COMPLEXITY-BASED OPTIMIZATION OF CARTOGRAPHIC DESIGN FOR MULTI-SCALE IMAGE-MAP GENERATION

QIAN PENG

PhD

The Hong Kong Polytechnic University

2022

The Hong Kong Polytechnic University

Department of Land Surveying and Geo-informatics

Complexity-based Optimization of Cartographic Design for Multi-Scale Image-Map Generation

Qian PENG

A thesis submitted in partial fulfillment of the requirements for the degree of Doctor of Philosophy

January 2022

CERTIFICATE OF ORIGINALITY

I hereby declare that this thesis is my own work and that, to the best of my knowledge and belief, it reproduces no material previously published or written, nor material that has been accepted for the award of any other degree or diploma, except where due acknowledgement has been made in the text.

________________________ (Signed)

Qian PENG (Name of student)

Complexity-based Optimization of Cartographic Design for Multi-Scale Image-Map Generation

Abstract

Maps are graphic representations of geographical features and their spatial relationship. However, maps appear abstract to many people due to the use of geometric symbols. Satellite images, on the other hand, appear more realistic owing to their resemblance to real-world scenery. A hybrid design with the advantage of maps' high interpretation efficiency and satellite images' realism is desired, leading to image-maps. However, the quality of such map is criticized by many people. When overlaying map symbols onto images, discrepancies have been found due to the limited geometric accuracy of map elements and/or scene changes on the images. And a breakdown of the map symbols and complex image may occur with camouflage. Map symbols are not easily recognized on complex image. Only with difficulty can you separate symbols from varying photographic representations of ground objects. Also when load map symbols onto complex background image, too much information may lead to symbol overload. The production of such maps is a big challenge, especially concerning the cartographic design. Therefore, it is very desirable to carry out a thorough investigation into the theories and key techniques for optimum cartographic design. From the problems occurred in the production of multi-scale image-map generation, the complexity-based strategies are proposed from four aspects: (a) the matching between the image and map, (b) the enhancement of background images, (c) the appropriate number of graphic symbols load on images, and (d) the appropriate label placement considering background images.

To address the first factor, a complexity-based method for matching image resolution and map scale has been proposed for multi-scale image-map generation. The matching is based on the complexity of line features (line networks and individuals), as indicated by length, density, area, and fractal dimension. Experimental evaluations are conducted on 15 representative areas (urban, rural, and mixed) in Hong Kong at seven scales and eight image resolutions. Results show that the proposed complexity-based method can obtain good matching between image resolution and map scale in terms of accuracy and users' preference.

To address the second factor, an experimental investigation has been conducted into the influence of the transparency of background images on the usability (i.e., effectiveness and efficiency) of image-maps. Image-maps with eleven levels of image transparency, at three scales and in nine areas have been designed and generated. An online questionnaire survey was conducted. A total of 1,263 participants took part in this experiment and they were asked to distinguish between natural and cultural features. Results show that (a) the usability of image-maps varies with the transparency of background images, mostly with a single peak; (b) the transparency level corresponding to the peak usability decreases as the background complexity increases. This serves as a guideline for the effective use of transparency in image-map design.

To address the third factor, an experimental investigation into the effects of the complexity of background images and the density of graphic symbol on the usability of image-maps has been conducted to obtain the optimum level of map symbols load. Image-maps with ten density levels of map symbols from ten test areas in Hong Kong were used in eye tracking and online questionnaire survey. Forty participants took part in this experiment and they were asked to search Areas of Interest (AOIs) from image-maps/maps. Results show that (a) the optimum density level for may symbol load, where the peak usability occurs, varies with the complexity of the background images/image-map; (b) a polynomial model can fit the relationship between optimum level of symbol load and the complexity of the background image/image-maps. This can help optimize map symbol load for image-map generation.

To address the fourth factor, complexity-based optimization is proposed for point label placement for image-maps. Both the general principles of point label placement and the complexity of background images were considered and integrated into the automated labeling optimization algorithm. The Boltzmann entropy of the patch (where the rectangular box of a label is located) is calculated as the complexity variable. Image-maps of three test areas in Hong Kong, which combined Points of Interest (POI) data and the corresponding satellite images, were used in the experiment. An experimental evaluation is conducted by a questionnaire in terms of "the ease level of finding the corresponding name labels", "congestion level" and "the satisfaction level". The proposed complexity-based strategy for point label placement

has better performance in target searching tasks and satisfaction than original placement and strategy with general principles.

In summary, this project has developed some complexity-based optimization methods of cartographic design for multi-scale image-map generation. In further research, more factors (e.g., automatic feature extraction methods, more image generalization methods, automatic symbol style design) can be explored.

Publications arising from the thesis

Peng, Q., Li, Z. L., Chen, J., and Liu, W. Z., 2021. Complexity-based matching between image resolution and map scale for multiscale image-map generation. *International Journal of Geographical Information Science*, 35:10, 1951-1974, (DOI:10.1080/13658816.2021.1885674)

Peng, Q., Li, Z. L. and Gong, X. Y., 2021. Exploring the effects of background image transparency on the usability of image-maps. *Transactions in GIS*, 25, 3002-3024. (DOI: 10.1111/tgis.12805)

Peng, Q. and Li, Z. L., Exploring the effects of background image complexity and map symbol load on the usability of image-maps. (in preparation)

Peng, Q., Li, Z. L. and Lan, T., Automated label placement for point feature based on complexity of background image and general principles. (in preparation)

Acknowledgements

I would like to express my highest gratitude to my supervisor Prof. Zhilin Li (PhD, DSc). He is not only a true researcher but also a conscientious teacher. He is very busy but always spends tremendous time supervising students and is always here when I need his help. He is knowledgeable, talented, energetic, patient and also strict. I would never forget one day before the confirmation of my PhD registration, he noticed I refrained from tears and said tears were necessary during the process of pursuing a PhD degree. When I walked out of his office, I could not hold back the tears but that was also my last time for tears until now. I'm extremely grateful to get his high standards, continuous guidance and warm encouragement.

I would like to express my sincere thanks to Prof. Man Sing Wong, Charles for his help and support during the last year of my study. Sincere thanks also go to Prof. Bo Wu (the chair of the Board of Examiners) for his precious time on my PhD examination. Prof. Qiming Zhou of Hong Kong Baptist University and Prof. Feng Lu of Chinese Academy of Sciences have served as the external examiners and have given many insightful and helpful comments. I really appreciate them.

I would also like to express my sincere thanks to my colleagues and friends, Dr. Peichao Gao, Dr. Tian Lan, Dr. Jicheng Wang, Dr. Zhicheng Shi, Ms. Jing Li, Ms. Meilian Wang, Mr. Keru Lu, Ms. Xinyu Gong, for their valuable suggestions to my research and warm help in my life.

Special thanks go to my former supervisors for bringing me to research and for enabling me to pursue this degree. They are Dr. Zhiyong Lin of Wuhan University, Prof. Bing Zhang and Dr. Xu Sun of Institute of Remote Sensing and Digital Earth, University of Chinese Academy of Sciences.

Finally, I must express my very profound gratitude to my beloved parents, Dengli Peng and Shengzhi Pan, for their unconditional love and support, which make it possible for me to walk so far.

Table of contents

Chapter 1 Introduction

1.1 Background and motivation

1.1.1 Image-map: a hybrid of remote sensing image and map symbols

Maps are the graphic representation of geographical settings and can improve the understanding of geospatial relationships (Robinson et al. 1995); however, maps still appear abstract to many people due to the use of geometric symbols. Remote sensing images, on the other hand, appear more realistic owing to their resemblance to real-world scenery. A hybrid design with the advantage of maps' high interpretation efficiency and remote sensing images' realism is desired, leading to image-maps. For such maps, remote sensing images function as the background, and selective map symbols are then overlaid on them (Figure 1.1). Various research communities have recognized that image-maps have a significant advantage in human interpretation of terrain features over plain images, as map symbols provide useful additional thematic information.

(a) Map (b) Image (c) Image-map

Figure 1.1 Examples of a map, an image, and an image-map from Google maps (accessed Jan 20, 2021, from https://www.google.com/maps).

For decades, aerial photographs have been assembled into mosaics and overprinted with selected map symbols to produce photomaps. Russel Bean (1955) introduced a new instrument, "orthophotoscope", to correct relief displacements in aerial photographs. Orthorectified photos have formed the base for orthophotomap productions (Zuylen 1969), enabling the addition of cartographical symbols, e.g., contours, to planimetrically correct aerial photographs, as the term "image" covers a wider range of remote sensing imagery than the term “photograph” (Vozenilek and Bělka 2016, Lillesand et al. 2015). “Orthoimage” is also defined in ISO/TC211. Image-map is used in this study and defined as the hybrid of orthorectified remote sensing images and map symbols. Figure 1.2 shows an example of early image-maps with different design styles (Albertz et al. 1992). Many researchers have focused on the characteristics, composition and capabilities (Dahlberg and Luman 1987, Dahlberg 1993, Thrower and Jensen 1976), basic concepts, principles and geometry (Petrie 1977), and production process (Schweinfurth 1985, Murphy 2014) of the design.

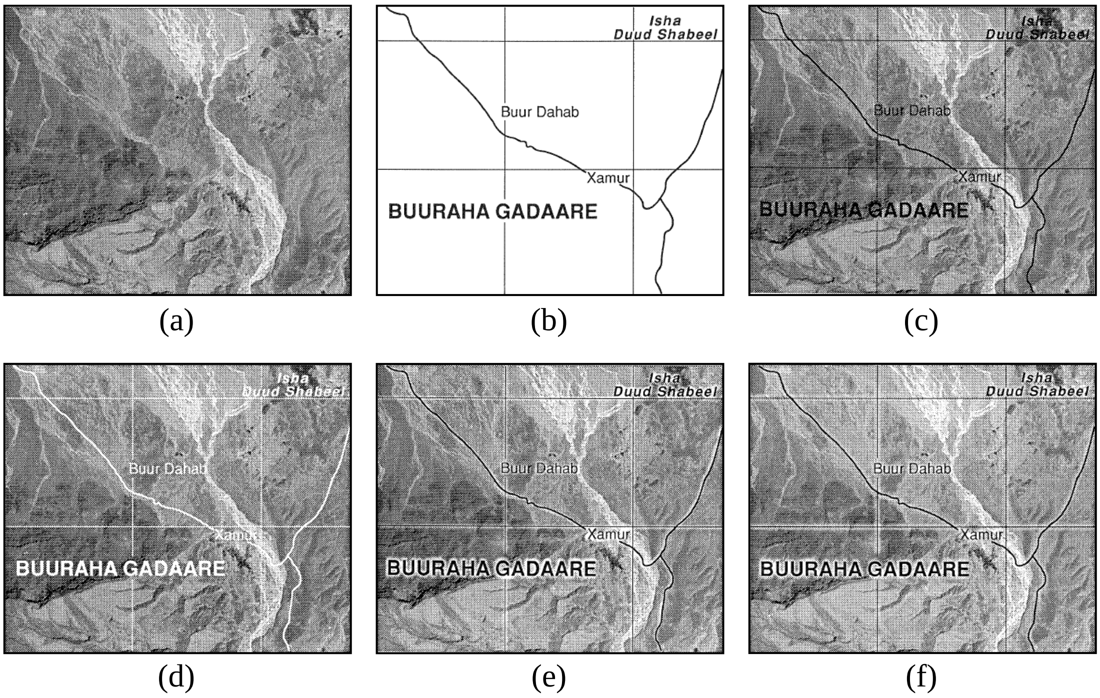

Figure 1.2 An example of early image-maps, (a) image data, (b) graphical elements to be integrated with image data, (c) integration of the graphical elements in positive form (letters, etc., printed in black), (d) integration of elements in negative form (letters, etc., removed from image data), (e) same as (c) with a brightened border around the graphical elements, (f) same as (d) with brightened borders around the graphical elements only in the dark areas (Albertz et al. 1992).

1.1.2 The importance of image-map

An image map has immense benefits and is in high demand in various disciplines, such as planning, environmental studies, property management, disaster and resources management, navigation, location-based services, and tourism (Landen 1966, Johansson 1967, Guzmán and Meyer 1967, Campodonico and Monopoli 1967, Arkesteijn 1967, Petrie 1977, Sunar Erbek et al. 2005, Cassettari 2004, Bělka 2013, Bělka and Voženílek 2014, Murphy 2014, Vozenilek and Bělka 2016, Meng et al. 2017, Dong et al. 2014). For example, Figure 1.3 (a) shows an image-map used in disaster management, global detection of current (near-real-time) and recent actively burning landscape fire map from Global Fire Monitoring Center, and Figure 1.3 (b) shows an image-map used in tourism: Hong Kong walking trails map.

(a)

(b)

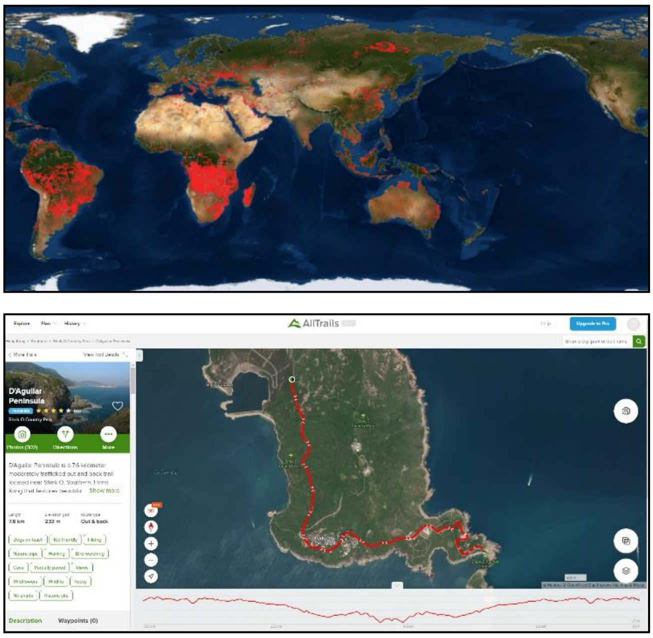

Figure 1.3 (a) an example of an image-map used in disaster management: global fire map (accessed August 12, 2021, data for August 6–12, 2021, from https://gfmc.online/current/globalfire-2.html), (b) an example of an image-map used in tourism: Hong Kong walking trails map (accessed August 12, 2021, from https://www.alltrails.com/explore/trail/hong-kong/southern/daguilar-peninsula).

In addition, many web map platforms also offer an image-map mode as an option, for example, the Tianditu map: https://map.tianditu.gov.cn/; the GeoInfo Map: https://www.map.gov.hk/gm/; the ArcGIS online map: http://www.arcgis.com/home/webmap/viewer.html; the Microsoft Bing Map: https://www.bing.com/maps; Maps of Switzerland: http://map.geo.admin.ch; the national geoportal of the Grand-Duchy of Luxembourg: https://www.geoportail.lu/en/maps/ (Figure 1.4). These online maps play an important role in geospatial information services for the general public.

However, many people have criticized the poor cartographic quality of such maps and pointed out that “the production of such maps is a big challenge, especially concerning the cartographic design”. Therefore, it is very desirable to carry out a thorough investigation into the theories and key techniques for optimum cartographic design.

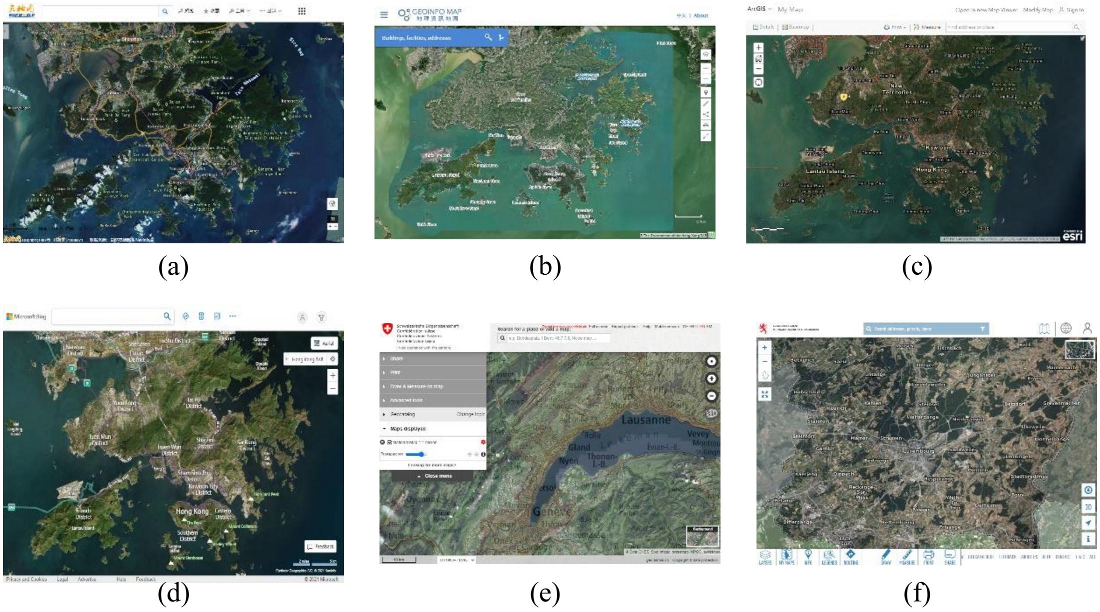

Figure 1.4 (a) a screen capture of the Tianditu Map (accessed May 13, 2021, from https://map.tianditu.gov.cn/), (b) a screen capture of the GeoInfo Map (accessed May 13, 2021, from https://www.map.gov.hk/gm/), (c) a screen capture of the ArcGIS online map (accessed May 13, 2021, from http://www.arcgis.com/home/webmap/viewer.html), (d) a screen capture of the Microsoft Bing Map (accessed May 13, 2021, from https://www.bing.com/maps), (e) a screen capture of the map viewer, with National Map 1:100 000 loaded semi-transparently (accessed May 13, 2021, from http://map.geo.admin.ch), (f) a screen capture of the national geoportal of the Grand-Duchy of Luxembourg (accessed May 13, 2021, from https://www.geoportail.lu/en/maps/).

1.2 Research for multi-scale image-map generation: state of the art

1.2.1 Main factors influencing the quality of multi-scale image-map

Main factors influence the quality of multi-scale image-map, including (1) the generation of background images, (2) overlaying map symbols onto images, (3) background image enhancements, and (4) map symbol representation (Figure 1.5).

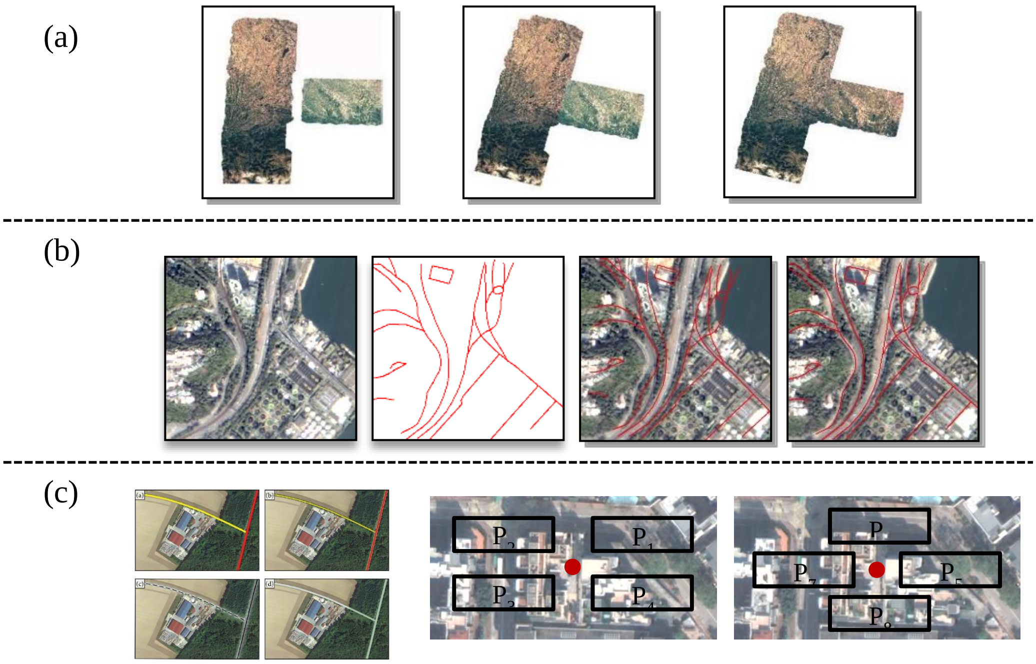

Figure 1.5 Main factors influencing the quality of multi-scale image-map.

(1) Generation of background images

To prepare the background images for the production of multi-scale image-map, the generation of background image are summarized as follows: orientation (vertical & oblique), standard rectification, orthorectification, mosaicking, and radiometric visual enhancement (Figure 1.5-a).

(2) Overlaying map symbols onto images

When overlay map symbols onto images, discrepancies have been found due to the limited geometric accuracy of map elements and/or scene changes on the images (Figure 1.5-b).

(3) The map symbol representation

Cartographic elements, such as names, symbols, and coordinates, can add essential meanings to an image, including points, lines, and areas, which play an important role in map readability. Sufficient labeling is necessary for indicating the location of objects and assigning a name or a description to an object (Figure 1.5-c).

1.2.2 Workflows for multi-scale image-map generation

Many researchers have studied multi-scale image-map generation, and their comprehension and emphasis on the production differ. Zuylen (1969) introduced the three main steps: the determination of coordinates for the geometric base, the representation of the landscape in the map, and the reproduction of the map. Tauch and Kähler (1988) overviewed the system of image map production developed at the Technical University of Berlin, which includes preprocessing, geometrical mosaicking and rectification, radiometric mosaicking and postprocessing, cartographical processing, and digital screening (Figure 1.6a). Albertz et al. (1992) also introduced this system and considered the visibility of topographic details and the lack of experience in cartographic processing. Bělka et al. (2013) proposed an integrated procedure (Figure 1.6b) consisting of five stages: task stage (map proposition), project stage (specification of image map type, area, scale, composition, data sources, and data collection), compilation stage (preparation of data layers for image and symbol components, compilation of map window, frame and marginalia), evaluation stage, and application stage (Vozenilek and Bělka 2016, Bělka and Voženílek 2014, Bělka 2013). And they posited research topics, e.g., the symbol component color specification automation in relation to the image component, and the creation of labeling and user issues in image map applications. Murphy (2014) reviewed the previous study on the production of image-maps and proposed a general workflow for image-map design, as shown in Figure 1.7.

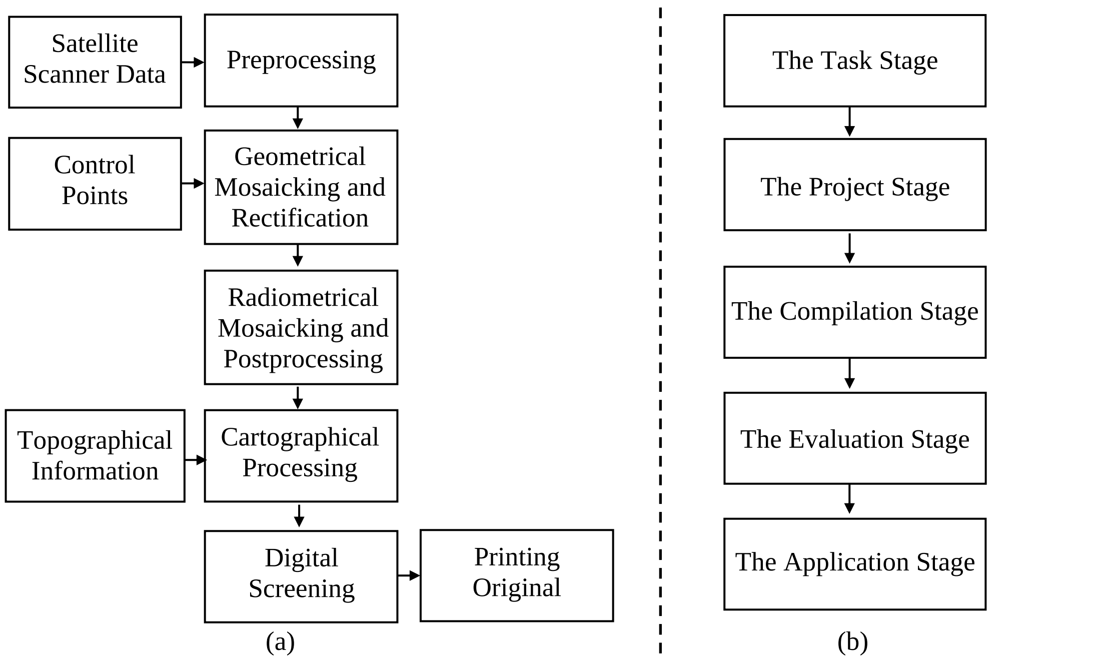

Figure 1.6 Workflows introduced by researchers: (a) redrawn from Tauch and Kähler (1988), (b) drawn from (Bělka 2013).

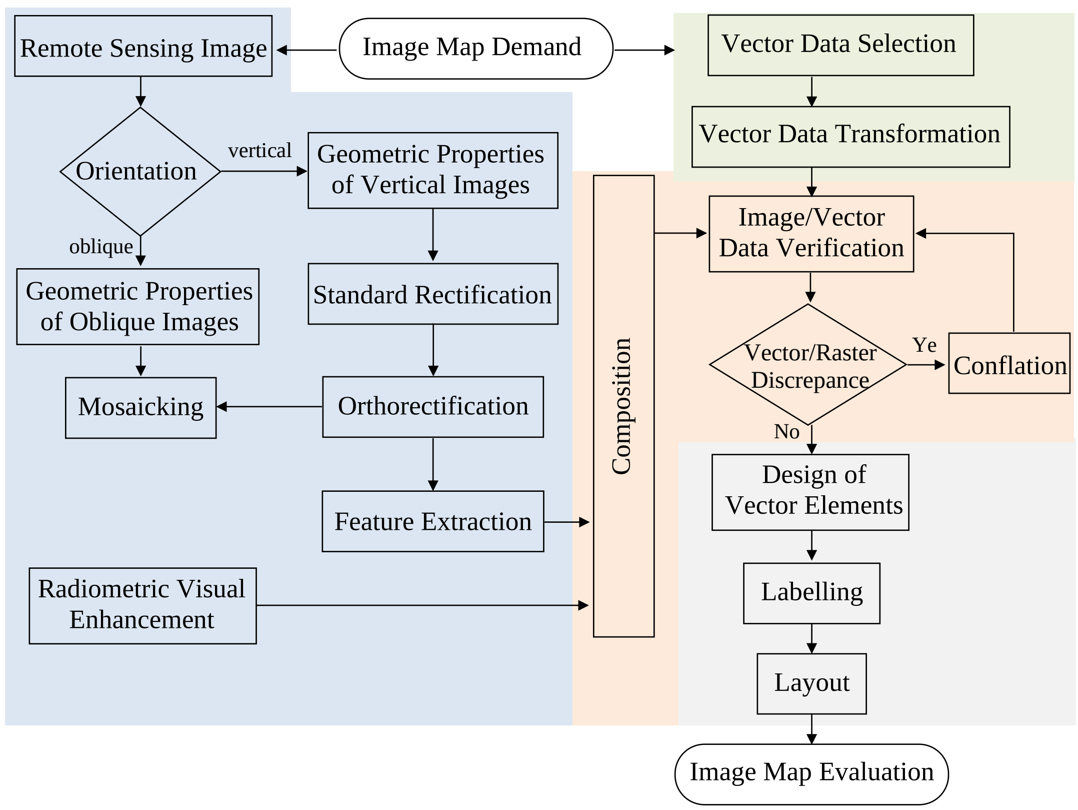

Figure 1.7 Standard workflow of image map design redrawn from Murphy (2014).

1.2.3 Research on main factors influencing the quality of multi-scale image-map

(1) Generation of background images

Remote sensing images play an important role in cartography, and many researchers have conducted several works to improve the quality of images for better mapping (Collins 1985, Tauch and Kähler 1988, Albertz and Tauch 1994, Albertz et al. 1992, Elshehaby and Taha 2011, Fleming 1973, Zuylen 1969). Many researchers have assessed the cartographic potential of images based on the accuracies of the images (Celikoyan et al. 2004, Alrajhi et al. 2016, Sisay et al. 2017, Thrower and Jensen 1976, Jacobsen 1990, Welch 1985, Elshehaby and Taha 2011, Fleming 1973). It has been reported (Pohl and van Genderen 1999) that discrepancies have been found when vector data are overlaid to raster orthoimages, due to the limited geometric accuracy of map elements and/or scene changes on the images.

Apart from these general methods for images, more image enhancements were explored for better usability of image-map. Complex background images make image-map cartographic design significantly more different from traditional mapping strategies. Most cartographic design rules in terms of simplicity, visual hierarchy, consistency, and legibility are violated by image maps (Meng et al. 2017). An image-map shows all sensed details, with varying photographic representations of objects. Even similar objects may appear dissimilar due to their varying surface colors and textures.

(2) Overlaying map symbols onto images

Images with different resolutions and maps with different scales should be selected in multi-scale image-map generation. The question "what scale of a map should be used to load symbols onto an image?" should be answered. An appropriate scale of a map should include supplementary spatial information about remote sensing images. The information content of maps should be consistent with images. Many researchers have assessed the cartographic potential of images based on the accuracies of the images (Celikoyan et al. 2004, Alrajhi et al. 2016, Sisay et al. 2017, Thrower and Jensen 1976, Jacobsen 1990, Welch 1985, Elshehaby and Taha 2011, Fleming 1973). Current solutions for matching image scales and image resolutions posit that the accuracy of images should satisfy the accuracy standard of maps. Images with a range of resolutions can satisfy the standard for a specific scale of the map after different image collection and preprocessing procedures (Fleming 1973, Welch 1985, Jacobsen 1990, Celikoyan et al. 2004, Elshehaby and Taha 2011, Sisay et al. 2017). However, the levels of detail (LoD) in images with different resolutions differ, which may also influence matching performance. This may lead to a situation in which the LoD in images may not match the complexity of map features despite matching planimetric accuracy. Not only are the horizontal accuracy of images and maps important, but the different LoD in images and maps may also influence matching performance.

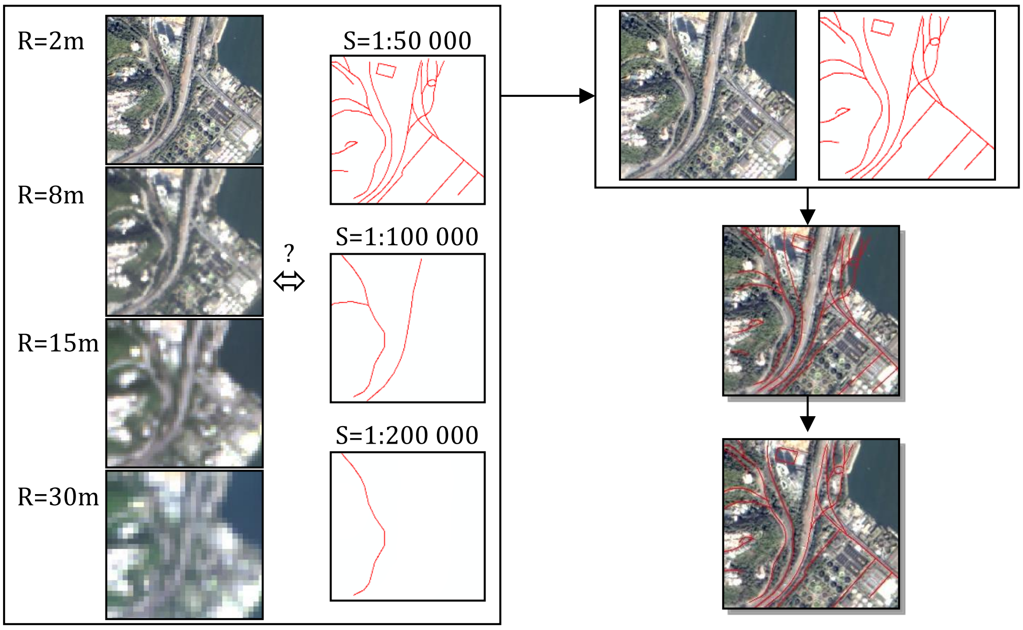

Figure 1.8 Choose the best matching between image resolution and map scale and the composition/conflation of image and map.

The conflation of these two data types should be conducted. Saalfeld (1988) states that conflation is the compilation or alignment of two different digital maps of the same region. Conflation can be classified into three classes based on the processing objects, namely, vector-vector, vector-image, and image-image, as well as from two aspects: horizontal and vertical (Yuan and Tao 1999). Many researchers have worked on the conflation of vector data and images (Zhang et al. 2016, Hackelöer and Andreas 2016, Hackeloeer et al. 2015, Zhang 2013, Zhang et al. 2011, Li and Goodchild 2011, Song et al. 2009, Blasby et al. 2002, Ruiz et al. 2011b). Conflation methods can be classified by the entities used for matching: point-based, line-based, and patch-based (Zhang 2013, Ruiz et al. 2011b).

(3) The map symbol representation

Vector elements can add essential meanings to an image, including points, lines, and areas, which play an important role in map readability. Vector elements can be topographic or qualitative, or quantitative thematic features. Sufficient labeling is necessary for indicating the location of objects and assigning a name or a description to an object. Labeling image-maps of background images with varying surfaces and textures is challenging.

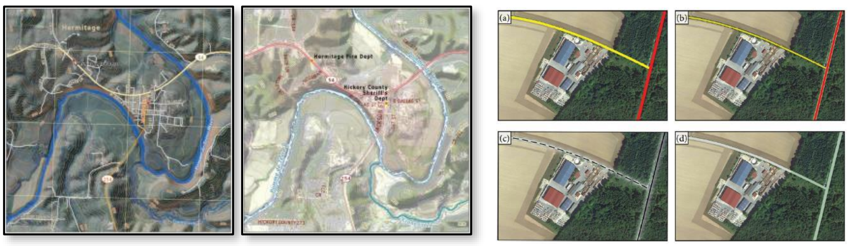

(a) Image-map style design

(b) Labeling

Figure 1.9 Design of map style/labeling.

The combination of image and map violates cartographic design rules in terms of simplicity because the map space is not masked by cartographic symbols but imagery depiction. Traditional map load considers the complexity of the loaded symbols; however, the background images are more complex. So if the amount of symbol loading remain the same as traditional map setting, the image-map may suffer from overload. The complexity of background image is not considered in current symbol loading problems in the production of image-maps.

The representations of graphic and text symbols have been explored to adapt to complex backgrounds, e.g., adapting the color of symbols depending on the radiometry of an image locally (Hoarau et al. 2013), adjusting the hues, color lightness levels, contrasts, halos, transparency, and layer order of labels to improve map readability (Raposo and Brewer 2013). The generalization of map contents, i.e., simplifying the map contents by load selected map features, is also related to this factor (Vozenilek and Bělka 2016).

The effectiveness of label position preference influences the quality of image-map. Although there are many rules for the placement of labels in traditional map design (i.e., the potential positions and the preferences of these positions), the traditional labeling preference may be not effective for image-maps with complex background images.

1.2.4 The evaluation of the usability of image-maps

To evaluate the usability of image-maps, three criteria for usability identified by the ISO 9241-11 standard can be adopted. The criteria are as follows:

- Effectiveness: "Accuracy and completeness with which users achieve specified goals" (ISO 2018).
- Efficiency: "Resources expended in relation to the results achieved, typical resources include time, human effort, costs and materials" (ISO 2018).
- Satisfaction: "Extent to which the user's physical, cognitive and emotional responses that result from the use of a system, product, or service meet the user's need and expectations" (ISO 2018).

These criteria are widely used in map evaluation (Brychtova and Coltekin 2016, Roth et al. 2017, Gao et al. 2018). Bevan et al. (2016) introduced quality measures used in ISO/IEC25022 which include measures for usability components defined in ISO 9241-11 (Table 1.1).

Table 1.1 Measures of effectiveness, efficiency, and satisfaction (ISO 9241-11, ISO/IEC 25022)

Effectiveness	**Efficiency**	**Satisfaction**
Tasks completed	Task time	Overall satisfaction
Objectives achieved	Time efficiency	Satisfaction with features
Errors in a task	Cost-effectiveness	Discretionary usage
Tasks with errors	Productive time ratio	Feature utilization

Task error intensity	Unnecessary actions	Proportion of users complaining
	Fatigue	Proportion of user complaints about a particular feature
		User trust
		User pleasure
		Physical comfort

1.3 Scope and objectives of this study

This project aims to optimize the cartographic design of image-maps. As discussed in Section 1.2, the challenges in the generation of image-map production are mainly because of the complex background image, which is different from traditional map. The complexity-based strategies are proposed for the optimization of image-map, i.e., to lower the complexity of image-map for better usability. From the main three aspects in image-map generation, four objectives are, therefore, proposed in this research:

- To develop a complexity-based strategy for matching image resolution and map scale;
- To explore the effects of background image transparency on the usability of image-map from the view of complexity
- To explore the effects of background image complexity and map symbol load on the usability of image-maps;
- To develop a strategy for the automated point label placement based on the complexity of background images.

Based on the general workflow proposed by Murphy (2014, Figure 1.7), the workflow for the optimization of multi-scale image-map generation in this study is shown in Figure 1.10. A more detailed review and analysis of related research will be given in Chapter 2.

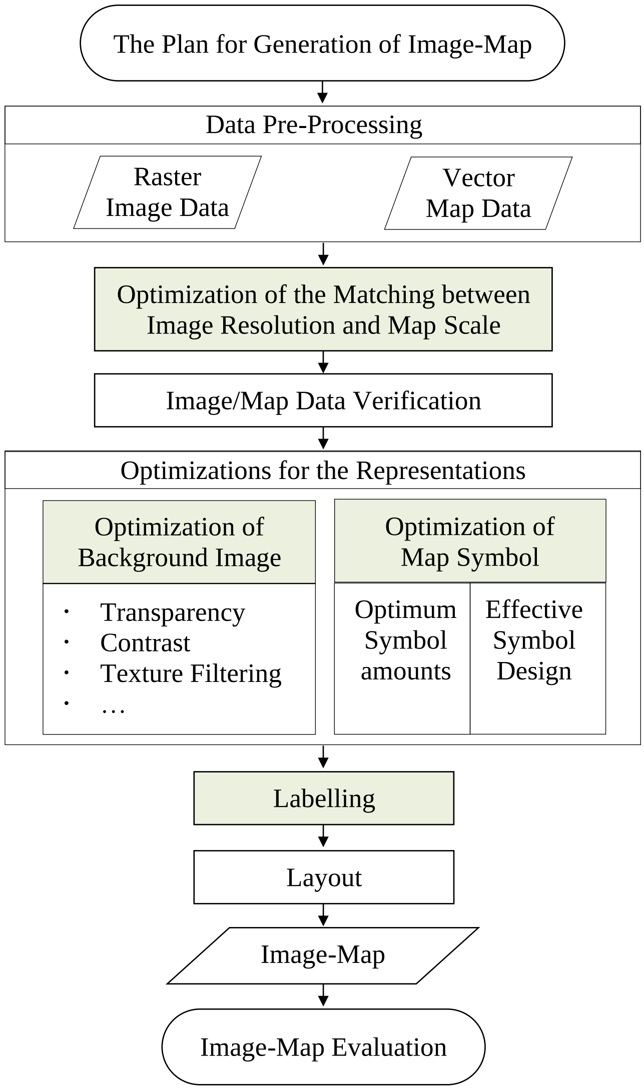

Figure 1.10 Workflow for the optimization of multi-scale image-map generation in this study.

1.4 Structure of the dissertation

This thesis is divided into seven chapters. A short preview of the remaining six chapters is given, as follows:

- Chapter 2: The current methodology and complexity-based strategy for multi-scale image-map generation are introduced.
- Chapter 3: A complexity-based strategy for matching image resolution and map scale for multi-scale image-map generation is proposed.
- Chapter 4: The effects of background image transparency on the usability of image-maps are explored.
- Chapter 5: The effects of background image complexity and map symbols load

on the usability of image-maps are explored.

- Chapter 6: An automated label placement strategy for point features based on the complexity of background image and general principles is proposed.
- Chapter 7: Our research work is summarized in this chapter. In addition, the limitations of this research are illustrated, and recommendations for future research are given.

Chapter 2 Optimizations for multi-scale image-map: review and analysis

To optimize the cartographic design of image-maps, a detailed review and analysis for current methodologies related to the four objectives in this study will be given in this chapter. And the complexity of image-map is introduced, i.e., the definition and measurements.

2.1 Current methodology for the multi-scale image-map optimization

2.1.1 Current solutions for matching image resolution and map scale

Matching image resolution and map scale is a commonly mentioned problem in production (Welch 1972, Albertz et al. 1992, Lam and Quattrochi 1992, Albertz and Tauch 1994, Vozenilek and Bělka 2016). For the selection of source images for multiscale image-map generation, horizontal accuracy is the main factor considered, which means the accuracy of the images should satisfy the accuracy standards of corresponding map scales. Map accuracy has been analyzed in many studies, and corresponding specifications have been issued (Authority 1998, Congalton and Green 2008, ASPRS 1990, ASPRS 2014). Table 2.1 presents examples of the horizontal-accuracy classes issued for digital planimetric data (ASPRS 1990, 2014). The horizontal root-mean-square error (RMSE) of images should be smaller than the accuracy standards for the corresponding map scales in the generation of a multiscale image-map. In general, the accuracy of an image is related to its resolution. High-resolution images commonly have high horizontal accuracy; however, remotely sensed images exhibit internal and external geometric errors (Poli and Toutin 2012). The errors of images with the same resolution may differ because of both internal and external conditions. The accuracy of images may differ because of different rectification methods used. Table 2.2 shows the GSD and RMSE_r (radial error) of many common satellite images. The geolocation accuracy of images is divided into two categories: horizontal accuracy not corrected by ground-control points (GCPs) or orthorectified using rational polynomial coefficients (RPC) models, digital elevation models (DEMs), and GCPs. Many researchers have assessed the cartographic potential of images based on their accuracies (Fleming 1973, Thrower and Jensen 1976, Welch 1985, Jacobsen 1990, Celikoyan et al. 2004, Elshehaby and Taha 2011, Alrajhi et al. 2016, Sisay et al. 2017). However, accuracy varies owing to different factors, such as sensors, atmospheric conditions, and elevation. Also, the RPC model, the quality of the DEM, the GCPs, and the terrain in the test area all influence RMSE and hence affect accuracy. The RMSEs listed in Table 2.2 were compiled from various sources.

Table 2.1. Horizontal accuracy/quality examples for high-accuracy digital planimetric data, based on positional-accuracy standards (ASPRS 1990, 2014).

ASPRS 2014			**ASPRS 1990**	
Horizontal accuracy class RMSE_x and RMSE_y(cm)	**RMSE_r (cm)**	**Approximate GSD of source imagery (cm)**	**Map scale**	
			Class 1	**Class 2**
0.63	0.9	0.31 to 0.63	1:25	1:12.5
1.25	1.8	0.63 to 1.25	1:50	1:25
…	…	…	…	…
250.0	353.6	125.0 to 250.0	1:10 000	1:5 000
300.0	424.3	150.0 to 300.0	1:12 000	1:6 000
500.0	707.1	250.0 to 500.0	1:20 000	1:10 000
1000.0	1414.2	500.0 to 1000.0	1:40 000	1:20 000
X	$1.4142 \times \mathrm{X}$	$0.5 \times \mathrm{X}$ to X	$1{:}\,(\mathrm{X} \times 40)$	$1{:}\,(\mathrm{X} \times 20)$

Note: RMSE_x and RMSE_y are horizontal linear values in X direction (Easting) and Y direction (Northing), and RMSE_r represents radial error, including both x- and y-coordinate errors. Class 1 is higher accuracy than Class 2; Class 2 means limiting errors are twice those allowed for Class 1. Circular map-accuracy standard” ($\mathrm{CMAS} = 2.146 \times \mathrm{RMSE_x}(\mathrm{RMSE_y})$) is 0.54 mm for all corresponding scales. [GSD, ground-sample distance; RMSE, root-mean-square-error]

Table 2.2. Selected satellite images.

Satellite images	**GSD (m)**	**$RMSE_r$ (m)**		**Resources**
		Without GCP	With GCPs	
WorldView-4	0.31	3.8	2.0	(DigitalGlobe 2017b, Vajsova et al. 2017)
WorldView-3	0.31	2.3	1.2	(DigitalGlobe 2017a, Barazzetti et al. 2016)
WorldView-2	0.46	2.5	0.3	(DigitalGlobe 2017a, Aguilar et al. 2013)
WorldView-1	0.5	2.8	0.9	(DigitalGlobe 2017a, Xiao et al. 2014)
GeoEye-1	0.41	2.5	0.4	(DigitalGlobe 2014, Aguilar et al. 2013)
TianHui-1	2, 5, 10	10	9	(Wang and Hu 2016)
ZiYuan-3	2.1, 3.6	15	4	(Li and Wang 2012, Yang et al. 2017)
GaoFen-2	1, 4	35	1.5	(Jiang et al. 2017)
GaoFen-4	50	1300	100	(Li et al. 2017)
SPOT-5	2.5, 5, 10	36	10	(Ma et al. 2017)
QuickBird-2	0.61	15	0.7	(DigitalGlobe 2012, Noguchi et al. 2004)
IKONOS	0.82, 3.2	10	1.3	(DigitalGlobe 2013, Jacobsen 2003)
HuanJing-1	30	1000	60	(Xiong et al. 2014)
Landsat-8	15, 30	43	8	(Storey et al. 2014)
Modis	250, 500	150	50	(Wolfe et al. 2002)

Note: GCP, ground-control point; GSD, ground-sample distance; RMSE, root-mean-square-error in radial direction.

Two problematic circumstances may result from the production of an image-map:

- First, although the detail of the image (resolution) may be satisfactory for map production, the image may not be well rectified, and the accuracy is thus not satisfied.
- Second, the accuracy of image may be satisfied, but the detail of images may be significantly different.

For images with different resolutions and maps with different scales, not only the accuracy should be considered but also the information content should be matched.

Resolution plays an important role in the interpretability of topographic details based on the smallest distinguishable objects. It can also be used as an indicator of LoD in multiscale representation (Li 2006). LoD is the concept applied to bridge the complexity and the efficacy of computer graphics by regulating the amount of detail used virtually to represent the physical world (Luebke et al. 2003). LoD can be used to explain the different scales that features may have when visualized within different multiscale representations. Map scale, as the degree of abstraction, implies the complexity of details shown in a map. The complexity of the details from images and maps can be regarded as an indicator for the matching.

2.1.2 Current adjustment methods for the background image

Many studies have been concentrated on the generalization of background images to reduce the complexity for better representation. Dong et al. (2014) enhanced the background image with histogram segmented stretch, co-occurrence-based texture filtering, and Gaussian low-pass filtering (Figure 2.1). Murphy (2019) proposed different highlighting or deemphasizing strategies for background images based on simplicity principle (Figure 2.2). Also the transparency and contrast of the background image were also been studied for better representation (Welch 1972, Albertz and Tauch 1994, Murphy 2014, Raposo and Brewer 2014) (Figure 2.3). Transparency refers to how the clearness of an image influences the observation of any images behind it and is widely used in image display. The use of transparency in the production of image-maps has been explored in a number of studies.

(a) (b)

Figure 2.1 The original (a) and enhanced (b) image basemap for a test area (3×5 km) in Hohhot (Dong et al. 2014).

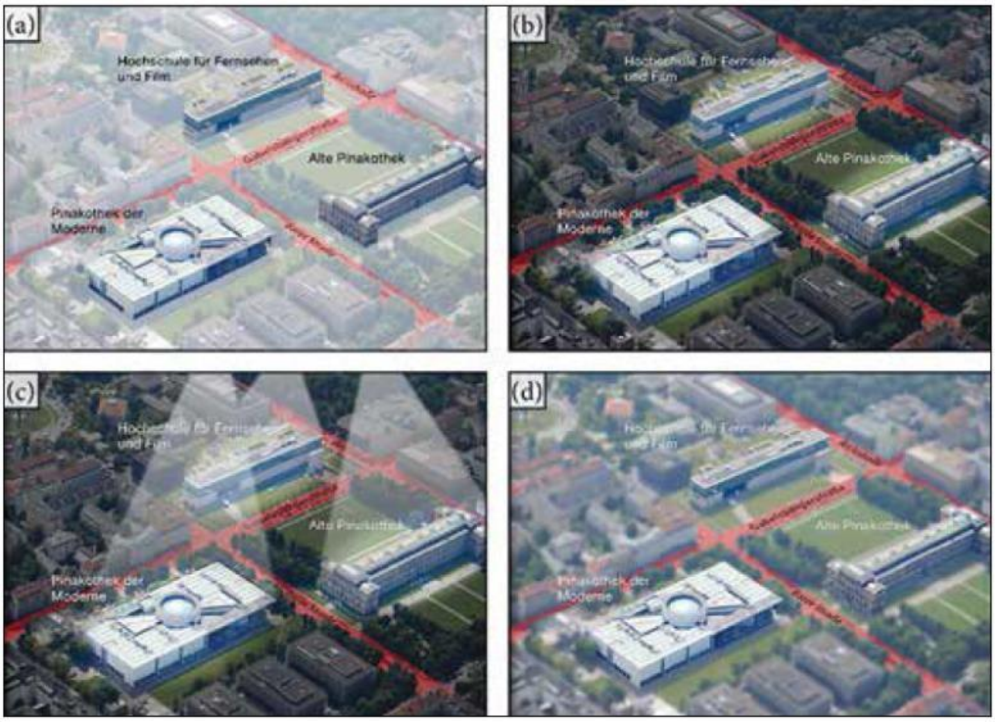

Figure 2.2 Four different highlighting or deemphasizing strategies for background images based on simplicity principle: (a) Selective Brightening, (b) Spotlight Highlighting, (c) Light Beam Guidance, (d) Semantic Focusing (Murphy 2019).

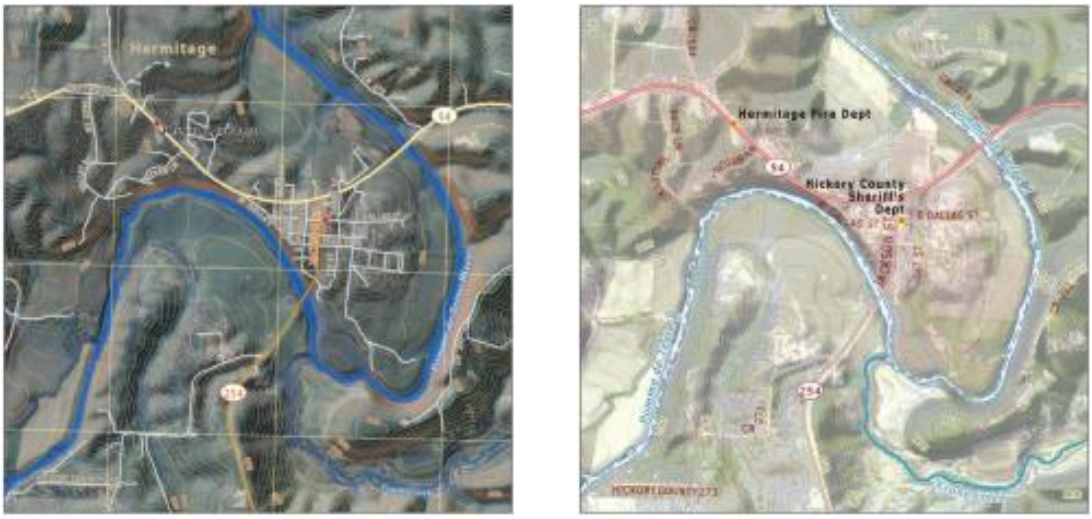

(a) (b)

Figure 2.3 Two selected designs of image-map with different transparency, greyscale, and vector features (Raposo and Brewer 2014).

Hoarau (2012) conducted a statistical analysis of a survey on the design choices of 45 cartographic websites using the API of the French Géoportail. Bělka (2013) dealt with the definition of image map and introduced the use of transparency in thematic image maps; the transparency of a displayed layer is an important factor considered in their study. Raposo and Brewer (2014) explored the landscape preferences and map readability in design evaluation for image-maps. Murphy (2014) found that higher symbol transparency resulted in the image being seen more clearly. The transparency of overlapping polygons and background images were considered important factors in design. Panchaud et al. (2017) demonstrated that changing layer transparency can reduce the visual importance of complex background satellite imagery. Additionally, many web maps provide functions allowing the users to modulate layer transparency in order to improve interpretation, for example, the ArcGIS online map, and the national geoportal of the Grand-Duchy of Luxembourg (Figure 1.4).

In these studies, different levels of layer transparency are used in the design of image-maps, usually based on the specific objective(s) of the study. In the case of online map websites, the transparency level is set manually by the users. The ad hoc transparency level varies when the background image changes. Herein, the effects of the transparency of a background image on the usability of image-map are explored systematically.

2.1.3 Current optimizations for the representations of map symbols

In image-map, the background image shows all sensed details and the photographic representation of objects are quite different. If vector elements represent important information to be visualized in the foreground, it is necessary to enable a good figure-ground segregation. This is a very difficult task when the background is seamlessly covered by a remote sensing imagery. The image is a collage of colored objects with varying pixel values in terms of intensity, hue and saturation. The image objects can appear in dark or light tones, their color values can change quickly over short distances. Moreover, the imagery can have rather homogenous colored areas adjacent to areas possessing high radiometric fluctuations. This challenges cartographers who should find design solutions to maintain the readability of vector and label designs upon imagery. Without any accentuation, however, relatively small points and thin lines are more likely to fade into the ground. Special symbolization strategies for image maps include saturated coloring, casing, brightened seam, and adaptive coloring (Murphy 2014). Each symbolization technique is shown in Figure 2.4.

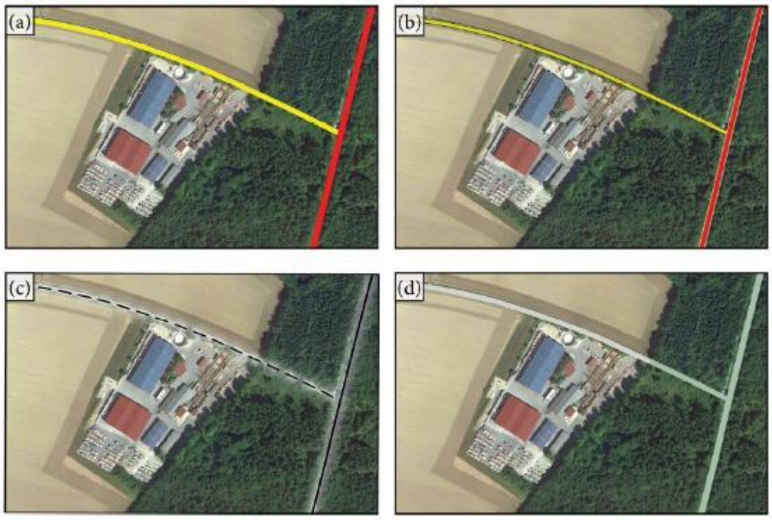

Figure 2.4 Image map symbolization techniques: (a) saturated coloring, (b) casing, (c) brightened seam, and (d) adaptive coloring (Murphy 2015).

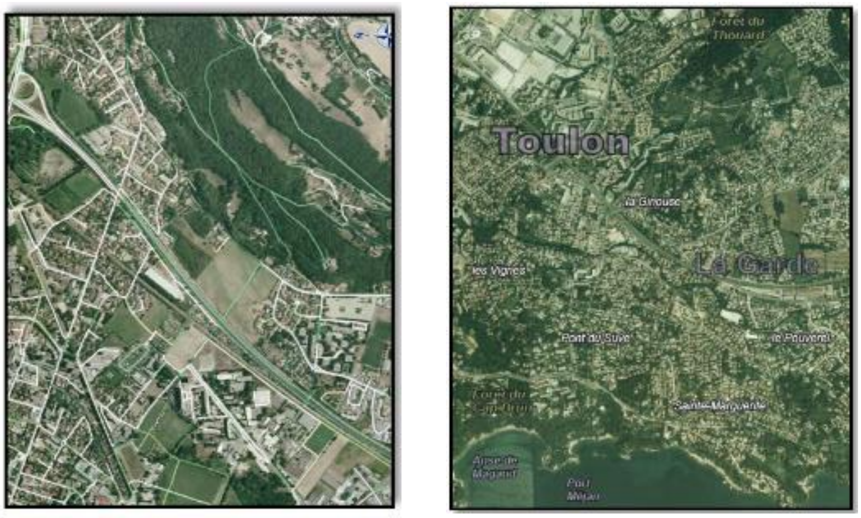

(a) (b)

Figure 2.5 Adaptive symbolization of the road network: (a) and toponym of cities (b) depending on the ortho-imagery radiometry (Hoarau et al. 2013)

Apart from the symbol design for maps, the visualization of map symbols with image background are getting more and more attention. Hoarau (2012) evaluated the existing design choices, such as favored base maps, transparency levels of the displayed layers, scale visualization, from mixed representations in use in geoportals Case study on the French Geoportal. Hoarau et al. (2013) showed adaptive symbolization when overlaying data shown in Figure 2.5. Raposo and Brewer (2014), Raposo and Brewer (2013), Raposo and Brewer (2011) explored the influence of hues, color lightness levels, contrasts, halos, transparency and layer order, casings on the readability of vector labels with background images (Figure 2.6). Murphy (2014) discussed basic characteristics of image and map as show in Table 2.3. As the background images are much more complex than traditional basemap with graphic symbols, selective map symbol load and symbol optimization can be further elaborated in future research.

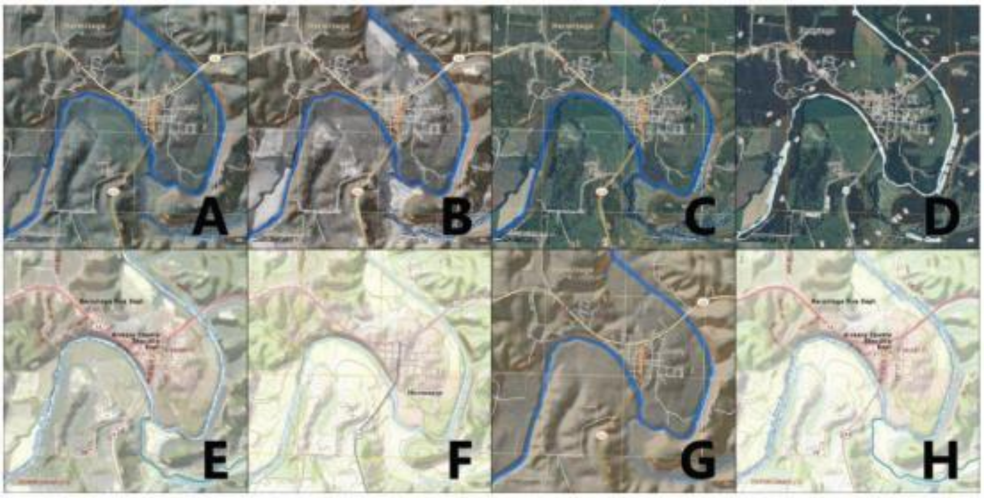

Figure 2.6 The eight design permutations considering such as favored base maps, transparency levels of the displayed layers, scale visualization (Raposo and Brewer 2014).

Table 2.3. Basic characteristics of images and maps (Murphy 2014).

Characteristic	**Image**	**Map**
Nature	Realistic	Abstract
General appearance	photographic	symbolised
Coverage	Seamless	Selective
Information	tangible objects	tangible and intangible
Appearance	Individual	Classified
Visual hierarchy	random	structured
Visual object separation	Vague	Distinctive
Declaration	unexplained	explained
Temporal representation	Moment	Period

2.1.4 Current point feature label placement

Point feature label placement (PFLP) is a fundamental task in cartography. Many automated cartographic labelling methods/algorithms for topographic maps (i.e., a kind of general-purpose maps) have been developed. Yoeli (1972) proposed eight potential positions with different weights and a three-step label placement process for PFLP (Figure 2.7 (a)). A set of fixed label candidates are predefined for each point (Christensen et al. 1995, Raidl 1998, Yamamoto et al. 2002, Klau and Mutzel 2003, Cravo et al. 2008, Do Nascimento and Eades 2008, Ribeiro and Lorena 2008). In addition to the fixed-positions-based methods, in some slider-based methods (Figure 2.7 (b)), the label can slide continuously in one or more directions (e.g. Hirsch 1982, Doddi et al. 1997, Van Kreveld et al. 1999, Strijk and Van Kreveld 2002, Kameda and Imai 2003, Ebner et al. 2004, Poon et al. 2004, Schwartges et al. 2014). That is, a continuous movement of a label around its point feature is allowed. Therefore, the space around the points can be better used for labels.

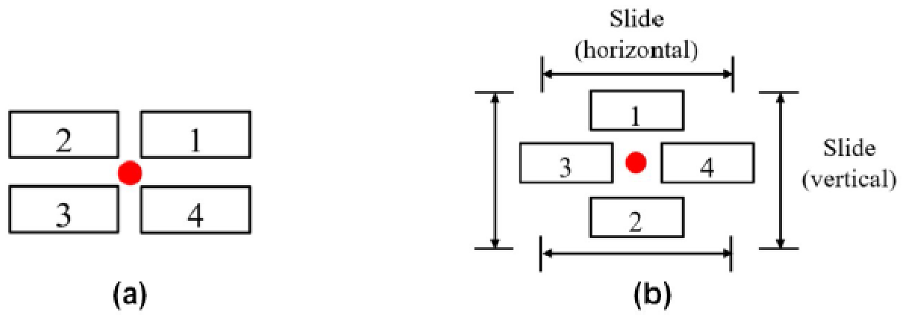

Figure 2.7 Two types of models for the construction of search space: (a) fixed-position model; and (b) slider model. (Lan et al. 2020)

Imhof (1975) is one of the earliest researchers concerning the rules of positioning labels on maps. In his work, six principles and requirements are proposed: (1) the name labels should be easily and quickly read, discriminated and located; (2) the name label and the object to which it belongs should be easily recognized; (3) names should disturb other map contents as little as possible; (4) names should assist directly in revealing spatial situation, territorial extent, connections, importance, and differentiation of objects; (5) name labels should reflect the classification and hierarchy of objects on the map; and (6) names should not be evenly dispersed over the map, nor should names be densely clustered. These principles and requirements are very helpful and have guided cartographic labeling for many years. However, they are not especially for automated labelling.

Currently, the point labelling methods for image-map mainly follow the methods above. The graphic features and labels are load to images without any further revisions adapting to the complex background images.

2.2 Measurements for the complexity of image-map

A large amount of research has been conducted to explore map complexity and the visual and intellectual complexities of maps are widely adopted in cartographic research. Visual complexity, also termed graphic complexity, refers to the spatial distribution of graphic content in geographic visualization. It includes the amount of information (statistical information) and its spatial distribution (structural information). According to this information, current measures for visual complexity in maps are summarized in Table 2.4, including indexes for vector and raster data.

Intellectual complexity deals with meaning, for example how symbols are understood and their significance to the map audience (Fairbairn 2006, Liao et al. 2018, MacEachren 1982). Intellectual complexity varies substantially between users and is not easily measured. Perceived map complexity is defined instead of intellectual complexity, which is measured by the subjective assessment of individuals.

Table 2.4 Classification of current measures for the visual complexity.

Map formats	**Measures for the visual complexity of maps**		**Resources**
Vector	Statistical	number of objects	(MacEachren 1982, Phillips and Noyes 1982, Fairbairn 2006, Harrie and Stigmar 2010, Schnur et al. 2010)
		number of vertices, links, length, and areas	(MacEachren 1982, Frank and Timpf 1994, Woodruff et al. 1998, Fairbairn 2006)
		density of map objects	(Stigmar and Harrie 2011, Fairbairn 2006)
		occupied space	(Kent and Tobias 1990, Frank and Timpf 1994, Harrie et al. 2015)
		entropy for symbol types and numbers	(Bjørke 1996)
	Structural	fractal dimension	(Goodchild 1980, Mandelbrot 1983, Lam and Quattrochi 1992, Lan et al. 2019)
		distribution of objects (graph theory)	(MacEachren 1982)

		entropy for spatial information	(Bjørke 1996, Li and Huang 2002)
		landscape shape index	(Fairbairn 2006)
Raster	Statistical	compositional entropy	(Sukhov 1970, Gatrell 1977, Rosenholtz et al. 2007)
		uniformity (energy)	(Gatrell 1977, Gonzalez and Woods 2002, Fairbairn 2006)
		variance (contrast)	(MacEachren 1982, Gonzalez and Woods 2002, Harrie et al. 2015)
		correlation	(Olson 1975, Gonzalez and Woods 2002)
	Structural	Boltzmann entropy	(Gao and Li 2019, Gao et al. 2017)
		relational descriptors	(Gonzalez and Woods 2002)

2.2.1 Complexity of line network and individual lines (vector)

The complexities of line networks and individual lines may be characterized by using indicators (Table 2.5). Overall length, line density, and fractal dimension are considered as indicators of the complexity of line networks. Length, shape, area, and fractal dimensions are considered as indicators of the complexity of individual lines.

Table 2.5. Indicators of complexity of line networks and individual lines.

Level		Indicators	Meanings
Line network complexity	Class level	$\mathrm{I_L}$	whole length of road networks
		$\mathrm{I_D}$	sum of the line density in all grids
		$\mathrm{I_F}$	box-counting geometric fractal dimension of networks
Individual line complexity	Feature level	$\mathrm{I_l}$	line length
		$\mathrm{I_s}$	line shape
		$\mathrm{I_a}$	line area formed by vertices
		$\mathrm{I_f}$	box-counting geometric fractal dimension of lines

The calculation of length, density, and fractal-dimension indicators of the line network are as follows:

- Length

Polyline T, formed from the set of vertices $\{t_1, t_2, \cdots t_n\}$, has a length defined as

$$I_L = \sum_{i=1}^{n-1}[(t_{i+1} - t_i)(t_{i+1} - t_i)^{\mathrm{T}}]^{\frac{1}{2}} \tag{2.1}$$

where $t_i = (x_{t_i}, y_{t_i}), i \in \{1,2,\cdots,n\}$. Although the length of an individual line is at the feature level, the entire length of road networks can give a macroscopic view of the road features (Chaudhry et al. 2009).

- Density

Line density, which has been taken as an index for the evaluation of line networks by many researchers (Hu et al. 2007, Chen et al. 2009, Liu et al. 2008, Li and Ti 2015), is calculated by the grid-based approach involving the creation of a regular grid (e.g., $1 \times 1\ km^2$) that is then intersected with road-network data to yield road density for each grid cell, according to:

$$\mathrm{I_D} = \frac{\sum_{\mathrm{i}}^{\mathrm{n}} \mathrm{D_i}}{n} = \frac{\sum_{\mathrm{i}}^{\mathrm{n}} \frac{\mathrm{L_i}}{\mathrm{A_i}}}{n} \tag{2.2}$$

where $\mathrm{D_i}$ is density in the $\mathrm{i^{th}}$ grid cell, n is the number of grids, $\mathrm{L_i}$ is the total length of roads in the $\mathrm{i^{th}}$ grid cell, and $\mathrm{A_i}$ is the area of the $\mathrm{i^{th}}$ grid cell.

- Fractal dimension

Mandelbrot (1983) developed the concept of fractal dimensions and the branch of geometry called fractal geometry. Box-counting is a primary means of calculating fractal dimension (Mandelbrot 1983, Zhang and Li 2012) and has been widely used in geometric fractal analysis. Box-counting uses overlays of grids of square boxes and involves counting the number of boxes that intersect objects of interest, such as lines representing roads (Figure 2.8). The number of boxes intersecting the objects changes with box size according to

$$\mathrm{N_g} \propto \ \ell_{\mathrm{g}}{}^{-\mathrm{D_g}} \tag{2.3}$$

where $\mathrm{N_g}$ is the number of intersecting boxes, ℓ_{g} is the size of the box, and $\mathrm{D_g}$ is the box-counting geometric fractal dimension. The indicators $\mathrm{I_F}$ and $\mathrm{I_f}$ are calculated by using the box-counting approach.

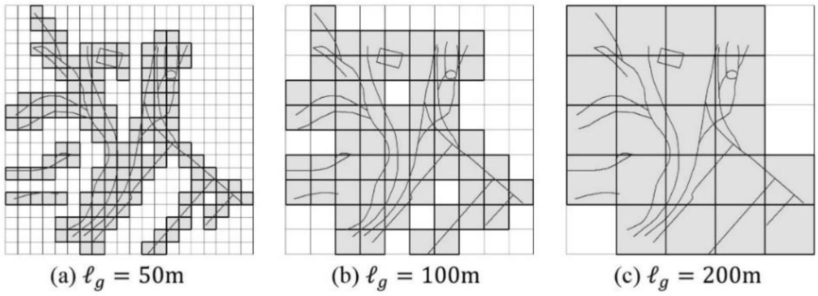

Figure 2.8. Box-counting geometric fractal dimension.

Length, shape, area, and fractal-dimension indicators for individual lines are used to evaluate line complexity. Line shape and area are introduced below.

- Shape

The shape indicator uses the cumulative angle function $\theta(s)$, also called the turning function, to yield the angle between the anticlockwise tangent and the X-axis as a function of arc length s. The function $\theta(s)$ tracks the turning that occurs; it increases with left-hand turns and decreases with right-hand turns (Arkin et al. 1991, Veltkamp 2001, Zhang 2009, Chehreghan and Ali Abbaspour 2017, Chehreghan and Ali Abbaspour 2018) (Figure 2.9).

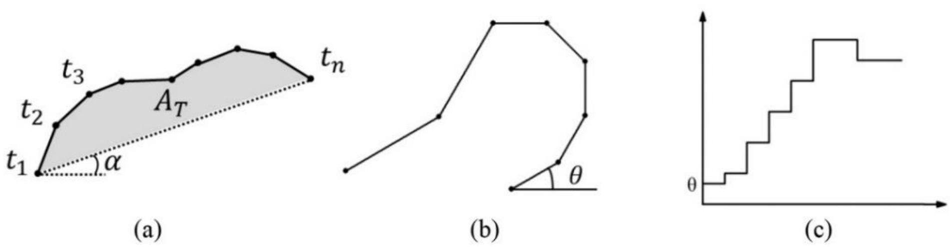

Figure 2.9. Polyline created from points t_{1-n}, area (A_T) of polygon created by points of polyline, and its turning function (θ).

Without losing any generality, each polyline can be rescaled such that its total length is 1, and then it can be defined as

$$\mathrm{I}_s = \left(\int_0^1 \theta(s)^p ds\right)^{\frac{1}{p}} \tag{2.4}$$

- Area

A polygon can be created by connecting its starting and ending points. $\mathrm{I_a}$ is the quotient of the area of polygon $\mathrm{A_T}$ and the distance between the starting and ending points (Figure 2.9) is given by

$$\mathrm{A_T} = \frac{1}{2}\sum_{1}^{n+1} \mathrm{t_i} \begin{vmatrix} 0 & 1 \\ -1 & 0 \end{vmatrix} \mathrm{t_{i+1}^T}, (\mathrm{t_{i+1}} = \mathrm{t_1}) \tag{2.5}$$

2.2.2 Complexity of background image (raster)

To assess combinations of different background images resolutions (raster) and scales of maps (vector), our final image-map outputs were produced in raster format. This enables measures of raster complexity considering the structural information adopted. Gao et al. (2017) proposed a feasible solution for calculating configurational entropy and, subsequently, Aggregation-based Absolute Boltzmann Entropy (AABE) was developed for calculating of the complexity of image-maps (Gao and Li 2019). For an image-map with dimensions of $M \times N$, the number of microstates is computed as the product of all possible decompositions of every aggregated cell, as shown in Eq. (2.6):

$$W = \prod_{i=1}^{(M/2)\times(N/2)} W_i \tag{2.6}$$

where W_i is the number of possible decompositions of the i th aggregated cell and $(M/2) \times (N/2)$ is the total number of aggregated cells. Decompositions are generated by the macrostate and microstate defined in Figure 2.10. The AABE (Figure 2.11) is computed as the sum of relative entropy S_R:

$$AABE = \sum_{k=0}^{n-1} S_R(L_k) = k_B \log\left(\prod_{k=0}^{n-1}\prod_{i=1}^{M\times N\div 4^{k+1}} W_{k,i}\right) \tag{2.7}$$

where n is the total number of hierarchical levels, L_k denotes the kth hierarchical level (L_0 is the original landscape gradient), $S_R(L_k)$ is S_R of L_k, and $M \times N \div 4^{k+1}$ represents the total number of aggregated cells in L_k.

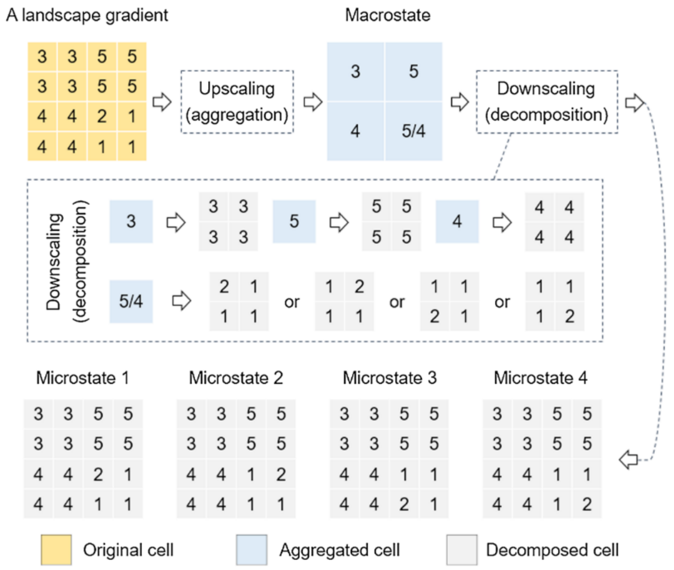

Figure 2.10. A landscape gradient with a microstate generated by the aggregation technique, and all possible microstates belonging to the microstate (Gao and Li 2019).

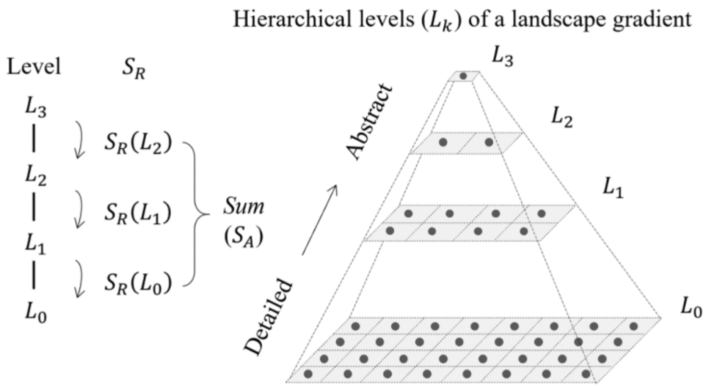

Figure 2.11. Relative Boltzmann entropies (S_R), absolute Boltzmann entropy (S_A), and the hierarchy generated using the aggregation of a landscape gradient with 4×8 cells (Gao and Li 2019).

Chapter 3 Complexity-based matching between image resolution and map scale for multi-scale image-map generation

In this chapter, a complexity-based matching between the image resolution and map scale is developed. The complexities of line network and individual line, as indicators of Level of Details (LoD), are considered to guide the matching between image resolution and map scale for multi-scale image-map generation.

3.1 Complexity-based strategy for matching image resolution and map scale

3.1.1 Matching based on complexities of line network and individual line

To produce an image-map, usually all superimposed graphical elements are required to allow the supplemental symbolism information to be used for interpretation of the satellite images. Because lines are one of the most common graphic elements for outlining features of interest in background images, the LoD of the line features in multiscale representations must be considered. To study the LoD of geometries featuring lines, the fractal is an appropriate spatial analytical tool in mapping sciences (Goodchild 1980, Mandelbrot 1983, Carstensen 1989). Fractal dimension can be an indicator for the complexity of curves and surfaces. The complexity of line features extracted from images differs from those extracted from maps. Li (2006) determined three levels of transformation of spatial representation: individual features (i.e., feature level), a class of features (i.e., class level), and the whole representation (i.e., map level). The complexities of line networks and individual lines concern the first two transformation levels. Accordingly, a strategy for matching between image resolutions and map scales is proposed:

- Use the complexity of line features as indicators of LoD to guide matching,
- Two levels of complexity are considered: class level and feature level, for line networks and individual lines, respectively.

Line features among graphical elements superimposed onto an image can be divided into two classes: formed lines and freeform lines. Formed lines result mainly from manmade features and comprise straight-line segments such as roads in urban areas. Freeform lines occur mainly in natural features and comprise curves, such as coastlines, but also may be derived from roads in rural or mountainous areas. The road network was selected as the research object because it includes both classes of lines. The line network studied in this research is specialized for application to road networks. An example of differences in the complexity of line networks and individual lines illustrates the two levels of complexity used herein (Figure 3.1).

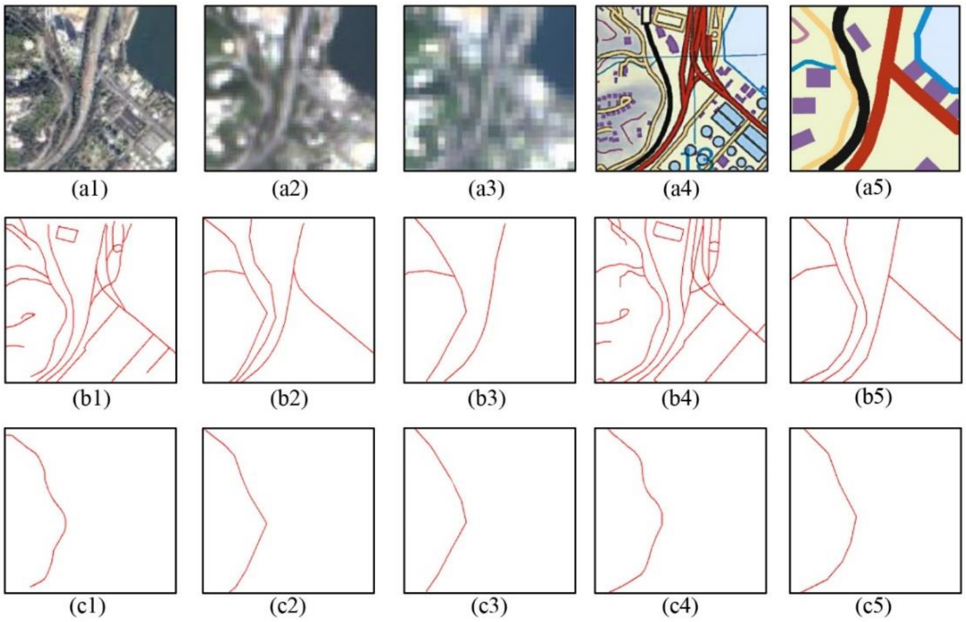

Figure 3.1. Different levels of details in multiscale representation. Images are shown at three resolutions (a1, 2 m; a2, 15 m; a3, 30 m) and two map scales (a4, 1:50,000; a5, 1:100,000). (b1–b5) Line networks (roads) extracted from images and maps; (c1–c5) Individual line extracted from these networks.

- Class level of complexity: The differing complexity of line network (b1–b5) derived from images (a1–a3) and maps (a4–a5).

Roads with smaller widths can be extracted from high-resolution images (a1), but only roads with larger widths (main roads) can be extracted from low-resolution images (a3). Therefore, the line network from high-resolution images is more complex than that from low-resolution images (b1–b3). On the other hand, the roads (b4–b5) shown on maps at different scales vary in appearance, and the complexity of line networks can be an indicator for matching between image resolution and map scale.

- Feature level of complexity: The variable complexity of individual lines (c1–c5) derived from images (a1–a3) and maps (a4–a5).

Roads extracted from high-resolution images show more detail (e.g., curved lines in c1). The length of the lines extracted from small-scale maps is shorter than those extracted from large-scale maps, as was revealed in Mandelbrot (1983) coastline paradox. Therefore, the complexity of an individual line feature can also be an indicator for matching because complexity increases for roads shown as having more detail.

The complexities of line networks and individual lines introduced above may be used for matching between image resolution and map scale. After matching based on line features, the horizontal position of lines should also be considered (Figure 3.2). From images of different resolutions, the line networks are manually extracted from background images, and polylines of transportation may be extracted from multiscale maps. Road polygons are extracted from high-resolution images, and the middle line of the polygons becomes the final road network. If using low-resolution images, polylines that capture the road pixels are extracted as the final road network. Typical lines are then chosen as study objects for matching the complexity of individual lines. After matching at the two levels (class and feature), the horizontal location of the line networks from the two sources should be considered. In the following three sections, the complexities of line networks and individual lines are analyzed to achieve the best quality of matching between the image resolution and map scale. After matching based on complexity, the horizontal location of the line networks should be reconsidered to satisfy accuracy standards.

The complexities of line networks and individual lines are characterized by using indicators introduced in Section 2.3.1. Overall length, line density, and fractal dimension are considered as indicators of the complexity of line networks. Length, shape, area, and fractal dimensions are considered as indicators of the complexity of individual lines.

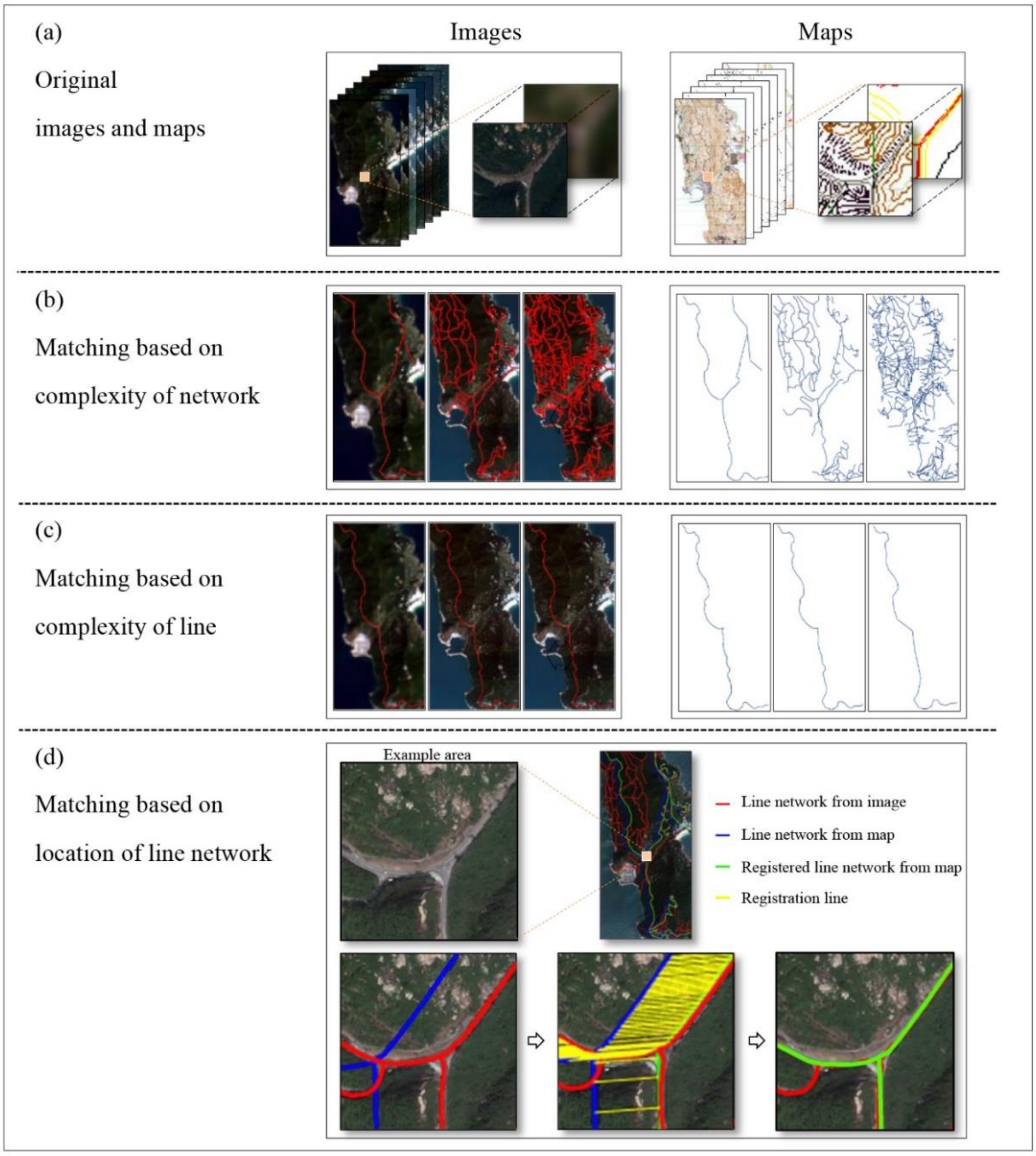

Figure 3.2. Matching of image resolution and map scale based on complexity of line networks, complexity of individual lines, and location of line network.

Matching should consider both the class and feature levels to ensure that all indicators of line networks and individual lines are used in such matching. For complexity indicators $\mathbf{I} = (\mathbf{I}_{\text{class}}, \mathbf{I}_{\text{feature}}) = [(\mathrm{I_L}, \mathrm{I_D}, \mathrm{I_F}), (\mathrm{I_l}, \mathrm{I_s}, \mathrm{I_a}, \mathrm{I_f})]$, the ones used in this study for matching can be divided into three types: $\mathbf{I}_{\text{class}}$ is for the first three indicators of line networks on the class level, $\mathbf{I}_{\text{feature}}$ is for the last four indicators of individual lines on the feature level, and $\mathbf{I}$ includes both levels. Given that the results do not conform to a normal distribution, the Friedman (1937) test is used to analyze the differences among and the effectiveness of the indicators. The Friedman test is a widely used nonparametric statistical test that is similar to classical balanced two-way analysis of variance, but it analyzes the values of ranks by columns.

For indicators collected from images and maps,

$$\{x_{ij}\}_{n,k} = \left| I_{\mathrm{S}} - I_{R_j} \right|_{A_i} \tag{3.1}$$

is a matrix with n rows, k columns, in which n rows (the blocks) mean n different experimental areas and k columns mean the absolute value of the difference between the indicators collected from a specific scale of maps and potential images. Then replace the data with the ranks $\{r_{ij}\}_{n,k}$, where r_{ij} is the rank of x_{ij} within block i. Finally, the rank matrix is used for the significance test. A sufficiently small p value suggests the column is significantly different from the reference column. When the complexity of line network is considered, $\mathbf{I}_{\mathrm{class}} = (\mathrm{I_L}, \mathrm{I_D}, \mathrm{I_F})$ are analyzed in the Friedman test; when the complexity of an individual line is considered, $\mathbf{I}_{\mathrm{feature}} = (\mathrm{I_l}, \mathrm{I_s}, \mathrm{I_a}, \mathrm{I_f})$ are analyzed; and the two levels are considered together.

3.1.2 Matching based on horizontal location of line networks

For the matching between the complexity of lines and networks, the matching of the horizontal location of the line networks from the two sources should also be considered to ensure horizontal accuracy. For this, it is necessary to register the spatial location of both the image and the map. Iterative closest-point (ICP) matching (Arun et al. 1987, Besl and McKay 1992, Zhang 1994, Williams 2000) is used to register the positions of both while using the same coordinates for both.

Numerous studies have been conducted on the registration of image and map; they mainly include two types of considerations: register the map based on image and register the image based on the map. Most studies are from the first aspect (Knoblock et al. 2006, Song et al. 2013), and this research followed. Automated registration of satellite imagery with vector map data is also an important aspect that can be explored (Hild and Fritsch 1998, Wu et al. 2007). Three kinds of feature matching for the conflation of image and map datasets were introduced by Zhang (2013): point-based, line-based, and patch-based matching. Point-based matching focuses on the location of feature points; line-based matching (Walter and Fritsch 1999, Conte et al. 2004) considers geometric, topologic, and semantic characteristics; and patch-based matching emphasizes enclosed meshes or polygons in road segments (Ruiz et al. 2011a, Zhang 2013). Point-based matching is conducted because it is simple and efficient to evaluate the horizontal locations of points from different images and maps. Other (topologic and semantic) characteristics were not considered in this study.

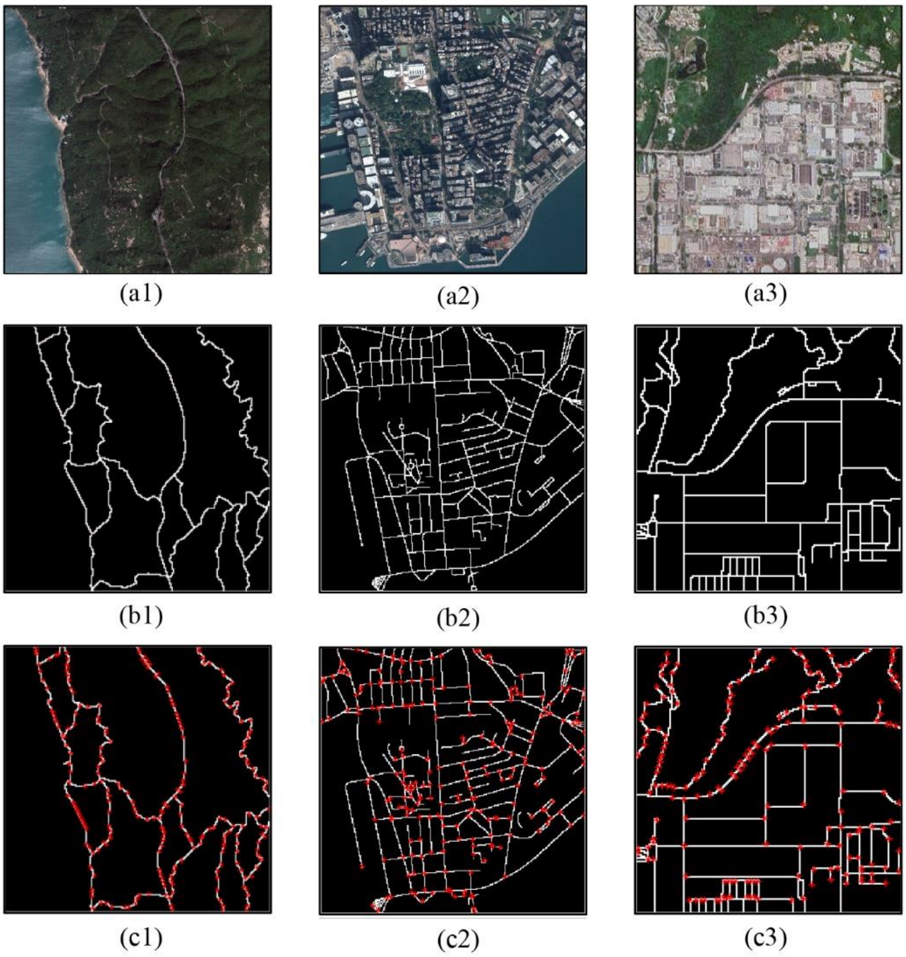

Figure 3.3. Three patterns of line networks: (a1–a3), original images; (b1–b3), line networks from images, and (c1–c3), feature points extracted from line networks.

ICP matching accounts for feature points in the line networks, in which three patterns were discerned (Figure 3.3). In (a1), most of the lines are freeform curves, from which it is difficult to extract feature points; in (a2), most of the lines are incorporate straight-line segments, and intersections can be extracted easily as feature points; and in (a3), the lines are the combination of two patterns. The feature points of line networks are extracted using a Harris corner detector (Harris and Stephens 1988). The number (N) of the corner points to be extracted depends on the line network patterns. More corners are needed for freeform curves than for grid-based networks. The maximum number (N_{max}) can be acquired by increasing the number of corners until the ICP matching errors of remain stable.

The objective function to be minimized in the registration is

$$F(\mathbf{R}, t) = \frac{1}{\sum_{i=1}^{m} p_i} \sum_{i=1}^{m} p_i d^2(\mathbf{R}x_i + \mathbf{t}, S') \tag{3.2}$$

where **R** is the rotation and **t** is the translation, p_i takes a value of 1 if point x_i can be matched to a point on S' and takes a value of 0 otherwise. The distance $d(x, S')$ is that between point x and shape S‘:

$$d(x, S') = \min_{x' \in S'} d(x, x') \tag{3.3}$$

The objective function is

$$D_L = \frac{1}{N} \sum_{i=1}^{N} ||\mathbf{R}x_i + \mathbf{t} - y_i||^2 \tag{3.4}$$

where **R** is the rotation, **t** is the translation, and x_i and y_i are the matching points. The ICP based registration (Zhang 1994) of image and map is summarized as follows:

- Inputs:

Two frames of line networks from images and maps and maximum tolerable distance:

$$D_{max} = \mu + \sigma, \mu = \frac{1}{N} \sum_{i=1}^{N} d_i, \sigma = \sqrt{\frac{1}{N} \sum_{i=1}^{N} (d_i - \mu)^2} \tag{3.5}$$

where *N* is the number of corners.

- Outputs:

Optimal motion between the two frames and final registration error of the two frames.

- Procedures:

(1) Preprocessing: Use Harris corner detector to determine N feature points from line networks. Use k-D tree search to determine closest points. (2) Iterations in ICP matching: Find closest points that satisfy tolerable distance (D_{max}) constraint. Determine points from freeform curves that satisfied orientation constraint. Update recovered matches and update motion calculation. Calculate the registration error for all matched points. End iteration when the absolute values of the last two motions of registration errors are smaller than the threshold. Output final motion and registration error for all matched points. (3) Iterations until convergence: Raise the number of feature points (N). Repeat ICP matching until registration error is smaller than the threshold, when iteration ends.

3.2 Experimental evaluation

3.2.1 Experimental design

In this section, the complexity-based method for matching image resolution and map scale is validated using maps at seven different scales and images at eight different resolutions. Vector data for the map scales (S1–S7: 1:1000; 1:5000; 1:10,000; 1:20,000; 1:50,000; 1:100,000; and 1:200,000) are digital maps from the Surveying and Mapping Office, Hong Kong Special Administrative Region (SMO 2019). The resolutions (R1–R8) of the eight images are 0.3 m, 1 m, 2 m, 4 m, 8 m, 10 m, 15 m, and 30 m, respectively, given by WorldView-4 (Pan-0.3 m, Mul-1.2 m), GaoFen-1 (Pan-1 m, Mul-4 m), GaoFen-2 (Pan-2 m, Mul-8 m), Sentinel-2 (Mul-10 m), and Landsat-8 (Pan-15, Mul-30). All images were obtained after radial and geometric corrections; orthophotos of Hong Kong were used for the 15 experimental areas, each 1 km × 1 km. Images 1–5 (top row in Figure 3.4) are of rural and mostly mountainous areas where most roads are freeform curves along the mountain range; images 6–10 (middle row) are of flat urban areas where most roads are organized as grids; and images 11–15 (bottom row) are of areas with mixed characteristics, where the road network combines both kinds of curves.

Figure 3.4. Fifteen experimental areas in Hong Kong used for testing.

3.2.2 Experimental results and analysis

The pairwise comparison results of the Friedman test using the seven indicators (I_L, I_D, I_F, I_l, I_s, I_a, I_f) in the 15 areas are shown in Figure 3.5. For all eight rows of grids (a–g), black squares (■) indicate the best match of image resolution for a specific map scale; dark-gray squares (■) refer to situations where $p > 0.1$ without being significantly different from the best situation; and white or light-gray squares (□) denote situations in which $p < 0.05$ or $0.05 < p < 0.1$, respectively, with significant differences from the best situation.

The first three rows of grids in Figure 3.5 show results based on the three indicators (I_L, I_D, I_F) for class-level matching, and the last four rows show results based on the four indicators (I_l, I_s, I_a, I_f) for feature-level matching. The first column in Figure 3.5 shows results based on all seven indicators used on all the data (image areas 1–15 in Figure 3.4), and the other three columns show the results of using indicators on data collected from areas 1–5, 6–10, and 11–15, respectively. The indicators (I_L, I_D, I_F) for line network all show the same trends for the best match between image resolution and map scale. However, the trends of indicators (I_l, I_s, I_a, I_f) for individual lines differ. The shape (I_s) and area (I_a) do not show any stable matching trends. Length (I_l) and fractal (I_f) data follow the trends in the rural (1–5) and mixed (11–15) areas but not in the urban (6–10) areas; this is because roads in areas 1–5 and 11–15 are more likely to be freeform curves, whereas those in areas 6–10 are more likely to be straight lines. However, the effectiveness of the indicators can be analyzed by the distribution of dark-gray squares (■) in each row. For the indicator I_L in all 15 areas (Figure 3.5 a), the two dark-gray squares in the first row mean that, based on the length of line networks, there is no significant difference between $\left|I_{S_1} - I_{R_2}\right|_{A_{1-15}}$, $\left|I_{S_1} - I_{R_3}\right|_{A_{1-15}}$ and $\left|I_{S_1} - I_{R_1}\right|_{A_{1-15}}$, where I_{S_1} represents the indicator from the map at the scale of S_1; I_{R_1}, I_{R_2}, and I_{R_3} represent indicators extracted from the images with resolutions R_1, R_2, and R_3; and $A_{1–15}$ means the data were collected from all 15 areas. The first three rows (a–c) in Figure 3.5 show similar matching trends, but the effectiveness of individual indicators for different areas is not reliable. Judging from the trend seen in the last four rows, only length (I_l) and fractal (I_f) data can be considered for matching. According to the pairwise comparison results of the Friedman test for the 15 areas (Figure 3.6), matching based on five indicators (I_L, I_D, I_F, I_l, I_f) from both class and feature levels are more stable and effective.

These results should be validated by ICP matching for the horizontal location of line networks (Table 3.1). The final column shows the corresponding accuracy standards (Class 2 in Table 2.1) for the horizontal positions at the different map scales. For each pair of scale and resolution, two data are given: the first is the mean horizontal accuracy of the 15 areas (upper row) and the second is the ratio of the areas in which the horizontal accuracy satisfies the standard of class 2 (lower row). The grids in which the mean horizontal accuracy or more than half (7/15) of the areas satisfy the standard of class 2 are in gray. The number of feature points for the 15 areas when the ICP iterations converge are 2500, 2500, 5500, 3000, 2500, 4000, 9000, 5500, 8500, 11000, 7000, 6000, 8500, 5000, 5500 in this experiment. It seems that more feature points are required to obtain convergence in flat urban areas (6)–(10). It can be seen from Table 2.2 that for a specific scale of maps, usually the images with higher resolutions will give better horizontal accuracy. The detailed information from high resolutions may also be redundant and interfere with the matching processing. For example, for the Scale S4 (1:20 000, Area 1–5), the best matching is R3 (2 m), the mean horizontal deviation is 6.14 m and all the five areas satisfy the accuracy standard (5/5). When the resolutions of images are higher than 2 m, the redundant feature points from images will lower the accuracy. However, when the resolutions of images are lower than 2 m, the feature points extracted from the images are not sufficient for obtaining the best matching with the road networks. To synthesize the result of the Friedman test for the five indicators and the horizontal standards, the pairs of scale and resolution in bold (Figure 3.1) are the best match.

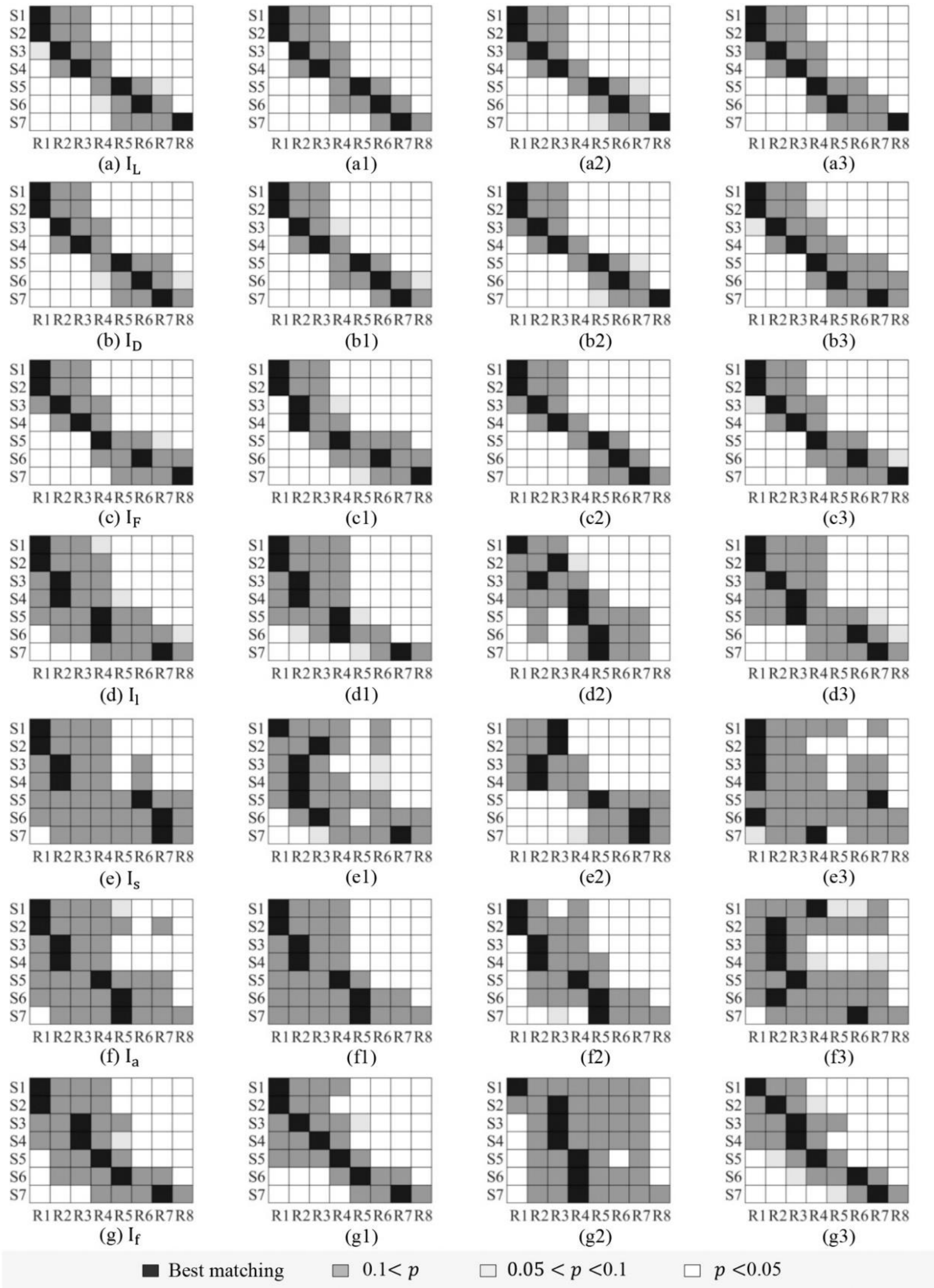

Figure 3.5. Pairwise comparison results of the Friedman test for indicators (I_L, I_D, I_F, I_l, I_s, I_a, I_f) in 15 different areas. First column was calculated from all 15 areas and identifies relevant indicators; the other three columns were calculated from areas 1–5, 6–10, and 11–15, respectively. The first three rows are based on class level, and last four rows are based on feature level.

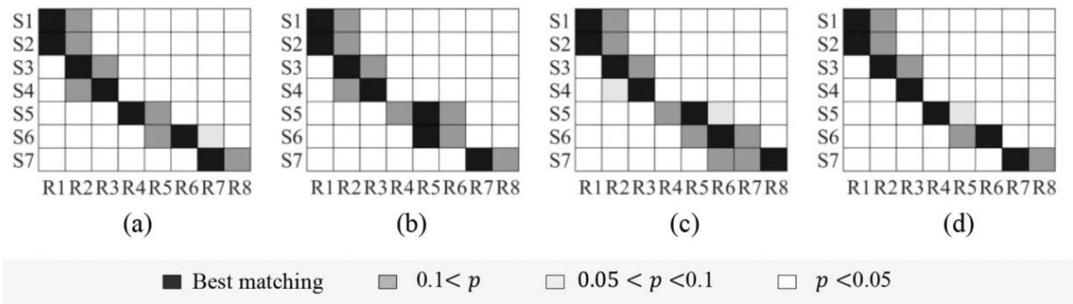

Figure 3.6. Pairwise comparison results of the Friedman test for all five indicators ($\mathbf{I_L}$, $\mathbf{I_D}$, $\mathbf{I_F}$, $\mathbf{I_l}$, $\mathbf{I_f}$), based on both class and feature levels of complexity. Areas: (a) 1–15; (b) 1–5; (c) 6–10; and (d) 11–15.

Based on the previous results, a visual user assessment test was designed via the social media platform (https://www.wjx.cn/) in June 2020. For every road network based on maps, four groups of images at different resolutions were provided for users to choose (shown in Figure 3.7). Twenty-one patches of road networks from the 15 areas shown in Figure 3.4 were chosen for this questionnaire. A total of 100 participants were recruited online randomly from over 15 areas in China, including Hong Kong, Hubei, Beijing, and Guangdong, and 65 effective answer sheets were collected after excluding the completion time is less than 1 min. Among the 65 participants, there were 35 males and 30 females aged from 22 to 35 years. Twenty-three of the participants had a background in geoscience. The participants were unpaid, but their internet access costs were covered for their online participations.

Figure 3.7. Example of multiple choices in the questionnaire.

Table 3.1. Horizontal location of line networks matching and corresponding to ASPRS (2014) positional-accuracy standards.

Scale	**Area**	**Resolution (m) & Horizontal location accuracy (m)**								**Standard Class 2 (m)**
		R1	R2	R3	R4	R5	R6	R7	R8	
		0.3	1.2	2	4	8	10	15	30	
S1 1:1 000	1–5	**3.57** **0/5**	32.57 0/5	45.50 0/5	120.42 0/5	134.49 0/5	128.43 0/5	155.88 0/5	188.73 0/5	**0.71**
	6–10	**8.46** **0/5**	14.19 0/5	18.11 0/5	30.41 0/5	48.78 0/5	57.86 0/5	85.36 0/5	142.81 0/5	
	11–15	**13.09** **0/5**	18.61 0/5	25.32 0/5	69.73 0/5	68.02 0/5	81.38 0/5	133.14 0/5	199.88 0/5	
S2 1:5 000	1–5	**2.39** **4/5**	32.31 0/5	41.96 0/5	121.50 0/5	135.43 0/5	142.19 0/5	156.20 0/5	185.57 0/5	**3.54**
	6–10	**1.22** **5/5**	6.06 3/5	15.12 0/5	26.33 0/5	37.68 0/5	54.60 0/5	75.75 0/5	147.61 0/5	
	11–15	**15.90** **4/5**	8.67 2/5	33.79 0/5	76.35 0/5	88.48 0/5	79.55 0/5	133.69 0/5	209.39 0/5	
S3 1:10 000	1–5	14.15 3/5	**10.86** **4/5**	11.27 2/5	99.19 0/5	109.85 0/5	103.74 0/5	138.92 0/5	171.04 0/5	**7.07**
	6–10	8.15 4/5	**6.03** **4/5**	11.04 2/5	23.99 0/5	43.79 0/5	54.47 0/5	87.47 0/5	142.14 0/5	
	11–15	16.90 2/5	**5.51** **4/5**	26.02 1/5	69.81 0/5	84.83 0/5	84.72 0/5	134.24 0/5	193.04 0/5	
S4 1:20 000	1–5	9.79 4/5	9.90 4/5	**6.14** **5/5**	91.52 0/5	89.62 0/5	96.80 0/5	119.34 0/5	139.78 0/5	**14.14**
	6–10	8.36 4/5	5.89 4/5	**1.97** **5/5**	22.32 1/5	37.30 0/5	50.44 0/5	67.83 0/5	134.76 0/5	
	11–15	17.90 2/5	6.70 4/5	**11.81** **4/5**	44.22 0/5	65.03 0/5	80.72 0/5	125.54 0/5	192.78 0/5	
S5 1:50 000	1–5	22.49 4/5	14.17 5/5	15.91 5/5	47.98 3/5	**24.30** **4/5**	29.52 4/5	57.58 2/5	96.32 0/5	**35.36**
	6–10	12.68 5/5	5.39 5/5	13.70 5/5	7.48 5/5	**27.59** **4/5**	46.23 2/5	68.62 0/5	127.11 0/5	
	11–15	21.71 4/5	10.21 5/5	16.88 4/5	**7.01** **5/5**	31.40 4/5	46.76 3/5	90.20 0/5	166.39 0/5	
S6 1:100 000	1–5	22.21 5/5	14.39 5/5	17.04 5/5	43.55 3/5	**25.21** **5/5**	24.65 5/5	54.02 4/5	87.06 2/5	**70.71**
	6–10	15.00 5/5	10.15 5/5	23.01 5/5	17.73 5/5	14.42 5/5	**24.63** **5/5**	41.95 5/5	116.88 0/5	
	11–15	14.62 5/5	18.62 5/5	26.36 5/5	26.49 4/5	28.95 4/5	**33.28** **4/5**	104.05 2/5	172.62 0/5	
S7 1:200 000	1–5	33.15 5/5	20.66 5/5	48.22 5/5	42.28 5/5	21.42 5/5	26.32 5/5	**37.22** **5/5**	50.06 5/5	**141.42**
	6–10	15.60 5/5	15.76 5/5	17.58 5/5	24.49 5/5	26.14 5/5	30.10 5/5	35.30 5/5	**65.15** **5/5**	
	11–15	18.56 5/5	20.89 5/5	20.46 5/5	53.03 5/5	31.50 5/5	38.70 5/5	**30.05** **5/5**	115.28 3/5	

Table 3.2. Results of the questionnaire on visual assessment.

Scale	**Resolution (m)**							
	R1	R2	R3	R4	R5	R6	R7	R8
	0.3	1.2	2	4	8	10	15	30
S1 1:1000	**82.05%**	**77.44%**	21.03%	6.15%	-	-	-	-
S2 1:5000	**88.21%**	**80.51%**	27.18%	7.69%	-	-	-	-
S3 1:10,000	**87.18%**	**75.90%**	51.28%	30.77%	-	-	-	-
S4 1:20,000	**88.72%**	**76.92%**	**73.59%**	18.46%	-	-	-	-
S5 1:50,000	-	-	**82.05%**	**79.49%**	35.13%	9.23%	-	-
S6 1:100,000	-	-	-	**92.31%**	**74.10%**	**64.62%**	7.18%	-
S7 1:200,000	-	-	-	-	**81.03%**	**66.92%**	**62.56%**	7.18%

Table 3.2 gives the percentage of the 65 participants who judged the matching to be acceptable, numbers >60% are shown in bold. The questionnaire is focused on the acceptance of corresponding image resolutions for road networks from different scales of maps. According to Table 3.2, the user's acceptance is decreased when the image resolutions become lower. The users are attempting to find out the roads from images corresponding to the given road networks, so the groups with the highest resolutions get high preference. The abundant information from the background images with higher resolutions may bring inefficiency but not be evaluated in this test; for example, when only the main roads are shown in the road network, but the footpaths can be clearly observed in high-resolution images and may bring inefficiency in the task. In this experiment, the lower limit of the resolutions is the main factor considered. The percentages in bold (>60%) are regarded as the image resolutions that can be accepted by the participants. Compared with results obtained by combining the previous two aspects (the resolution and scale pairs in bold in Table 3.1), the user study shows approximately the same trends. For scale S3, S4, S6, S7, the accepted image resolutions are the same as those in the previous study, and for scale S1, S2, S5, the users are more tolerant to the resolutions. More visual experiments can be conducted to study the cognition process, for example, using eye tracking technologies to

evaluate the effectiveness and efficiency of visual tasks conducted with images having different resolutions (Dong et al. 2014, Duchowski 2017).

3.3 Summary

The above-mentioned validation of the matching between image resolution and map scale took the complexity indicators and the horizontal-accuracy standards into consideration and was realized through visual assessment. Two levels of complexities for line features were considered for the matching: class level (complexity of line network) and feature level (complexity of individual lines). The horizontal location of line networks from images and maps were matched using the ICP method. A user visual assessment was conducted to acquire the participants' acceptance of image resolutions. The results showed approximately the same trends as those obtained using the previous two aspects but slightly more tolerance to the image resolutions. The strategy has been evaluated using actual experimental data in the form of vector maps at seven scales and raster images at eight resolutions. The complexity-based method can determine the best matching between image resolution and map scale, which can satisfy the horizontal accuracy standard of map production and evaluate by visual assessments. Complexity-based matching's consideration of LoD differences from multiscale representation in image-map generation can improve the final match between image resolution and map scale.

Chapter 4 Effects of background image transparency on the usability of image-maps

In chapter 3, a complexity-based matching between image resolution and map scale has been developed for multi-scale image-map generation. In this chapter, the effect of generalization of the background image, changing the characteristic, i.e., transparency, on the usability of image-map is explored.

4.1 Strategy for exploring the effects of background image transparency

For images with different landscape features, the optimum transparency level to obtain the highest degree of usability varies depending on the complexity of background images. On the other hand, the usability of image-maps with similar transparency levels may also differ as a result of the complexity of background images. When the transparency changes, landscape features in the background images may fade. Other properties, such as contrast and complexity, are also influenced by the transparency of the background image. The effects of transparency, contrast, and complexity will therefore be considered in the exploration of their effects on usability. Two hypotheses are made:

- Firstly, for the same image-map with different levels of background transparency, usability should increase and then decrease when either the transparency or contrast rises. A peak value of usability should exist for a series of image-maps with different background image transparency levels (Figure 4.1-a).
- Secondly, for different image-maps, the optimum background transparency level, at which the peak value of usability exists, should vary with the contrast and complexity of background images (Figure 4.1-b). The optimum background transparency level is related to the contrast and complexity of background image.

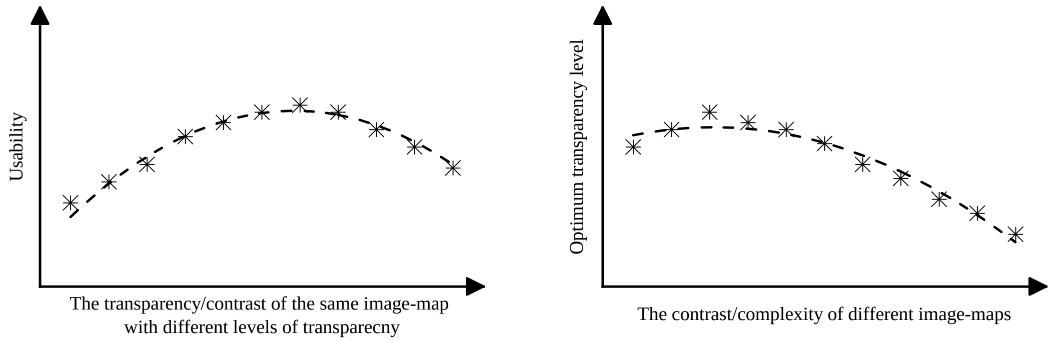

(a) The relationship between usability and transparency/contrast

(b) The relationship between optimum transparency level and contrast/complexity

Figure 4.1. Virtual visualization of the two hypotheses raised in this paper.

To verify these hypotheses, an experiment was carried out through surveys using online questionnaires. Testing data were selected to include different landscapes and scales, and different levels of transparency were applied to the chosen image-maps. Features such as annotations and lines were also uploaded onto the image-maps. The usability of image-maps was evaluated by user study in terms of two aspects, satisfaction and effectiveness (ISO 2018). The framework of the experimental evaluation is shown in Figure 4.2.

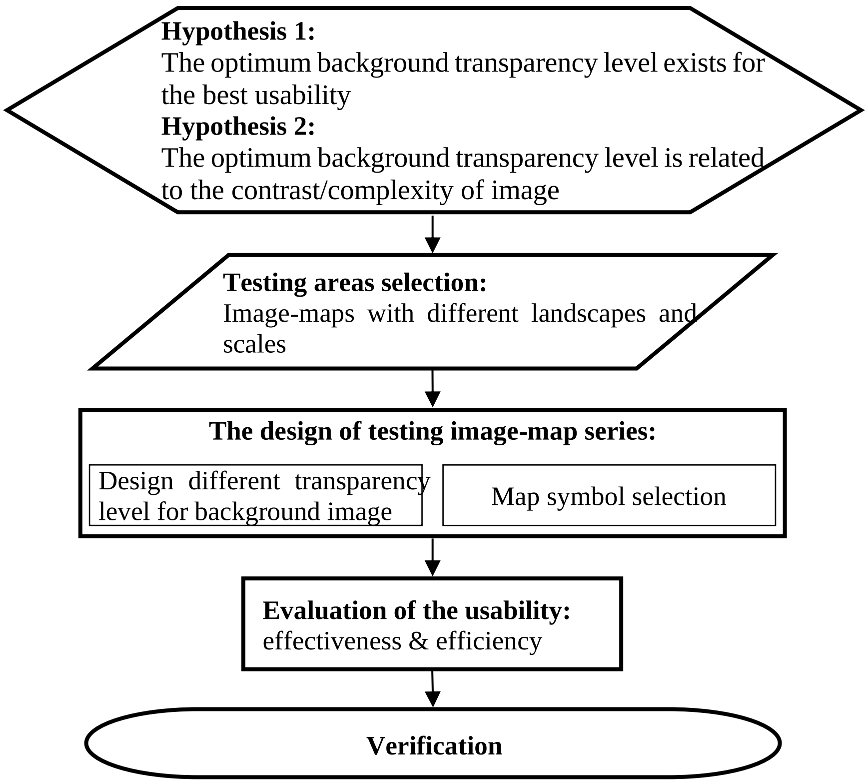

Figure 4.2. The framework of the experimental evaluation.

The measuring of transparency/contrast and selection of indicator for complexity will be introduced in the following paragraphs.

Eleven transparency levels were used in this study, i.e., 0% to 100% at intervals of 10%, as shown in Figure 4.3. The 0% level refers to the original condition of the background image whereas the 100% levels indicates that the image has completely faded away, i.e., only graphic map remained.

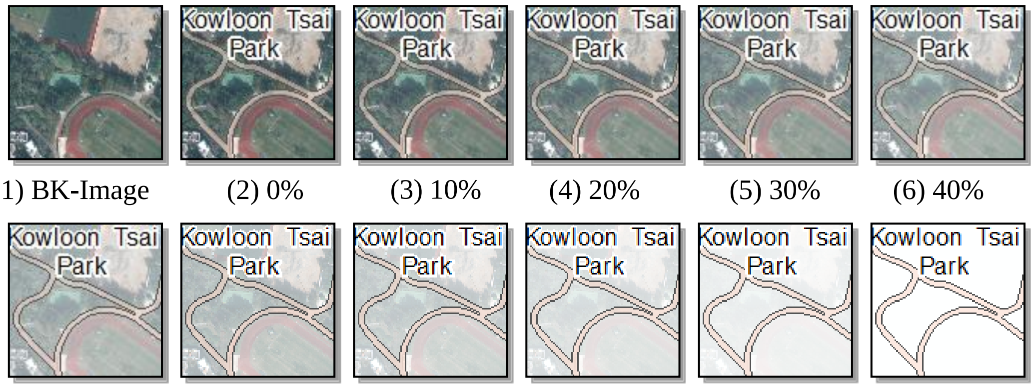

(1) BK-Image (2) 0% (3) 10% (4) 20% (5) 30% (6) 40%

(7) 50% (8) 60% (9) 70% (10) 80% (11) 90% (12) 100%

Figure 4.3. Original image and ten levels of transparency for the background image.

Contrast is another important characteristic of image-maps, and is strongly related to their usability. It affects both the amount of details visible and their clarity for interpretation (Fleming 1973). Contrast enhancement is conducted during the production of image-maps for numerous applications (Albertz and Tauch 1994, Murphy 2014, Welch 1972). The contrast values of image-maps are calculated according to the method introduced by Gonzalez and Woods (2002). Let z_i, $i = 0,1,2,\cdots,L-1$, denote the values of all possible intensities in an $M \times N$ digital data. The probability $p(z_k)$ of intensity level z_k occurring in a given image is thus estimated as follows:

$$p(z_k) = {}^{n_k}/_{MN} \tag{4.1}$$

where n_k is the number of times that a specific intensity occurs in the image and MN is the total number of pixels. Thus $\sum_{k=0}^{L-1} p(z_k) = 1$. The mean (average) intensity is given by

$$m = \sum_{k=0}^{L-1} z_k p(z_k) \tag{4.2}$$

And the contrast value (variance of the intensities) is as follows:

$$Contrast\ value = \sqrt{\sum_{k=0}^{L-1}(z_k - m)^2 p(z_k)} \tag{4.3}$$

Boltzmann Entropy, introduced in section 2.3.2, is employed to measure the complexity of final image-map outputs in raster format, which combine different background images (raster) and scales of maps (vector).

4.2 Experimental evaluation

4.2.1 Design of image-map series for the questionnaire

Experimental data sets included satellite images and maps from nine areas in Hong Kong (Figure 4.4). The resolutions of these images were 2 m (A–C, top row left in, Figure 4.4), 1 m (D–F, middle row left, and 0.5 m (G–I, bottom row left), i.e., the corresponding map scales are 1:20 000, 1:10 000, and 1:5 000. These areas in these image-maps show two main kinds of landscapes features: natural (mountains, plain, water bodies, etc.) and cultural (buildings, roads, parks, etc.).

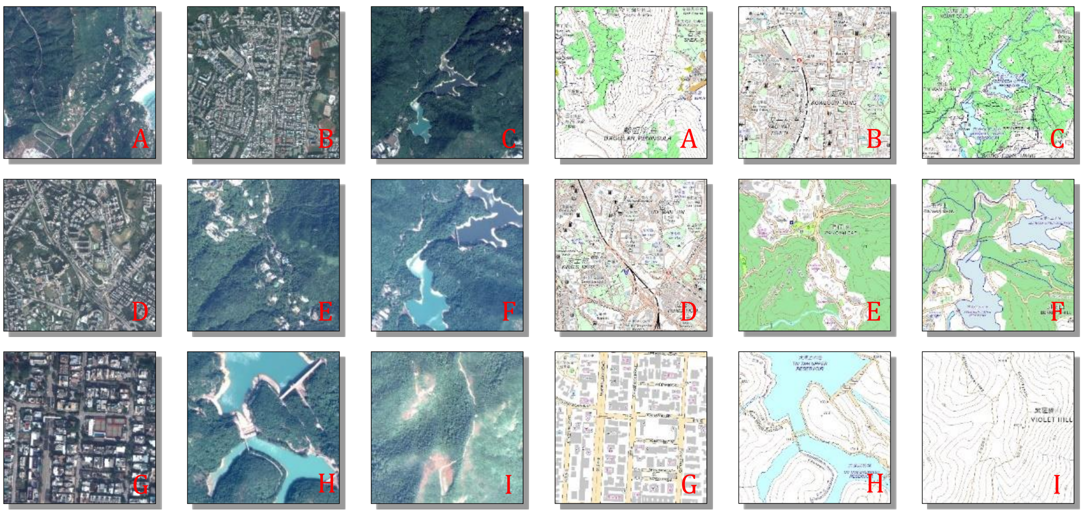

Figure 4.4. Images (A~I, left) and maps (A~I, right) of the nine testing areas for the study.

The design of image-maps for study considers two main variables: the features to be uploaded onto images and the transparency level of background images. Figure 4.5 shows an example of this design flow using the image-map of area A. At the first step, only the map annotations are uploaded onto the images, after which eleven transparency levels are generated ($A_{1,1}, A_{1,2}, \ldots, A_{1,11}$). Image-maps with uploaded annotations and line features (e.g., roads, contours, streams), and further image-maps ($A_{2,1}, A_{2,2}, \ldots, A_{2,11}$) with eleven transparency levels, are then generated. Annotations are in white with a black border while line features are in their original colors. For the other eight areas in the chosen dataset (B–I in Figure 4.4), the design and serial numbers are the same as in image-map A. The image-maps generated were 800×800 pixels and all designs were created and implemented using Esri ArcMap 10.2 software.

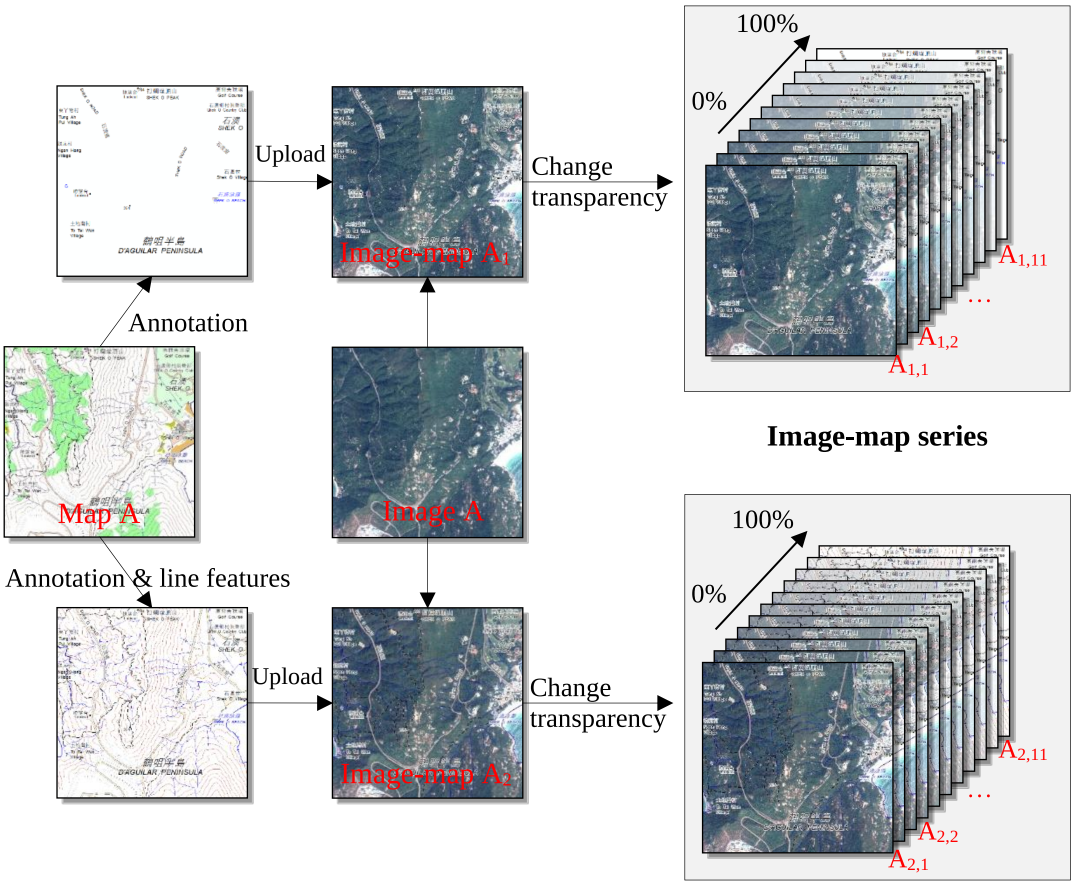

Figure 4.5. Example image-map (using image-map A) showing the design of image-map series based on the map features uploaded and the transparency level of the background images.

4.2.2 Design of image-map permutations and questionnaire

Permutations of the series of image-maps used are shown in Table 4.1, and include eleven groups of tests for one series of image-maps. For image-maps A_1–I_1, eleven groups of questionnaires were conducted using image-maps with different transparency levels arranged in a disordered manner. Another eleven groups were conducted for image-maps A_2–I_2. The user randomly chose the group of questionnaires.

Table 4.1. Image-map permutations ($A_{i,j}{\sim}I_{i,j}$, $i \in (1,2), j \in (1,2,\ldots,11)$) of the two design series for image-map A~I prepared for user study. $A_{1,j}{\sim}I_{1,j}$, $j \in (1,2,\ldots,11)$ refers to image-maps with only their annotations uploaded; $A_{2,j}{\sim}I_{2,j}$, $j \in (1,2,\ldots,11)$ refer to image-maps with both annotations and line features uploaded.

Groups	**Questions**								
	1	**2**	**3**	**4**	**5**	**6**	**7**	**8**	**9**
G1	$A_{i,1}$	$B_{i,2}$	$C_{i,3}$	$D_{i,4}$	$E_{i,5}$	$F_{i,6}$	$G_{i,7}$	$H_{i,8}$	$I_{i,9}$
G2	$A_{i,2}$	$B_{i,3}$	$C_{i,4}$	$D_{i,5}$	$E_{i,6}$	$F_{i,7}$	$G_{i,8}$	$H_{i,9}$	$I_{i,10}$
G3	$A_{i,3}$	$B_{i,4}$	$C_{i,5}$	$D_{i,6}$	$E_{i,7}$	$F_{i,8}$	$G_{i,9}$	$H_{i,10}$	$I_{i,11}$
G4	$A_{i,4}$	$B_{i,5}$	$C_{i,6}$	$D_{i,7}$	$E_{i,8}$	$F_{i,9}$	$G_{i,10}$	$H_{i,11}$	$I_{i,1}$
G5	$A_{i,5}$	$B_{i,6}$	$C_{i,7}$	$D_{i,8}$	$E_{i,9}$	$F_{i,10}$	$G_{i,11}$	$H_{i,1}$	$I_{i,2}$
G6	$A_{i,6}$	$B_{i,7}$	$C_{i,8}$	$D_{i,9}$	$E_{i,10}$	$F_{i,11}$	$G_{i,1}$	$H_{i,2}$	$I_{i,3}$
G7	$A_{i,7}$	$B_{i,8}$	$C_{i,9}$	$D_{i,10}$	$E_{i,11}$	$F_{i,1}$	$G_{i,2}$	$H_{i,3}$	$I_{i,4}$
G8	$A_{i,8}$	$B_{i,9}$	$C_{i,10}$	$D_{i,11}$	$E_{i,1}$	$F_{i,2}$	$G_{i,3}$	$H_{i,4}$	$I_{i,5}$
G9	$A_{i,9}$	$B_{i,10}$	$C_{i,11}$	$D_{i,1}$	$E_{i,2}$	$F_{i,3}$	$G_{i,4}$	$H_{i,5}$	$I_{i,6}$
G10	$A_{i,10}$	$B_{i,11}$	$C_{i,1}$	$D_{i,2}$	$E_{i,3}$	$F_{i,4}$	$G_{i,5}$	$H_{i,6}$	$I_{i,7}$
G11	$A_{i,11}$	$B_{i,1}$	$C_{i,2}$	$D_{i,3}$	$E_{i,4}$	$F_{i,5}$	$G_{i,6}$	$H_{i,7}$	$I_{i,8}$

For each group, nine questions were asked based on the main landscape features in the area (Table 4.2); the efficiency scores of obtaining the answer to the corresponding question were collected. Ground features relevant to the questions were divided into five groups: direction of stream flow (A & F), direction of sites (B & E), point elevation (C & I), roads (D & G), and facility symbols (H).

The effectiveness and efficiency of the image-maps were evaluated according to the ISO 9241-11 standard, wherein effectiveness is defined as the accuracy and completeness with which users achieve specified goals, and efficiency as the resources used in relation to the results achieved; such resources include time, human effort, money, and materials (ISO 2018). These criteria are widely used in map evaluation (Harrie and Stigmar 2010, Leung and Li 2002, Liao et al. 2018, Raposo and Brewer 2014, Schnur et al. 2018, Stigmar and Harrie 2011). To assess the fulfillment of each criterion, the percentage of correct answers (correctness) is employed as the criteria of effectiveness and the difficulty noted by subjects is used to evaluate efficiency.

Efficiency scores ranged from 1 to 5, where higher scores indicated high efficiency. The usability of an image-map is evaluated by combining these two indicators.

$$\text{Effectiveness:} \qquad \text{Correctness} = \frac{\text{The number of the correct answers}}{\text{The number of the whole answers}} \tag{4.4}$$

$$\text{Efficiency:} \qquad \text{Difficulty} = \frac{\sum \text{Difficulty score}}{\text{The number of the whole answers}} \tag{4.5}$$

$$\text{Usability:} \qquad \text{Correctness \& Difficulty} = \text{Correctness} \times \text{Difficulty} \tag{4.6}$$

Table 4.2. Tasks designed for the evaluation and corresponding landscape feature considered.

Area	Questions for subjects	Correct answers	Landscape features
A	Which is the correct direction of stream flow between A and B? (From A to B/From B to A)	From A to B	Natural
B	What is the direction of Kowloon Tsai Park towards City University of Hong Kong? (East/North-east/North/North-west/West/South-west/South/South-east)	South-east	Anthropogenic
C	Which point is higher? (Point A/Point B)	Point B	Natural
D	Which road does not appear in this area? (Waterloo Road/Chatham Road North/Gascoigne Road/Wuhu Street)	Wuhu Street	Anthropogenic
E	What is the correct direction from Carolina Gardens towards the Police Museum? (East/North-east/North/North-west/West/South-west/South/South-east)	South-west	Anthropogenic
F	Which is the correct direction of flow of stream between A and B? (From A to B/From B to A)	From A to B	Natural
G	Which road does not appear in this area? (Waterloo Road/Cambridge Road/Moray Road/Lancashire Road)	Lancashire Road	Anthropogenic
H	How many declared monuments (✾) are present in this area? (4/5/6/7)	7	Anthropogenic
I	Which point is higher? (Point A/Point B)	Point B	Natural

4.2.3 Study participants

Participants were recruited via advertisements in geo-informatics lectures (at Southwest Jiaotong University, China) and social media networks (https://www.wjx.cn/vj/txPrGeA.aspx) in December 2019, June 2020 and March 2021. A total of 1,263 participated in the experiment. Answer sheets were excluded if the completion time was less than 2 minutes, or if the correctness was less than 4/9. 1092 answer sheets were valid for final considerations, including 513 females and 579 males, of whom 371 had backgrounds in the geosciences (supposed to have prior experience of using maps) and 721 did not, representing more than 30 districts in China, aging from 18 to 35. Participants were randomly divided into 22 groups, each of which contained more than 25 members. They were informed on the intention of the questionnaire before starting, i.e., "to explore the effects of background image transparency on the usability of image-maps".

4.3 Usability of image-map with different image transparency levels

4.3.1 Analysis of relationships between the usability of image-maps and the transparency and contrast of the background image

The experimental results of the effectiveness and efficiency based on the indicators of correctness and difficulty of the two series of image-maps $A_{i,j} \sim I_{i,j}$, $i \in (1,2), j \in (1,2,\ldots,11)$ are listed in Table 4.3 and Table 4.4. In Figure 4.6 and Figure 4.7, lines with circles (, red) represent the effectiveness (with a background in Geoscience light red, without a background in Geoscience , light red) whereas lines with stars (, blue) indicate the corresponding efficiency (with a background in Geoscience light blue, without a background in Geoscience , light blue).

Table 4.5 and Figure 4.8 show usability, determined combining the above two aspects as a comprehensive representation. Image-maps with annotations $A_{1,j} \sim I_{1,j}, j \in (1,2,\ldots,11)$ are represented as red lines with diamonds (), whereas image-maps with annotations and line features $A_{2,j} \sim I_{2,j}, j \in (1,2,\ldots,11)$ are shown as blue lines with squares (). The light red/blue line with triangles/inverted triangle indicate the participants with/without geoscience background for the two series of image-maps. The peak data for all eleven transparency levels are in solid red/blue; these peaks appear at different transparency levels for each image-map.

A significance test was conducted on the usability of image-maps with different transparency levels. The null hypothesis is that no significant difference exists between the eleven levels of transparency in image-maps $A_{i,j} \sim I_{i,j}$, $i \in (1,2), j \in (1,2,\ldots,11)$. To test this hypothesis, a one-way analysis of variance test (one-way ANOVA) was conducted. All p-values were smaller than 0.05, demonstrating that the null hypothesis is rejected at 95% confidence. In other words, the usability of an image-map varies significantly depending on the inline level.

Table 4.3. Correctness of two series of image-maps $A_{i,j}{\sim}I_{i,j}$, $i \in (1,2), j \in (1,2,\dots,11)$.

Correctness		**Transparency level (%)**										
		0	**10**	**20**	**30**	**40**	**50**	**60**	**70**	**80**	**90**	**100**
Series 1: image-maps with annotations	A_1	0.21	0.24	0.23	0.24	0.31	0.45	0.47	0.45	0.41	0.38	0.32
	B_1	0.94	0.83	0.82	0.85	0.85	0.88	0.86	0.86	0.95	0.88	0.92
	C_1	0.65	0.83	0.86	0.76	0.83	0.76	0.81	0.75	0.65	0.62	0.60
	D_1	0.80	0.86	0.88	0.83	0.87	0.87	0.96	0.97	0.96	0.92	0.96
	E_1	0.94	0.90	0.95	0.94	0.90	0.96	0.88	0.96	0.91	0.95	0.89
	F_1	0.69	0.77	0.80	0.80	0.81	0.68	0.80	0.86	0.85	0.85	0.85
	G_1	0.90	0.92	0.80	0.80	0.88	0.85	0.88	0.88	0.88	0.96	0.96
	H_1	0.56	0.78	0.77	0.89	0.89	0.95	0.84	0.88	0.96	0.92	0.90
	I_1	0.38	0.46	0.52	0.61	0.49	0.53	0.62	0.76	0.59	0.53	0.50
Series 2: image-maps with annotations and line features	A_2	0.51	0.53	0.55	0.55	0.67	0.62	0.62	0.64	0.75	0.73	0.70
	B_2	0.91	0.93	1.00	1.00	0.92	0.91	0.95	0.93	0.86	0.77	0.85
	C_2	0.82	0.89	0.87	0.83	0.86	0.90	0.93	0.94	0.86	0.85	0.82
	D_2	0.79	0.78	0.81	0.83	0.85	0.82	0.88	0.94	0.94	0.88	0.82
	E2	0.74	0.83	0.85	0.86	0.83	0.88	0.86	0.88	0.81	0.89	0.80
	F_2	0.77	0.75	0.73	0.82	0.81	0.81	0.87	0.84	0.86	0.90	0.85
	G_2	0.82	0.88	0.90	0.85	0.85	0.88	0.95	0.87	0.86	0.87	0.94
	H_2	0.62	0.75	0.78	0.70	0.81	0.66	0.76	0.87	0.81	0.82	0.71
	I_2	0.58	0.70	0.75	0.84	0.83	0.87	0.92	0.93	0.87	0.82	0.82

The trends of effectiveness, efficiency and satisfaction for the two series of image-maps from participants with different backgrounds (with/without geoscience background) are quite different. For the first series of image-maps, just annotations and no line features uploaded, the scores from participants with different backgrounds have approximately the same trends. The geosciences background didn't show any advantages in the tasks. And for the second series of image-maps, with annotations and line features uploaded, the scores for different backgrounds were quite different for tasks A2, C2, F2 and I2, which line features (e.g., contours) can be used to assist the tasks. The participants with geoscience background were more familiar with image-maps with distinguished line features and higher transparency level (approach 100%). On the contrary, participants without geoscience background did not prefer that kind of image-maps. As shown in Figure 4.8, most usability indicators from participants with geoscience background in the second series (—△—) for tasks A2, C2, F2 and I2, are greater than those in the first series (—△—). This is because these four areas mainly comprise natural landscapes and thus use questions about the height of two points or stream flow direction. Although information from images can enable such interpretation, line features (contours) are very helpful in their determination, especially for skilled map users. For the other five areas B, D, E, G and H, the first series generally has higher usability. The two classes of participants shown no big difference between these tasks. In these five areas, the questions involved finding the names of places or roads, or identifying symbols. Such tasks require less information from the whole image-map, but necessitate that local information around the targets make sense. Participants need to quickly locate targets from the whole image-map. In these cases, line features (contours and roads) are redundant information and increase the complexity of the image-map.

The evaluation of contrast and usability was also conducted, the results of which are shown in Figure 4.9 and Figure 4.10. In the first series of image-maps (with annotations uploaded), some situations $(\mathrm{A_1, D_1, F_1, H_1, I_1})$ denote slightly decreasing usability when the contrast is increased. In the second series (with annotations and line features uploaded), relatively few series $(\mathrm{D_2, F_2, H_2, I_2})$ show the same trends. In almost all situations, the usability indicator does not show similar trends as contrast increases.

Table 4.4. Efficiency of the two image-map series $A_{i,j}$~$I_{i,j}$, $i \in (1,2), j \in (1,2,\ldots,11)$.

Efficiency		**Transparency level (%)**										
		0	10	20	30	40	50	60	70	80	90	100
Series 1: image-maps with annotations	A_1	3.51	3.57	3.51	3.83	3.88	3.29	3.34	3.33	3.23	3.30	3.20
	B_1	4.77	4.53	4.80	4.58	4.64	4.85	4.52	4.55	4.57	4.59	4.63
	C_1	3.67	3.82	3.36	3.38	3.81	3.66	3.67	3.66	3.49	4.08	3.87
	D_1	4.43	4.52	4.48	3.95	4.46	4.27	4.30	4.63	4.56	4.49	4.48
	E_1	4.62	4.67	4.68	4.69	4.60	4.57	4.70	4.62	4.68	4.57	4.56
	F_1	3.77	3.84	3.76	3.54	3.59	3.55	3.22	3.33	3.67	3.54	3.08
	G_1	4.38	4.37	4.51	4.84	4.78	4.45	4.32	4.65	4.18	4.66	4.34
	H_1	4.36	4.40	4.44	4.66	4.36	4.42	4.59	4.71	4.68	4.62	4.55
	I_1	4.20	4.10	3.21	3.62	3.37	3.79	3.55	3.83	3.74	3.72	3.66
Series 2: image-maps with annotations and line features	A_2	3.24	3.61	3.47	3.76	3.79	3.10	3.70	3.83	3.94	3.94	3.91
	B_2	4.61	4.04	4.37	4.75	4.63	4.19	4.18	4.51	4.28	4.39	4.91
	C_2	3.75	3.75	3.49	3.30	3.49	3.73	3.63	3.61	3.52	3.50	3.48
	D_2	2.88	2.80	3.14	3.10	3.43	3.73	3.39	4.11	4.19	3.83	3.78
	E2	4.33	4.70	4.57	4.42	3.84	4.11	4.46	4.90	4.23	4.27	4.47
	F_2	3.68	3.60	3.70	4.31	4.27	4.18	4.11	4.06	3.96	3.84	3.74
	G_2	4.02	3.91	4.10	3.82	4.09	3.79	4.48	3.69	3.76	3.50	3.26
	H_2	3.17	3.31	3.98	3.61	4.05	3.97	3.79	4.06	4.13	3.89	3.65
	I_2	4.03	3.89	4.03	4.11	3.89	3.50	3.82	3.80	4.24	3.88	4.02

Table 4.5. Usability of the two image-map series $A_{i,j}{\sim}I_{i,j}$, $i \in (1,2), j \in (1,2,\ldots,11)$.

Usability		**Transparency level (%)**										
		0	**10**	**20**	**30**	**40**	**50**	**60**	**70**	**80**	**90**	**100**
Series 1: image-maps with annotations	A_1	0.73	0.86	0.81	0.92	1.21	1.48	1.57	1.51	1.32	1.25	1.03
	B_1	4.48	3.74	3.94	3.89	3.93	4.28	3.88	3.91	4.33	4.03	4.26
	C_1	2.37	3.18	2.90	2.57	3.16	2.79	2.97	2.76	2.27	2.51	2.32
	D_1	3.55	3.86	3.94	3.28	3.86	3.71	4.14	4.47	4.38	4.13	4.31
	E_1	4.36	4.18	4.42	4.39	4.14	4.40	4.15	4.44	4.26	4.34	4.06
	F_1	2.61	2.95	3.01	2.83	2.90	2.40	2.58	2.86	3.13	3.01	2.61
	G_1	3.94	4.00	3.60	3.85	4.21	3.79	3.80	4.09	3.70	4.49	4.17
	H_1	2.43	3.43	3.40	4.13	3.86	4.19	3.87	4.14	4.49	4.26	4.09
	I_1	1.61	1.87	1.67	2.19	1.63	2.01	2.20	2.91	2.21	1.95	1.83
Series 2: image-maps with annotations and line features	A_2	1.67	1.90	1.89	2.07	2.53	1.92	2.28	2.44	2.95	2.87	2.73
	B_2	4.19	3.74	4.37	4.75	4.24	3.82	3.97	4.20	3.70	3.38	4.17
	C_2	3.06	3.34	3.04	2.73	3.00	3.36	3.37	3.39	3.03	2.97	2.85
	D_2	2.27	2.19	2.54	2.56	2.91	3.07	2.97	3.85	3.94	3.39	3.09
	E2	3.22	3.90	3.88	3.79	3.18	3.60	3.86	4.29	3.43	3.80	3.58
	F_2	2.83	2.70	2.70	3.53	3.45	3.37	3.58	3.26	3.20	3.02	2.88
	G_2	3.31	3.42	3.71	3.24	3.46	3.34	4.24	3.21	3.23	3.05	3.07
	H_2	1.95	2.50	3.11	2.54	3.28	2.62	2.88	3.53	3.34	3.20	2.57
	I_2	2.32	2.72	3.00	3.46	3.23	3.03	3.52	3.52	3.69	3.19	3.27

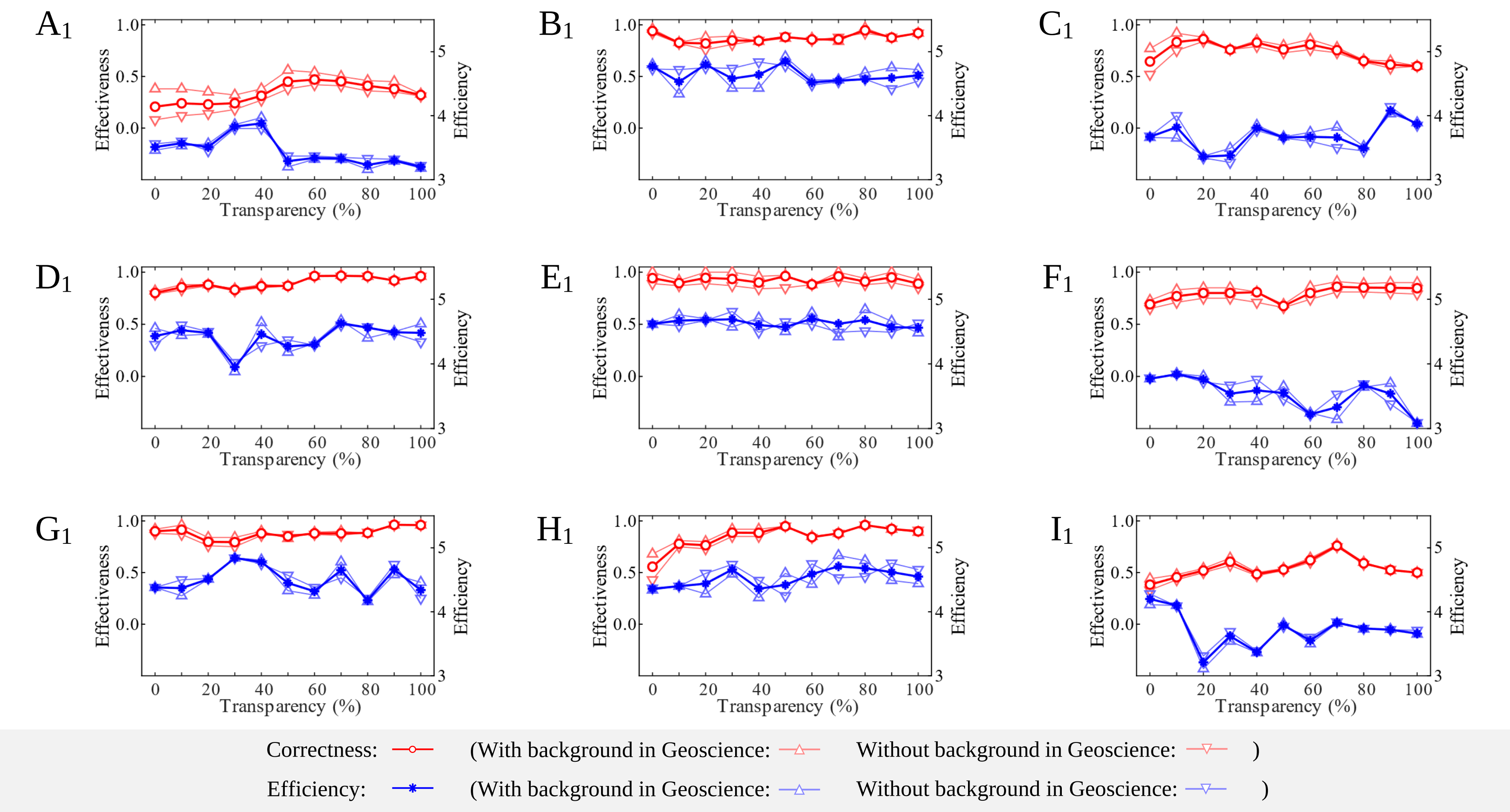

Figure 4.6. Correctness and difficulty for the first series of image-maps $A_{1,j} \sim I_{1,j}, j \in (1,2,\dots,11)$ with annotations uploaded.

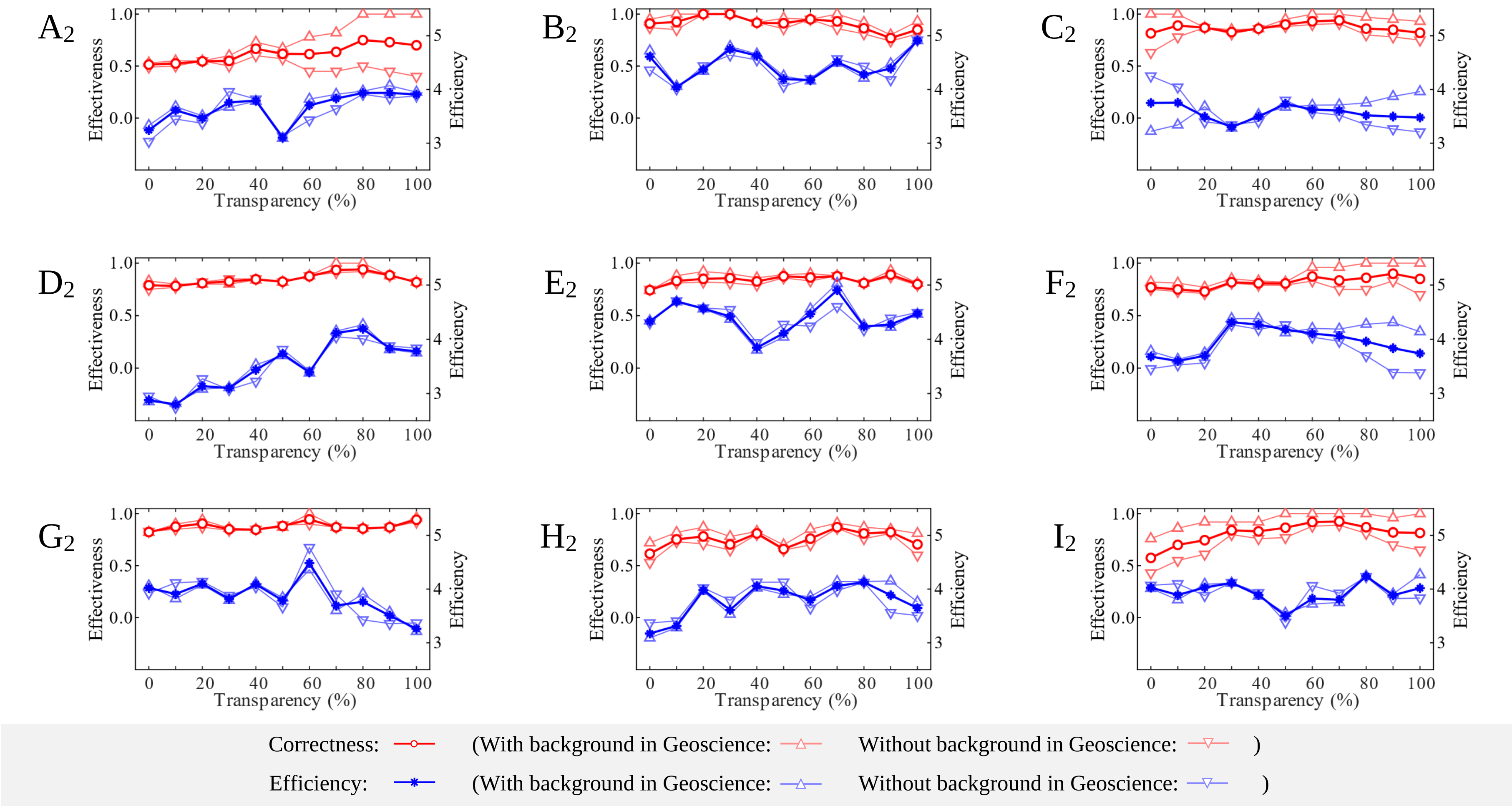

Figure 4.7. Correctness and difficulty for the second series of image-maps $A_{2,j}$~$I_{2,j}, j \in (1,2,\ldots,11)$ with annotations and line features uploaded.

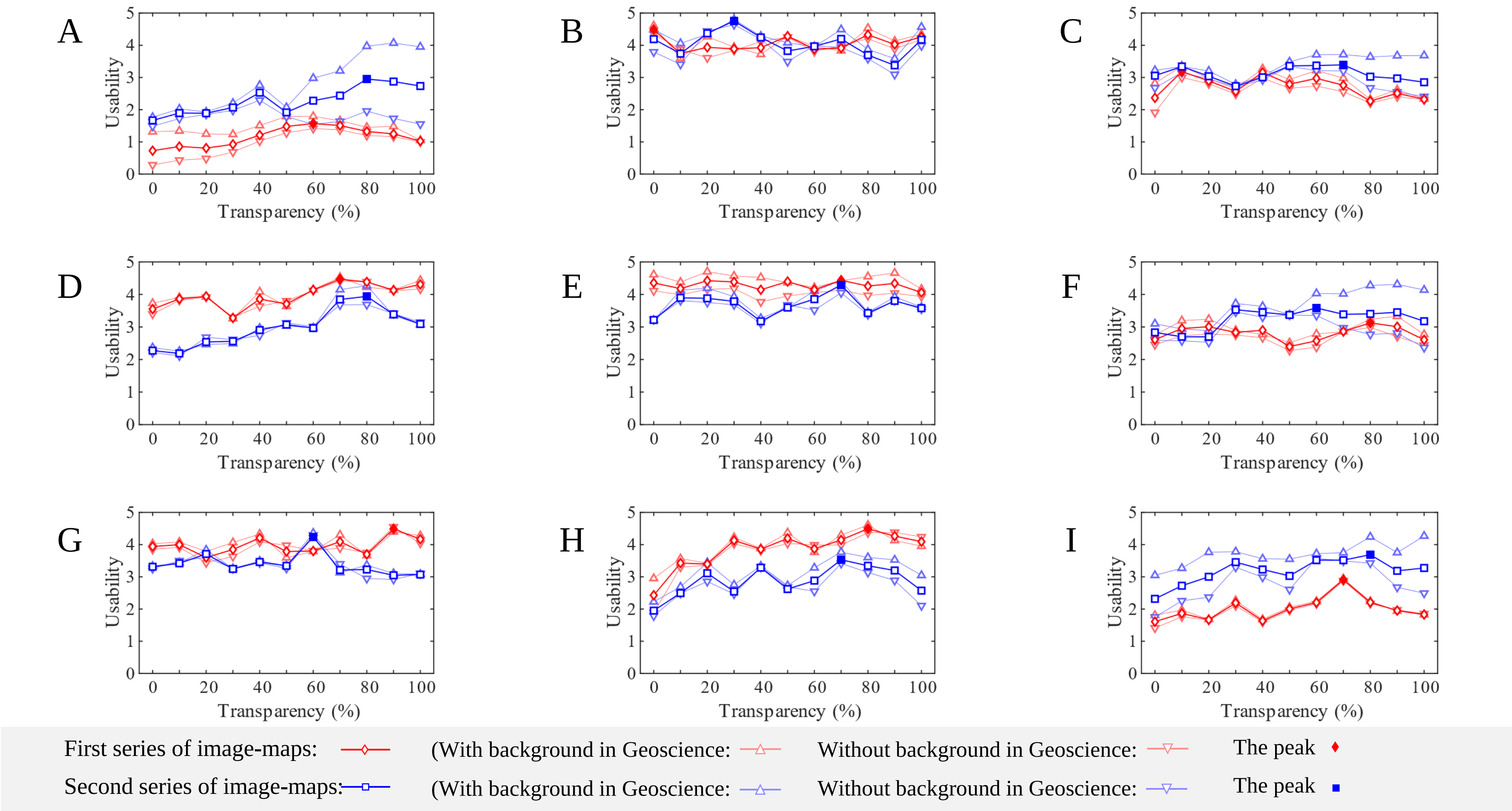

Figure 4.8. Usability of the two image-map series: first, with annotations uploaded, $A_{1,j} \sim I_{1,j}, j \in (1,2,\ldots,11)$; second, with annotations and line features uploaded: $A_{2,j} \sim I_{2,j}, j \in (1,2,\ldots,11)$.

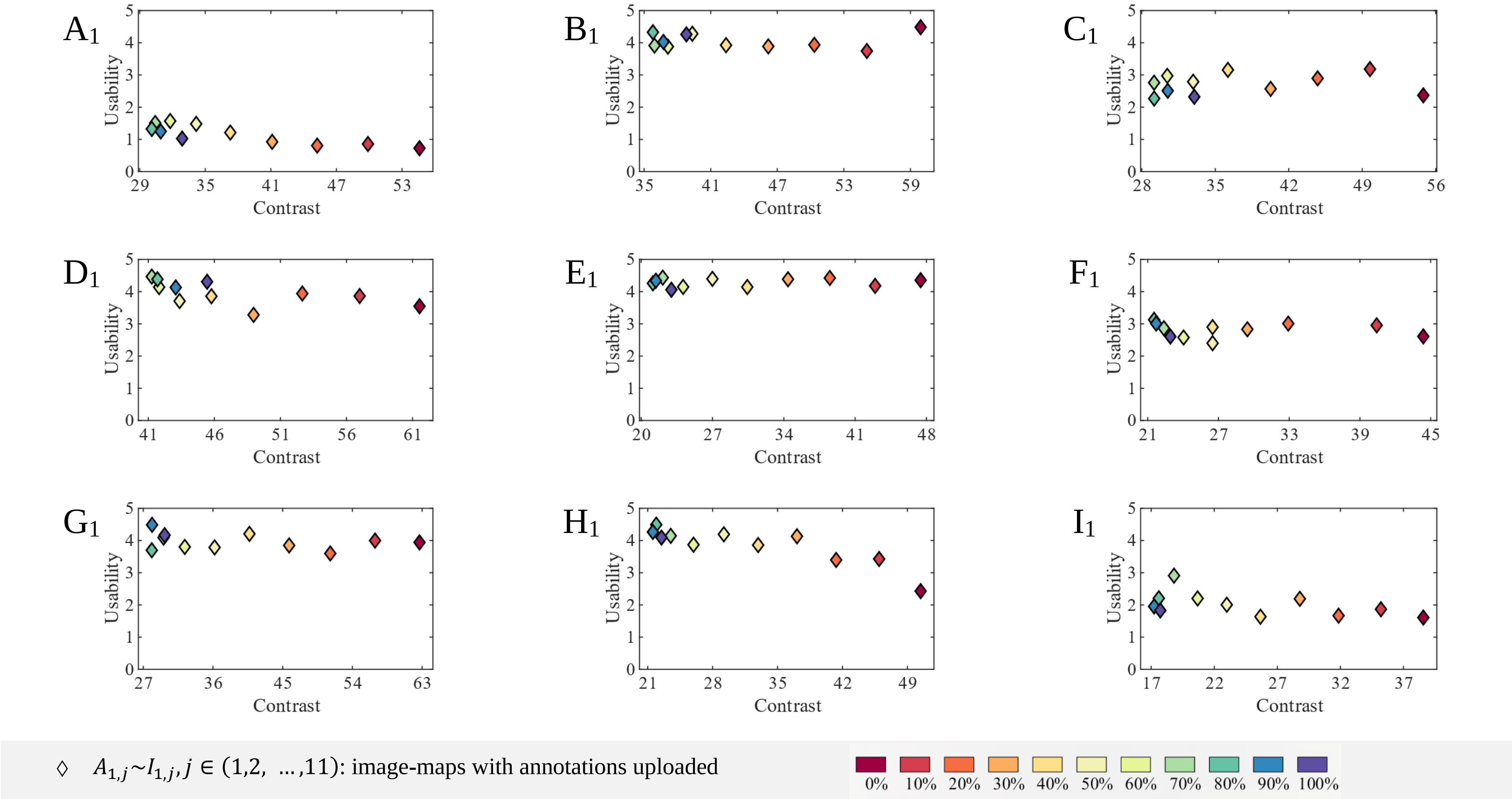

Figure 4.9. Usability and contrast for the first series of image-maps $A_{1,j} \sim I_{1,j}, j \in (1,2, \ldots, 11)$ with annotations uploaded.

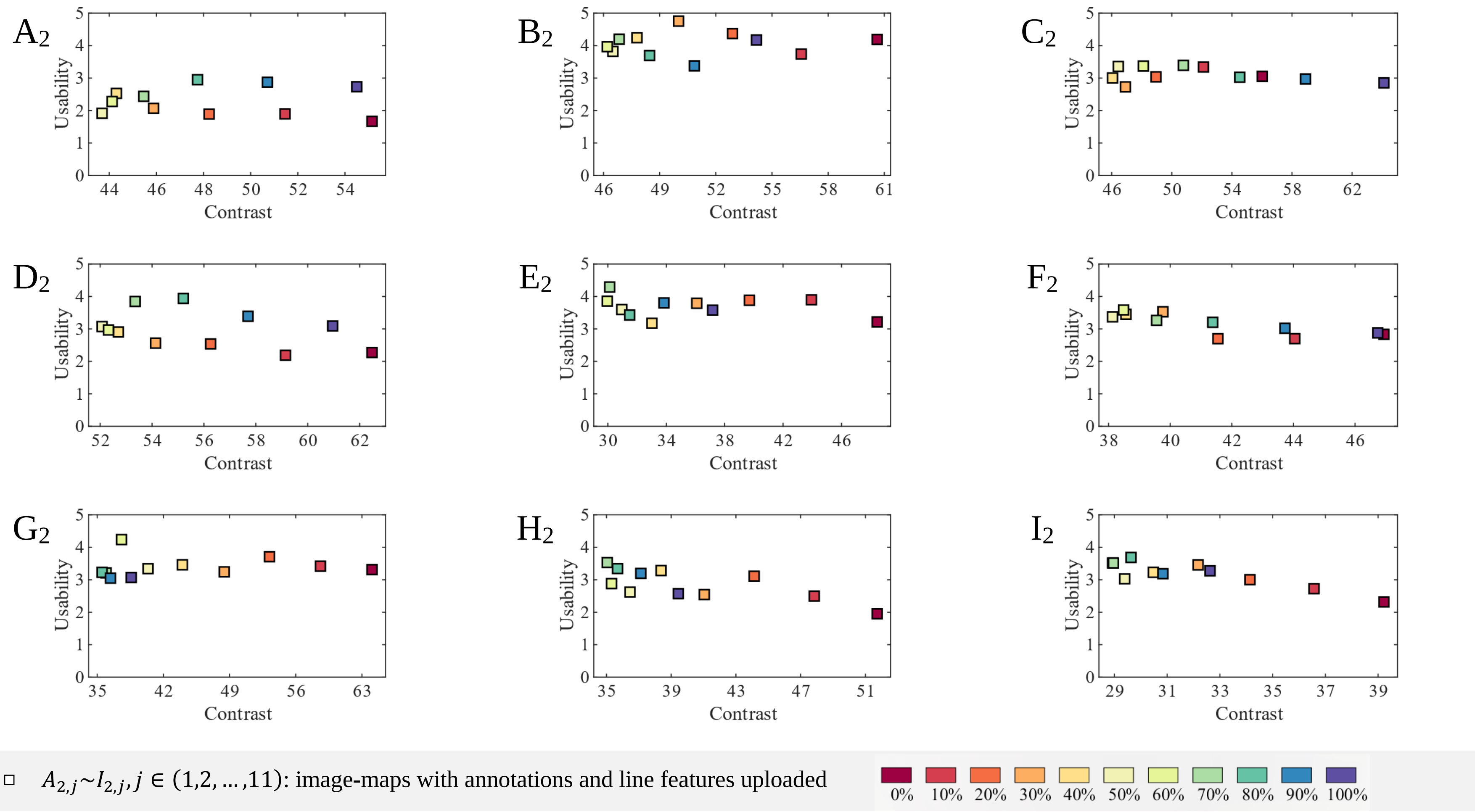

Figure 4.10. Usability and contrast for the second series of image-maps $A_{2,j}$~$I_{2,j}$, $j \in (1,2,\ldots,11)$ with annotations and line features uploaded.

Table 4.6. Optimum transparency level and corresponding contrast/complexity of the original background image/image-map with original background image/image-map with optimum transparency.

			Contrast			**Complexity**		
		Optimum transparency level (%)	**Original background image**	**Image-map with original background image**	**Image-map with optimum transparency**	**Original background image**	**Image-map with original background image**	**Image-map with optimum transparency**
Series 1: image-maps with annotations	A_1	60	44	55	32	463230	466098	386731
	B_1	0	50	60	60	478837	478665	478665
	C_1	10	35	55	50	479283	483290	474209
	D_1	70	48	62	41	466706	467842	372950
	E_1	70	(1) 40	(3) 47	(5) 22	(7) 466616	(9) 465387	(11) 363685
	F_1	80	38	44	22	445572	447389	308936
	G_1	90	54	63	28	427030	430500	224685
	H_1	80	47	50	22	390425	395315	257273
	I_1	70	36	39	19	436952	438290	335591
Series 2: image-maps with annotations and line features	A_2	80	44	50	48	463230	475386	364424
	B_2	30	50	61	50	478837	477219	457238
	C_2	70	35	50	51	479283	485152	407987
	D_2	80	48	50	55	466706	467270	370552
	E_2	70	(2) 40	(4) 61	(6) 30	(8) 466616	(10) 462761	(12) 375092
	F_2	60	38	50	38	445572	446050	378409
	G_2	60	54	50	38	427030	428914	355412
	H_2	70	47	61	35	390425	404383	314010
	I_2	80	36	50	30	436952	450847	324985

4.3.2 Relationships between optimum transparency and the complexity of the background image

The optimum transparency level and corresponding contrast/complexity of original background images/image-maps are compared with the original background images/image-maps with optimum transparency in Table 4.6. Five different fitting models are applied: linear, exponential, logarithmic, power, and polynomial. The goodness of fit (R-square and Root Mean Squared Error (RMSE)) are evaluated. R-Square, defined as the ratio of the sum of squares of the regression and the total sum of squares, is the square of the correlation between the response values and predicted response values, indicating the success of the fit in explaining data variation. RMSE is an estimate of the standard deviation of a random component in the data. These terms are defined as follows:

$$\text{R-square}=\frac{SSR}{SST}=\frac{\sum_{i=1}^{n}(\widehat{y_i}-\bar{y})^2}{\sum_{i=1}^{n}(y_i-\bar{y})^2} \tag{4.7}$$

$$RMSE=\sqrt{\frac{\sum_{i=1}^{n}(y_i-\hat{y})^2}{n}} \tag{4.8}$$

where $\widehat{y_i}$ is the predicted response value, y_i is the response value, $\bar{y}$ is the mean value, and n is the number of observations. R-square can take on any value between 0 and 1, with a value closer to 1 indicating that a greater proportion of variance is accounted for by the model. The R-square (R^2) and RMSE values for all models with a 95% confidence interval are shown in Table 4.7.

From the models listed in Table 4.7, the polynomial fit was chosen by virtue of its goodness of fit for scatters and its simplicity. Fitting curves are drawn with a solid line on the scatter diagrams in Figure 4.11 and Figure 4.12.

Table 4.7. Comparison between the R-square and RMSE of different fitting models.

No.	**Linear** $a*x+b$		**Exponential** $a*e^{b*x}$		**Logarithmic** $a*\log(x)+b$		**Power** $a*x^b$		**Polynomial** $a*x^2+b*x+c$	
	R^2	RMSE	R^2	RMSE	R^2	RMSE	R^2	RMSE	R^2	RMSE
(1)	0.02	33.71	0.02	33.72	0.02	33.68	0.02	33.69	0.03	36.25
(2)	0.45	25.11	0.36	27.25	0.43	25.66	0.34	27.66	**0.77**	**17.67**
(3)	0.08	32.64	0.08	32.64	0.08	32.65	0.08	32.58	0.07	32.76
(4)	0.47	24.66	0.37	26.97	0.45	25.22	0.35	27.38	**0.78**	**17.05**
(5)	0.77	16.44	0.65	20.06	0.67	19.46	0.56	22.66	**0.85**	14.25
(6)	0.83	13.93	0.67	19.42	0.74	17.33	0.59	21.72	**0.98**	**5.49**
(7)	0.17	15.44	0.16	15.50	0.16	15.53	0.15	15.59	0.20	16.31
(8)	0.04	16.59	0.03	16.61	0.03	16.62	0.03	16.64	0.11	17.23
(9)	0.12	15.88	0.12	15.88	0.12	15.87	0.12	15.87	0.12	15.88
(10)	0.01	16.86	0.01	16.86	0.01	16.86	0.01	16.86	0.02	18.11
(11)	0.02	16.70	0.03	16.68	0.03	16.61	0.04	16.59	0.02	16.70
(12)	0.52	11.77	0.45	12.53	0.47	12.30	0.41	12.99	**0.72**	**9.61**

Figure 4.11 shows the fitting between the optimum transparency level and contrast (Nos. 1, 3, & 5) /complexity (Nos. 2, 4, & 6) for the first series of image-maps. For image-maps with annotations uploaded, the R-square of fitting is very poor for first two conditions (Nos. 1 & 3). When the transparency level changes, the annotations (black with white halo) exert a substantial influence on the contrast of the whole image-maps. Consequently, the fitting between the optimum transparency level and the contrast of the original image/image-map with the original image are poor. The fitting between the optimum transparency level and the contrast of the image-map with optimum transparency (No. 5) improves considerably, and can thus be better modeled. Clearly, the fittings for groups of complexity (Nos. 2, 4 & 6) are better than those for groups of contrast, especially for the relationship between the optimum transparency and the complexity of image-map with corresponding transparency.

Figure 4.12 shows the fitting between the optimum transparency level and contrast (Nos. 7, 9, & 11) / complexity (Nos. 8, 10, & 12) for the second series of image-maps. When compared with the first series of image-maps, the annotations and line features in the second series play an important role, resulting in the significant lowering of the R-square value. The different backgrounds of participants also influenced the results. The experienced map users may prefer more transparent image and distinguished line features. On the other hand, the line features may be useless and redundant for participants without geoscience background. The trends for complexity of image-maps and the optimum transparency show quite different for the two groups of participants, with geosciences background (—△—), without geosciences background (—△—). Questions A, C, F, and I concern the interpretation of the height of points or flow of streams, which rely primarily on line features (contours) and the landscape shown in background images. The two groups of participants show deviation between these tasks. Questions B, D, E, G, and H relate to the location of buildings, roads, and signs, which rely more on annotation and less on the background image. The fittings based on two kinds of questions focusing on different landscapes can be analyzed separately from contrast. The questionnaire conducted included four groups; however, the inclusion of more experiment groups could be conducted to verify these predictions.

Combining annotations and line features causes the R-square value to slightly decrease because the uploaded features influence the complexity of the background image. The models of optimum transparency level and the image-map complexity with optimum transparency (Nos. 6 & 12) showed the best fitting. Thus, there is potential to predict peak usability based on the complexity of background images.

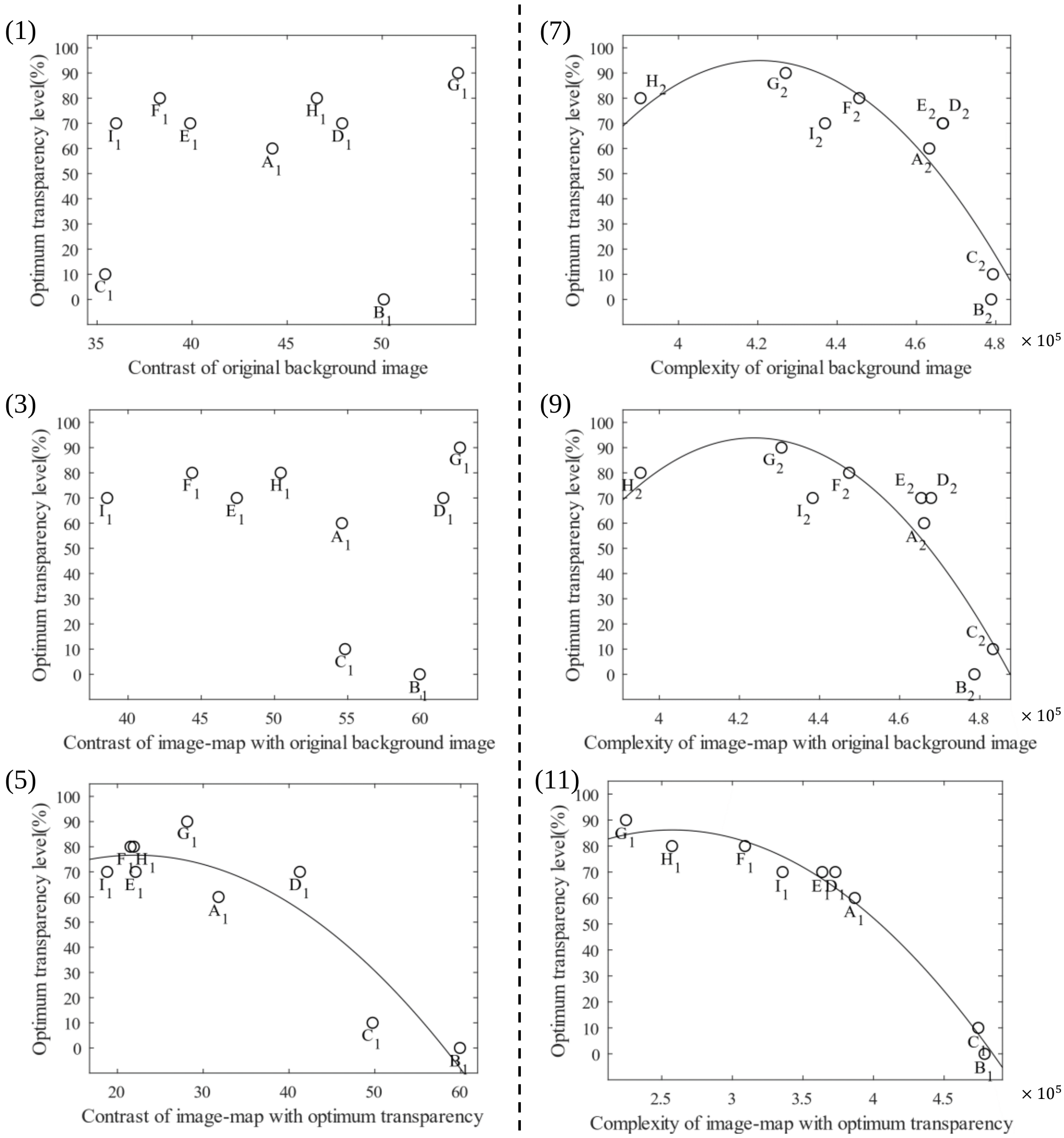

Figure 4.11. Optimum transparency and corresponding contrast / complexity for the first series of image-maps, $A_{1,j} \sim I_{1,j}, j \in (1,2,\ldots,11)$ with annotations uploaded.

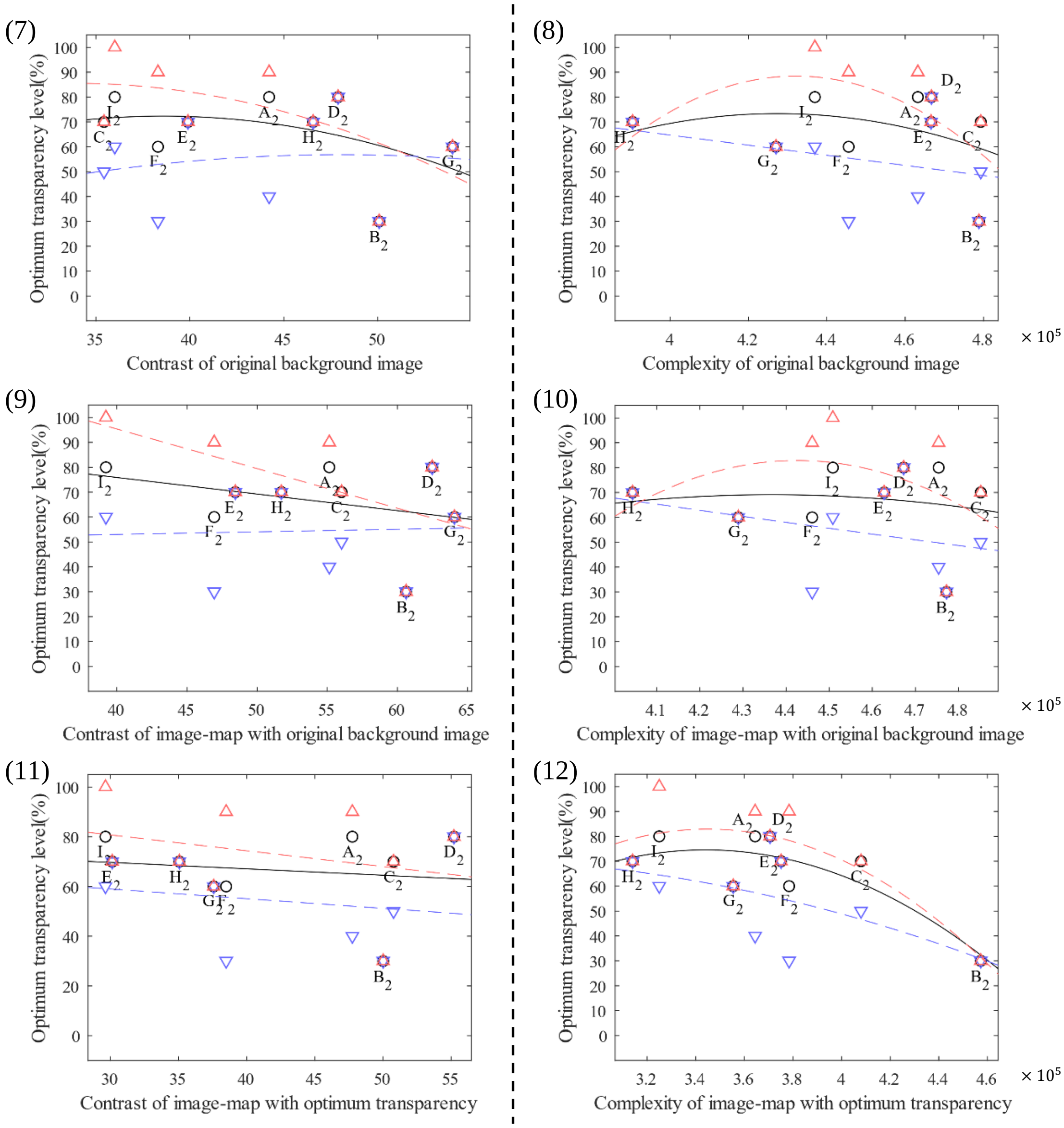

Figure 4.12. Optimum transparency and corresponding contrast / complexity for the second series of image-maps, $A_{2,j} \sim I_{2,j}, j \in (1,2,\ldots,11)$ with annotations and line features uploaded.

4.4 Summary

In this study, the usability of image-maps was evaluated in terms of effectiveness and efficiency. Image-maps were produced with eleven background image transparency levels and three map scales using nine areas. The image-maps were evaluated *via* online surveys. Changing transparency level was shown to influence the usability of image-maps. The transparency level at which the image-map reaches peak usability changes according to the data from different areas. The relationship between two characteristics, contrast and complexity, and the usability were evaluated, enabling the following conclusions to be drawn based on our experimental results:

(1) The usability of image-maps is influenced by the transparency of background images. Peak usability occurs at different transparency levels depending on the landscape and scale of the image-map.

(2) A quadratic polynomial model can fit the trend between usability and Boltzmann Entropy as a measure of complexity for image-maps. The complexity of background images shows advantages compared with contrast. This may reflect the fact that Boltzmann Entropy characterizes the structural information of image-maps.

When dealing with image-maps featuring only annotations, background images play an important role in the interpretation of natural landscapes. Line features influence the entirety of the representation and considerably improve the usability of image-maps, which weakens the relationship between usability and background images. For map users with different levels of map skills, the line features (e.g., contours) may greatly influence the results of tasks regarding with relative height. Relationships between the complexity of the original image and image-maps with peak transparency levels and usability indicates potential for image enhancement during the production of image-maps.

Chapter 5 Effects of background image complexity and map symbol load on the usability of image-maps

In the last chapter, the generalization of background images to reduce the complexity for better representation of image-map has been studied. On the other hand, the representations of graphic and text symbols can also be explored to adapt to complex backgrounds. In this chapter, the effects of background image complexity on map symbol load are explored.

5.1 Strategy for exploring the effects of background image complexity and map symbol load on the usability of image-maps

The combination of image and map contradicts cartographic design rules concerned with simplicity because the map space is not masked by cartographic symbols but imagery depiction. Traditional map load considers the complexity of the loaded symbols, but image-map should also consider the complexity of the image to get the optimum amount of symbols to be loaded. The hypotheses were made that the complex background image influenced the effectiveness and efficiency of image-maps, which is different from traditional maps with the same level of symbol density:

- Firstly, for the same background image, the usability should increase and then decrease when the amount of symbol load rises. A peak value of usability should exist for a series of image-maps with different levels of symbol load.
- Secondly, for different image-maps, the optimum level of symbol load at which the peak value of usability exists, should vary with the complexity.

To verify the hypotheses, an experiment was carried out using eye-tracking and online questionnaire surveying. As over-crowded situations with high-density labels mainly exist in urban areas, ten different urban areas were selected and ten density levels of map symbols were applied to the chosen image-maps. Annotations for polygon features, such as building, park, waterbody, were loaded to the image-maps. The usability of image-maps was evaluated by user study in terms of two aspects, effectiveness and efficiency (ISO 2018). The framework of the experimental evaluation is shown in Figure 5.1.

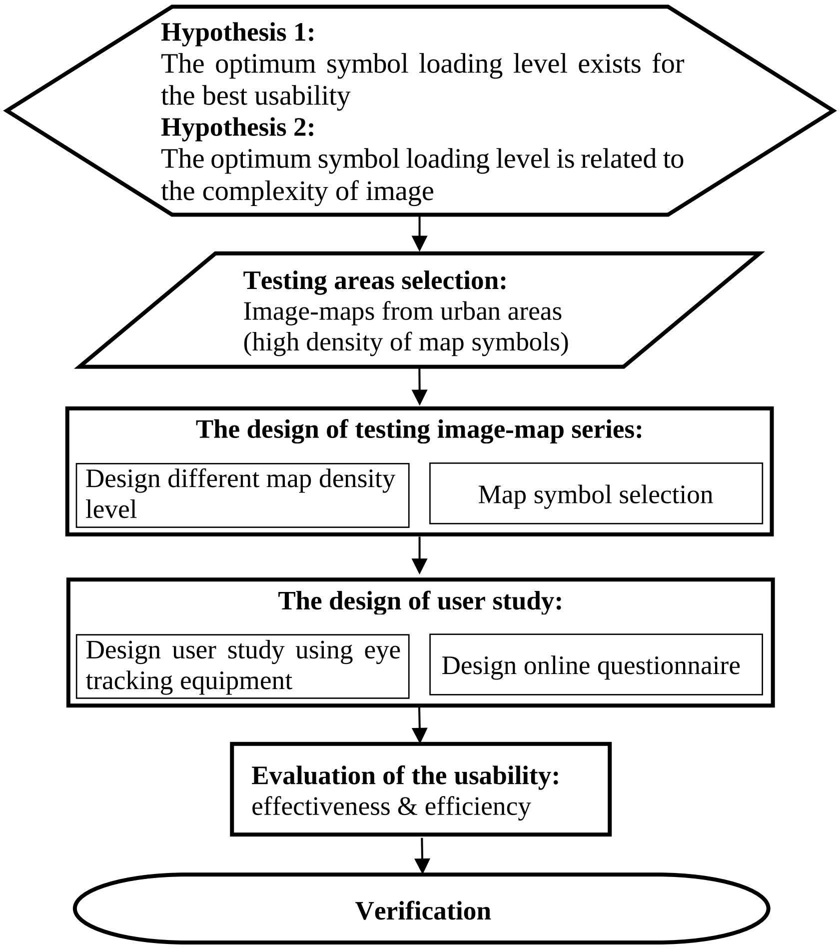

Figure 5.1. The framework of the experimental evaluation.

Boltzmann Entropy, introduced in section 2.3.2, is also employed to measure the complexity of background image and final outputs of combinations of image and different density levels of map symbols.

The symbols to be loaded onto images were classified into ten classes based on the original area sizes of the corresponding feature polygons. Figure 5.2 shows the original background image (a), the original map (b), image-map with annotations for all polygon features (c), and ten classes of polygon features based on the area sizes. All the polygon features, i.e., buildings, facilities, were sorted in order from largest to smallest. Every 10% of the polygon features were classified as an individual class, and corresponding labels were loaded onto the images. Ten different density levels of labels were loaded onto the images. The corresponding polygons for the labels were sorted from largest to smallest based on the area sizes, and ten different levels were classified: L_1 (first 10% labels with the largest sizes loaded), L_2 (first 20% labels with the largest sizes loaded), …, L_{10} (100% labels loaded), as shown in Figure 5.3.

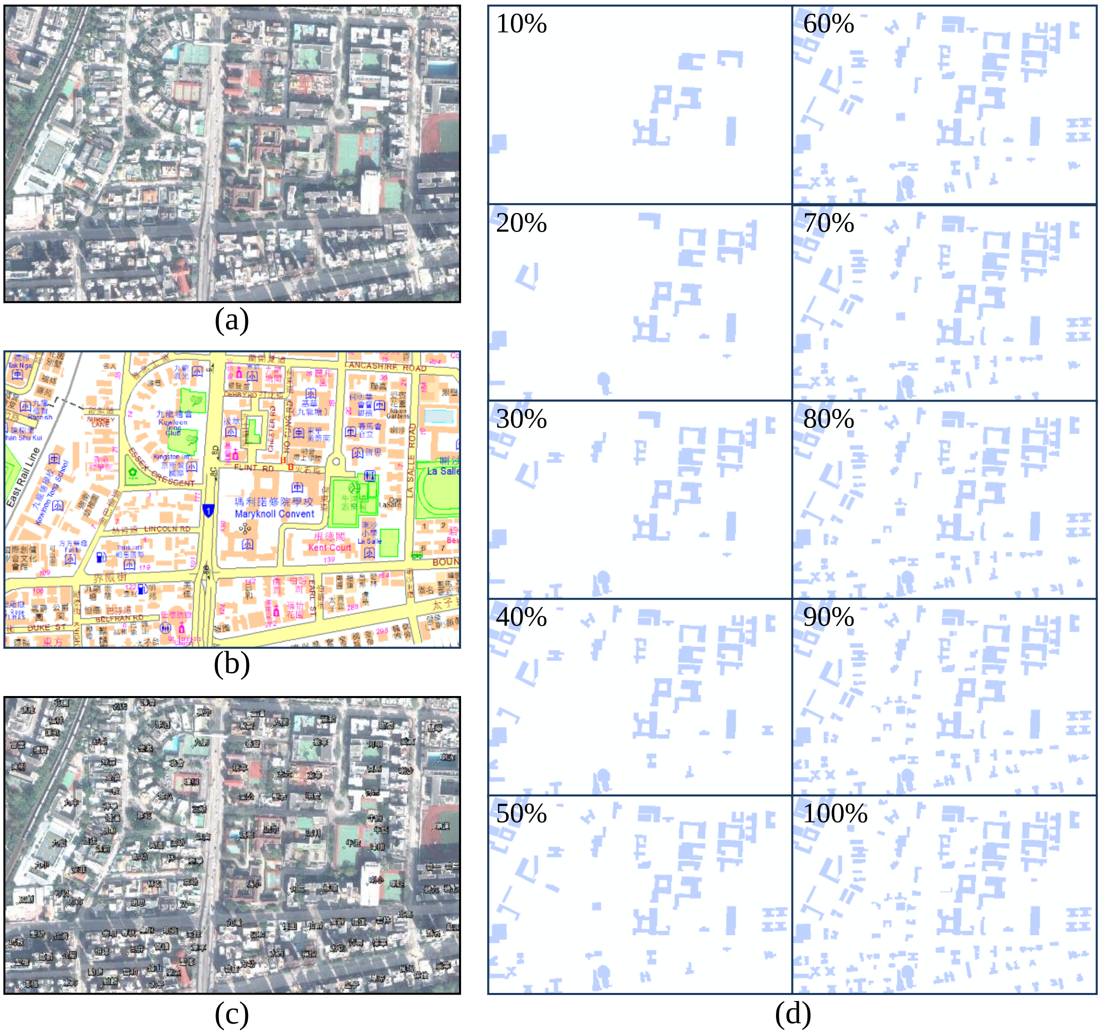

Figure 5.2. Load the map symbols onto images: (a) original background image, (b) original map, (c) load all the annotations for polygon features onto images, (d) ten different levels of polygon features based on the area sizes.

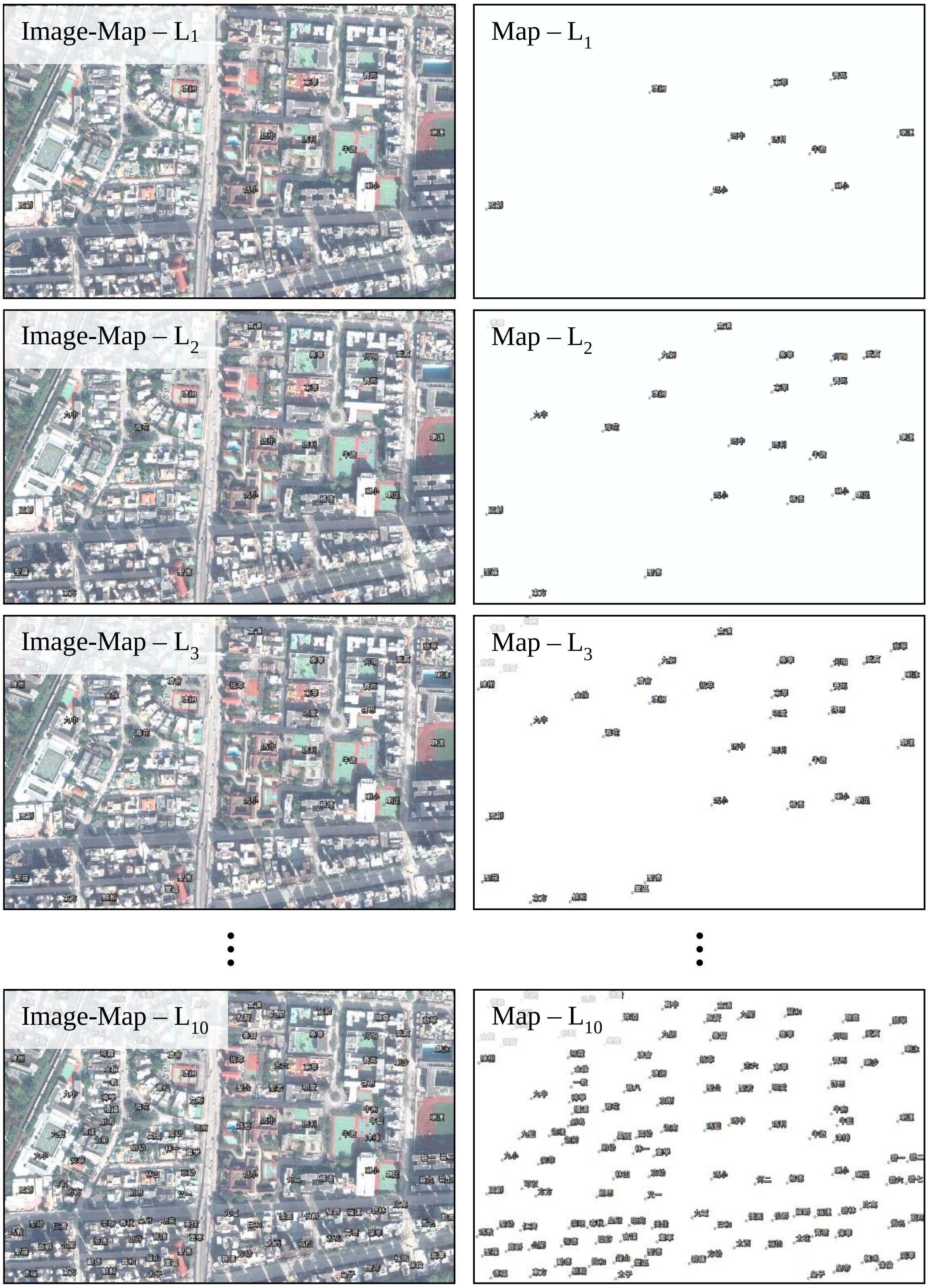

Figure 5.3. Image-maps and maps with different levels of label density ($L_1, L_2, \ldots, L_{10}$).

5.2 Experimental evaluation

Experimental data sets included satellite images and maps from ten areas in Hong Kong (Figure 5.5). The resolution of the images was 0.8 m, and the digital maps (scale 1:10 000) were from the Surveying and Mapping Office, Hong Kong Special Administrative Region (SMO 2019). All images were obtained after radial and geometric corrections; orthophotos of Hong Kong were used for the ten experimental areas, each 800 m × 520 m. Only polygon features, i.e., building, facilities, and corresponding annotations as labels, were employed for the following experiments. The ten areas were urban areas with high-density ground features, so when all the labels were loaded onto the images, the image-map would be too complex. The optimum level of symbol load can be explored.

5.2.1 Design of survey using eye-tracking equipment and online questionnaire

Gazepoint GP3 eye tracker (Gazepoint 2021) was used in this surveying. The eye tracker is at research-grade and utilizes a 60Hz machine-vision camera. The visual angle accuracy is 0.5~1 degrees. The equipment was set up with a 17-inch monitor (1280*1024). The surveyings were all finished in the cartography laboratory with the same stable environment. The image-maps and maps (Figure 5.3) used in the experiment were at the scale of 1:3000, and the resolutions were 1000*600 pixels. Target search was a common experiment used by many researchers with eye-tracker (Dong et al. 2016, Liao et al. 2018). In this experiment, the participants were asked to seek five specific labels in each image-map/map, and then gaze at the label until pre-set time ends. The labels were selected from the five different levels of symbols, $L_2, L_4, L_6, L_8, L_{10}$, i.e., the first 20%, 40%, 60%, 80%, 100% labels with the largest sizes loaded and well-distributed on the screen. The areas around target labels (120*72 pixels) were set as Area Of Interests (AOI). The average time to first view and average revisits of AOIs were recorded, and the fixation map and heat map recording the eye movements were also provided for analysis (Figure 5.5). The gaze points and fixations are the basic measurements for eye tracking. A fixation is constituted by a series of gaze points in very close time and/or space. The fixation map shows the gaze points and gaze time, which can measure visual attention. Heatmap shows the distribution of gaze points. The red, yellow, and blue colors represent the number of gaze points in descending order. The average revisits and average time viewed of the AOI were recorded. The revisits of and viewed-time of AOIs reflect the effectiveness and efficiency of searching the target label. The more revisits and less viewed time imply the difficulty for finding target label. The usability of an image-map is evaluated by combining these two indicators.

$$\text{Usability:} \qquad \text{Efficiency \& Effectiveness} = \frac{\text{Average Time Viewed}}{\text{Average Revisits}} \tag{5.1}$$

For the online questionnaire (https://www.wjx.cn/vj/YDqzvwn.aspx), the questions were about the perceived complexity for the same sets of image-maps and maps. The questionnaire was conducted when the participants finished the eye-tracking experiment.

5.2.2 Study participants

Participants were recruited via advertisements posted on the campus of the Hong Kong Polytechnic University. Forty volunteered students aged from 18 to 35 participated in the experiment, including 22 females and 18 males, of whom 15 had backgrounds in geosciences. All the participants are with normal eyesight (or corrected to normal eyesight with contact lenses). They were informed of the intention of the questionnaire before starting, i.e., “to explore the effects of background image complexity on the usability of image-maps”. The whole experiment lasted 60 minutes. Every participant was paid HK$50 for their participation.

Figure 5.4. Ten testing areas.

(a)

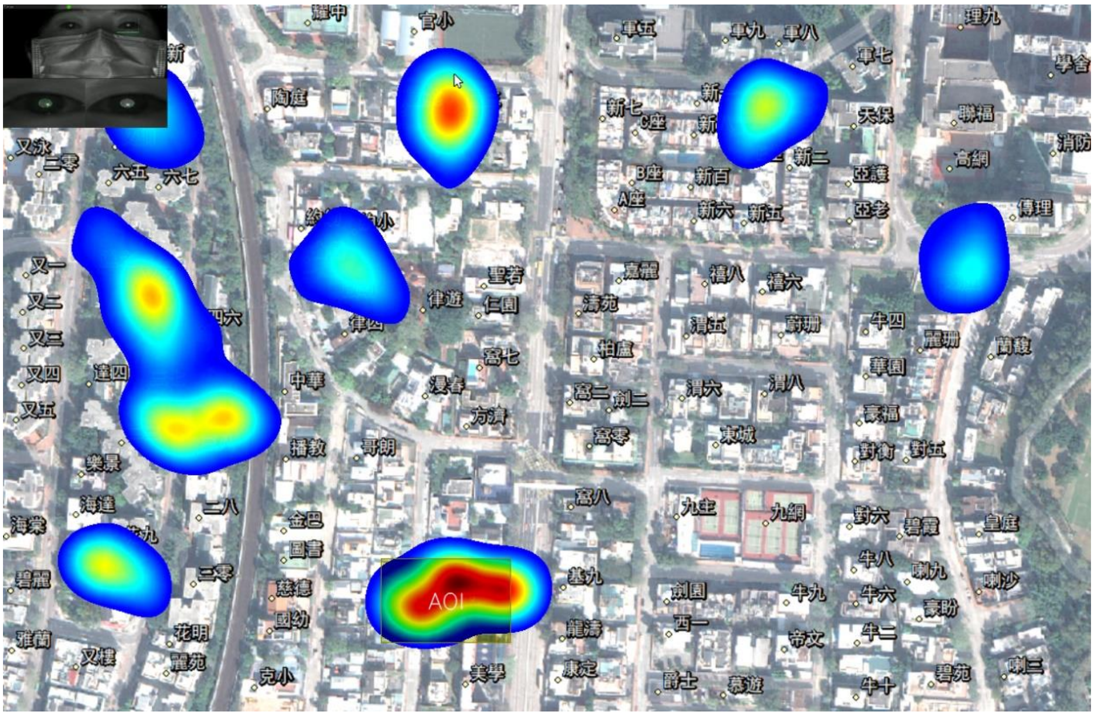

(b)

Figure 5.5. Fixation map (a) and heatmap (b) of gaze for searching AOI.

5.3 Usability of image-map with different levels of map symbols load

5.3.1 Analysis of relationships between the usability of image-maps and the complexity of image-maps

The eye tracker recorded the movements of the eye and the average time viewed, average revisits of AOIs and the corresponding complexity of two series of image-maps and maps in ten areas (A-J) with different levels of label density $(L_1, L_2, \ldots, L_{10})$ are shown in Table 5.1 and Table 5.2. In Figure 5.6 and Figure 5.7, the boxplots show the average time viewed and average revisits of AOIs for image-maps and maps with different levels of label density $(L_1, L_2, \ldots, L_{10})$. On each box, the central mark (-/-) indicates the median, and the bottom and top edges of the box indicate the 25th and 75th percentiles, respectively. The whiskers extend to the most extreme data points not considered outliers, and the outliers are plotted individually using the '+/+' symbol.

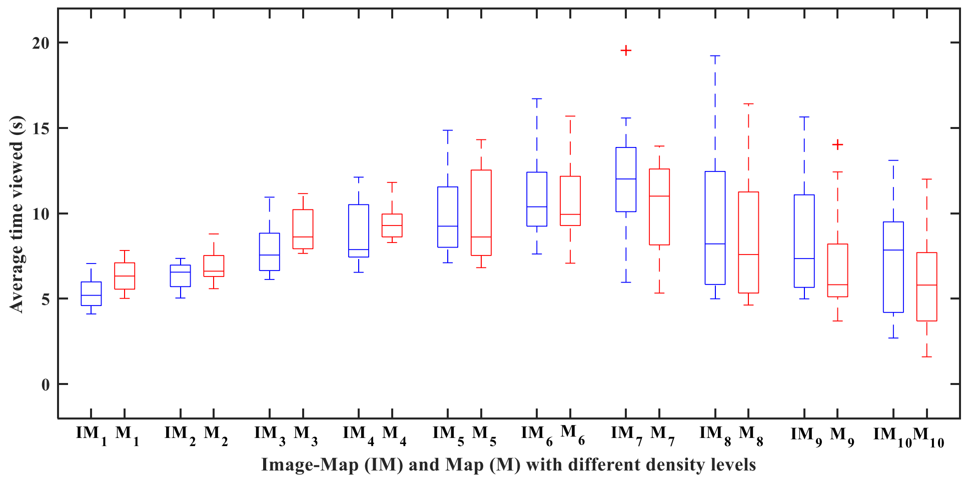

Figure 5.6. Average time viewed of AOIs for image-maps and maps with different levels of label density $(L_1, L_2, \ldots, L_{10})$.

A significance test was conducted on the average time viewed and average revisits of AOIs for image-maps and images with different density levels. The null hypothesis is that no significant difference exists between the ten levels of density $(L_1, L_2, \ldots, L_{10})$ in image-maps and maps. To test this hypothesis, a one-way analysis of variance test (one-way ANOVA) was conducted. All p-values were smaller than 0.05, demonstrating that the null hypothesis is rejected at 95% confidence. In other words, the usability of an image-map varies significantly depending on the density level of symbol load.

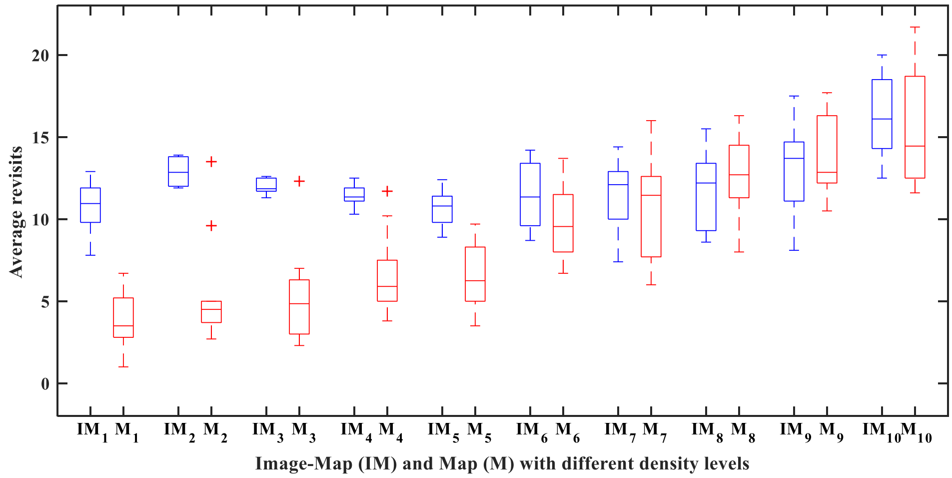

Figure 5.7. Average revisits of AOIs for image-maps and maps with different levels of label density ($L_1, L_2, \dots, L_{10}$).

In Figure 5.6, the boxplots of the average time viewed of AOIs for image-maps (blue) and maps (red) with different levels of label density ($L_1, L_2, \dots, L_{10}$) show that the average viewed time increased and then decreased when the label density increased. If the target label exists in the image-map, the time for searching will be influenced by the complexity of image-map. If the target label not exist, then the searching will last until time ends. When the label density is low (L_1~L_4), the time used for target searching is less but more targets cannot be found, so the average time viewed is low. When the label density is high (L_8~L_{10}), although more targets can be found, it takes more time for searching due to the high density of labels. The viewed times for AOIs in maps are higher than those in image-maps when the density level is low (L_1~L_4). On the other hand, when the density level is high (L_8~L_{10}), the complex background images improve the viewed times for AOIs. The viewed times for AOIs in maps are lower than those in image-maps with dense symbols. The complex background image may have an effect on the monotonous map labels and improve the searching efficiency.

Table 5.1. Average time viewed, average revisits of AOIs, corresponding complexity of image-maps, and rated complexity from user questionnaire in ten areas (A-J) with different levels of label density ($L_1, L_2, \ldots, L_{10}$).

Image-maps	Area	L_1	L_2	L_3	L_4	L_5	L_6	L_7	L_8	L_9	L_{10}
Average time viewed (s)	(A)	6.0	5.4	10.9	10.5	14.9	16.7	15.6	14.8	15.6	13.1
	(B)	4.1	5.7	7.7	6.5	8.7	10.3	10.1	7.0	5.7	3.3
	(C)	5.1	7.2	8.1	7.5	9.8	9.8	11.8	5.7	6.6	8.0
	(D)	4.6	5.0	6.1	7.5	7.1	8.1	13.1	11.5	8.1	2.7
	(E)	5.2	7.0	6.3	7.0	8.1	12.4	13.9	5.0	5.7	7.7
	(F)	4.5	6.4	7.4	8.2	8.0	9.2	12.2	9.4	5.0	5.9
	(G)	5.6	6.9	6.6	7.4	7.6	10.5	10.7	6.8	8.4	9.0
	(H)	6.2	6.1	8.8	12.1	11.1	7.6	6.0	5.8	6.2	4.2
	(I)	7.1	7.4	10.3	11.4	11.5	15.3	19.5	19.2	15.2	10.7
	(J)	5.2	6.7	7.0	9.7	11.8	11.4	10.0	12.5	11.1	9.5
Average revisits	(A)	15.5	11.9	12.6	12.5	12.7	13.4	13.5	13.4	14.7	20.0
	(B)	14.2	13.1	12.5	11.9	10.9	13.6	10.0	13.8	9.5	20.0
	(C)	14.9	12.7	11.8	11.2	9.1	9.6	12.6	15.5	11.1	12.5
	(D)	13.8	12.8	11.3	12.1	10.9	12.2	14.4	12.0	14.9	13.7
	(E)	13.8	11.9	12.2	10.9	9.8	10.5	8.7	12.4	14.6	18.5
	(F)	14.6	13.8	11.9	10.3	11.4	14.2	11.7	9.1	17.5	16.5
	(G)	14.4	13.8	11.7	11.4	12.4	9.4	11.3	8.6	8.1	17.0
	(H)	12.9	12.9	11.7	11.1	12.2	13.0	12.9	10.2	12.1	14.6
	(I)	12.5	13.9	12.6	11.3	10.5	8.7	7.4	9.3	14.6	15.7
	(J)	12.9	12.0	11.3	11.9	8.9	9.8	12.5	12.4	12.8	14.3
Complexity ($\times 10^7$)	(A)	19.5	19.6	19.7	19.7	19.8	19.9	20.0	19.9	19.9	20.0
	(B)	17.7	17.9	17.9	18.1	18.3	18.3	18.4	18.5	18.5	18.5
	(C)	17.4	17.6	17.7	17.8	17.9	18.0	18.2	18.2	18.3	18.4
	(D)	18.7	18.7	18.8	18.8	18.9	19.1	19.2	19.2	19.3	19.5
	(E)	19.5	19.6	19.7	19.9	19.9	20.0	20.3	20.6	20.7	20.9
	(F)	18.0	18.2	18.5	18.6	18.8	18.8	19.1	19.2	19.4	19.6
	(G)	17.7	18.0	18.3	18.5	18.6	18.7	18.9	19.0	19.1	19.2
	(H)	17.9	17.9	17.9	17.9	17.9	18.0	18.1	18.1	18.2	18.2
	(I)	17.9	17.8	17.8	17.8	17.8	17.9	17.9	18.0	18.0	18.0
	(J)	18.1	18.2	18.2	18.1	18.1	18.2	18.2	18.3	18.3	18.3
Rated complexity from user questionnaire	(A)	4.5	4.7	5.6	5.3	6.1	6.3	6.4	7.4	7.6	8.9
	(B)	6.2	7.4	7.7	8.1	8.5	8.6	9	9.7	9.6	9.5
	(C)	3	3.1	3.3	3.3	4	5.1	6.2	7.3	7.2	7.6
	(D)	4.1	4.3	4.7	5.1	6.3	7.5	8.1	9.1	9.3	9.2
	(E)	3.7	4.6	5.3	5.4	7.1	7.2	7.5	8.7	8.6	8.8
	(F)	2	3.2	3.5	4.1	4.3	6.3	6.4	7.7	8.2	8.5
	(G)	3.3	4.4	4.5	4.4	5.2	5.7	6.7	7.5	8.1	8.5
	(H)	3.4	3.4	4.3	4.4	4.4	6.1	6.3	7.2	8.7	8.8
	(I)	4.1	3.8	4.2	4.3	5.2	5.1	6.5	6.4	7.6	7.7
	(J)	5.1	5.5	5.6	7.1	7.2	8.3	8.4	8.7	8.9	9.1

Table 5.2. Average time viewed, average revisits of AOIs, and corresponding complexity of maps in six areas (a-f) with different levels of label density ($L_1, L_2, \ldots, L_{10}$).

Maps	Area	L_1	L_2	L_3	L_4	L_5	L_6	L_7	L_8	L_9	L_{10}
Average time viewed (s)	(A)	6.2	5.6	11.2	9.6	14.3	15.5	12.9	16.4	14.0	8.7
	(B)	4.0	5.6	7.9	6.6	6.8	9.3	10.6	5.3	5.1	3.7
	(C)	5.2	7.9	8.5	6.9	7.6	9.3	8.3	4.6	6.2	1.6
	(D)	4.4	5.2	6.8	8.9	6.9	8.3	11.5	8.3	5.5	7.0
	(E)	5.1	7.5	7.8	8.3	7.5	12.2	12.6	6.9	3.8	4.6
	(F)	4.6	6.6	8.3	8.6	8.0	10.4	6.4	6.6	6.2	7.7
	(G)	5.6	8.3	9.0	7.6	9.2	9.6	8.2	8.3	3.7	2.5
	(H)	5.8	4.4	7.2	10.0	9.6	7.1	5.3	5.1	5.3	4.3
	(I)	6.8	6.3	10.6	11.8	12.7	15.7	13.9	15.6	12.4	12.0
	(J)	5.3	6.6	7.7	10.5	12.5	10.3	11.4	11.3	8.2	7.6
Average revisits	(A)	2.8	4.7	5.7	13.0	11.8	14.8	15.7	12.9	16.5	21.7
	(B)	3.0	4.0	7.0	11.3	9.9	11.6	9.5	9.5	10.9	13.0
	(C)	4.0	3.7	5.0	11.8	10.2	12.9	12.2	12.5	17.3	12.5
	(D)	5.0	4.7	2.3	11.5	9.0	9.8	10.0	12.0	12.6	15.5
	(E)	3.0	2.7	3.0	9.9	10.8	13.9	13.2	10.8	13.5	18.7
	(F)	4.5	4.3	6.3	10.7	11.7	9.8	16.0	14.3	16.4	19.5
	(G)	5.3	5.0	4.0	10.5	10.7	11.2	8.5	16.1	11.9	17.7
	(H)	6.7	5.5	8.3	13.6	12.6	12.7	13.6	13.5	12.6	13.6
	(I)	1.2	7.6	4.7	10.9	9.8	10.6	11.3	14.8	13.5	12.2
	(J)	2.8	3.4	2.7	11.7	8.7	11.3	12.7	13.3	12.4	13.4
Complexity ($\times 10^7$)	(A)	0.3	0.7	1.1	1.5	1.9	2.4	2.8	3.2	3.7	4.2
	(B)	0.6	1.6	2.7	3.6	4.7	5.7	6.8	7.8	8.7	9.6
	(C)	0.6	1.1	1.6	2.0	2.5	3.2	3.9	4.5	5.1	5.7
	(D)	0.7	1.4	2.0	2.5	2.9	3.6	4.1	4.8	5.4	6.0
	(E)	0.5	1.3	2.2	2.9	3.7	4.8	5.5	6.3	7.1	7.8
	(F)	0.4	1.3	2.1	2.8	3.5	4.2	4.9	5.7	6.6	7.6
	(G)	0.3	1.2	2.0	2.9	3.6	4.2	5.0	5.8	6.5	7.1
	(H)	0.3	0.7	1.2	1.7	2.1	2.6	2.9	3.3	3.8	4.2
	(I)	0.1	0.4	0.7	1.1	1.4	1.7	2.1	2.5	2.9	3.2
	(J)	0.3	0.8	1.2	1.7	2.1	2.6	3.0	3.3	3.8	4.2
Rated complexity from user questionnaire	(A)	1.4	2.1	3.4	3.8	3.8	4.2	4.3	5.6	5.7	6.1
	(B)	1.7	2.4	3.7	5.1	6.5	7.6	8.3	8.7	8.6	8.3
	(C)	2.3	3.1	3.3	3.3	4	5.1	6.2	7.3	7.2	7.6
	(D)	2.5	4.3	4.7	5.1	6.3	7.5	7.1	7.1	8.3	7.2
	(E)	1.9	2.6	3.3	5.4	7.1	7.2	7.8	7.7	7.6	7.8
	(F)	2	3.2	3.5	4.1	4.5	6.5	6.4	7.7	7.2	7.5
	(G)	1.5	2.4	3.4	4.4	5.2	4.7	5.7	6.5	7.1	7.5
	(H)	1.2	2.1	2.6	3.6	4.5	5.8	5.8	6.6	6.5	7.6
	(I)	1	1.7	3.2	3.7	4.7	5.6	5.4	6.6	6.5	7.6
	(J)	1.2	2.3	3.2	4.2	4.3	4.3	5.6	6.5	7.8	8.5

In Figure 5.7, the boxplots of the average revisits of AOIs for maps (red) with different levels of label density ($L_1, L_2, \ldots, L_{10}$) show that the average revisits increased when the label density increased. When the density level is low ($L_1 \sim L_4$), the difference between the image-map and map are more apparent than the situations for high-density level ($L_8 \sim L_{10}$). The average revisits for image-maps (blue) at low-density levels ($L_1 \sim L_4$) are higher because of the complex background images. More revisits of AOIs indicate the low effectiveness of searching. For medial density levels ($L_5 \sim L_6$), the difference of average time viewed and revisits of AOIs between image-maps and maps are not distinguished.

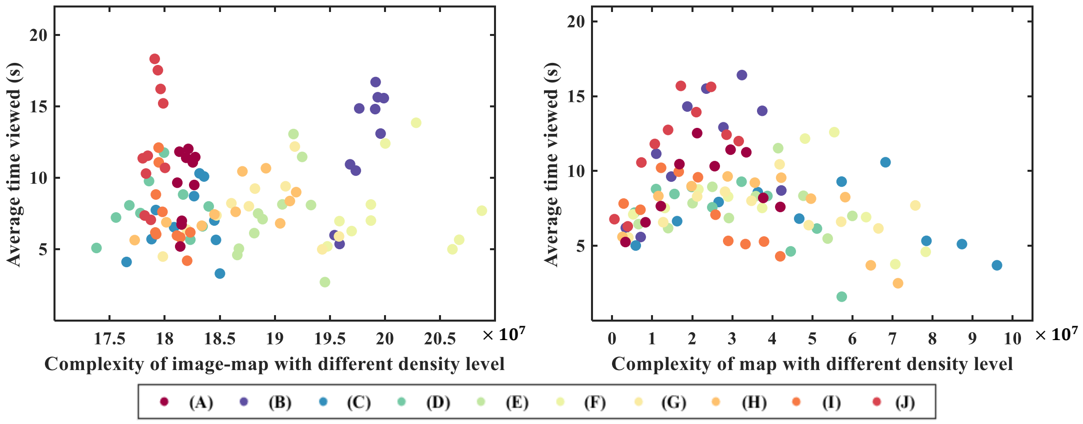

Figure 5.8. Average viewed time of AOIs and corresponding complexity for image-maps and maps.

Figure 5.8 shows the scatter diagrams for the average viewed time of AOIs and corresponding complexity for image-maps and maps. The ten different colors represent the ten areas (A-J). Obviously, the average viewed time and complexity of map (Figure 5.8-right) shows an increasing and decreasing trend when the complexity increase. However, the combination of image and map influences this trend. The complex background images weaken the relationship between the viewed time and maps with different density levels (Figure 5.8-left). The efficiency is reflected by the viewed time. The influence of density level on the efficiency in image-maps is smaller than that in maps. Figure 5.9 shows the scatter diagrams for the average revisits of AOIs and corresponding complexity for image-maps and maps. The average revisits increase when the complexity of map symbols increases (Figure 5.9-right). There is no apparent trend in the relationship of average revisits and complexity in image-maps (Figure 5.9-left).

Figure 5.10 shows the results of complexity rated by users in the online questionnaire. The rated complexity of image-map is much higher than those of the map for low levels of density ($L_1 \sim L_3$) and high levels of density ($L_8 \sim L_{10}$). But for the medium density level ($L_4 \sim L_7$), the rated complexity is equivalent. So for extreme situations, when the labels are dense or sparse, the rated complexity between the image-maps and maps varies. However, when the labels are at a medium level, there is no big difference between the rated complexity.

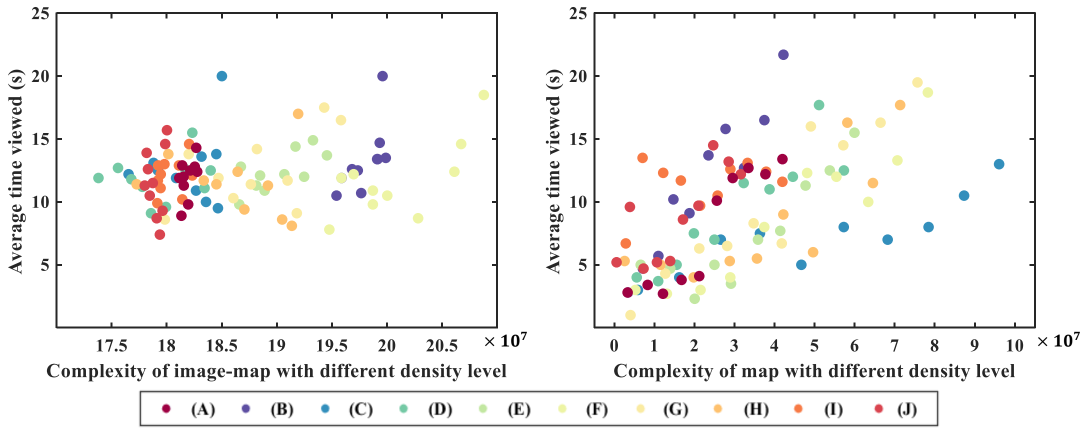

Figure 5.9. Average revisits of AOIs and corresponding complexity for image-maps and maps.

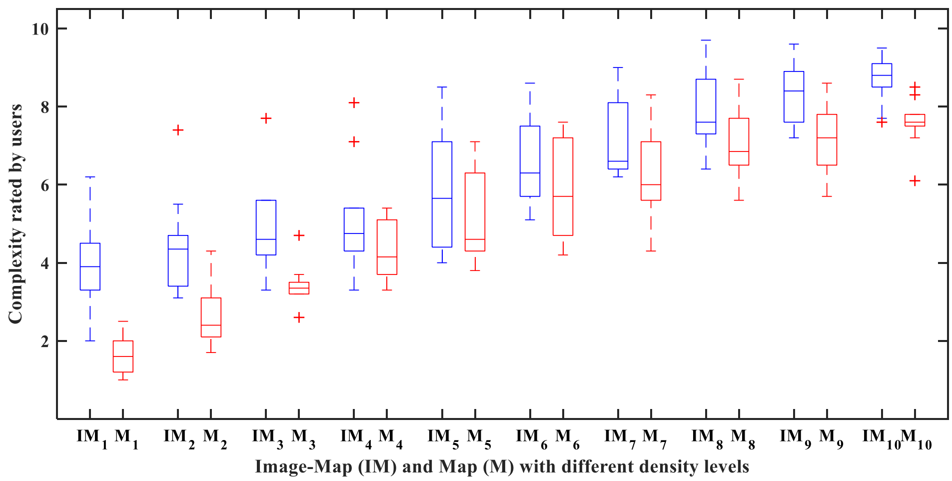

Figure 5.10. The perceived complexity rated by user study using online questionnaire.

5.3.2 Relationships between optimum level of map symbol load and complexity of image-map

In maps without background images, the more symbols load, the higher complexity of the map is. In image-maps, the complex background images influence the increasing trend when more symbols load. The relationship between the optimum level of map symbol load and the complexity of image-map is explored. Five different fitting models, i.e., linear, exponential, logarithmic, power, and polynomial models, were applied to fit the relationship between the optimum level of map symbol load and complexity of original background images and image-maps (Table 5.3). The R-square (R^2) and RMSE values for all models with a 95% confidence interval are shown in Table 5.3. From the models listed, the polynomial fit was chosen by virtue of its goodness of fit for scatters and its simplicity. Fitting curves are drawn with a line on the scatter diagrams in Figure 5.11. The figure shows the fittings between the optimum level of map symbol load and the complexity of original background images (left) and image-maps at the peak level (right). The optimum level of map symbol load is based on the usability of image-maps calculated with Equation 5.1. The optimum levels of map symbol load increased and then decreased when the complexity of the original background images increased. The model of optimum levels of symbol load and the image-map complexity with optimum level showed better fitting. Thus, there is potential to predict peak usability based on the complexity of background images.

Table 5.3. Comparison between the R-square and RMSE of different fitting models for the relationships between optimum level of map symbol load and complexity of image-map.

Fitting models		**Relationship with complexity of original image**		**Relationship with complexity of image-map**	
		R^2	RMSE	R^2	RMSE
Linear	$a * x + b$	0.13	1.22	0.25	1.13
Exponential	$a * e^{b*x}$	0.12	1.22	0.24	1.14
Logarithmic	$a * \log(x) + b$	0.23	1.22	0.16	1.28
Power	$a * x^b$	0.13	1.22	0.24	1.13
Polynomial	$a * x^2 + b * x + c$	**0.34**	**1.13**	**0.39**	**1.09**

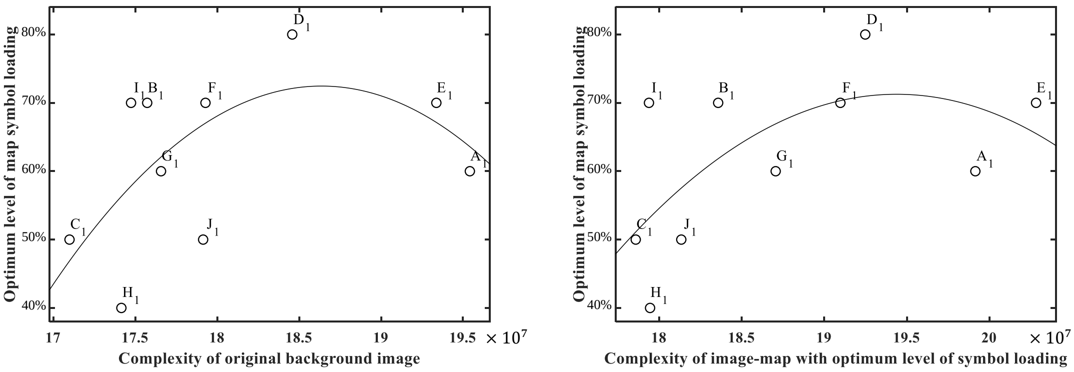

Figure 5.11. The optimum level of map symbol load for image-maps and corresponding complexity for original images (left) and image-maps (right).

5.4 Summary

In this chapter, the effects of background image complexity on map symbol load are explored. An experiment was carried out using eye-tracking and online questionnaire surveying to evaluate the usability of image-maps in comparison to maps with the same level of label density. It can be found from the experimental results that: (1) The usability of image-maps is influenced by the complexity of background images. Peak usability occurs at different levels of symbol load depending on the complexity of the image-map; (2) A quadratic polynomial model can fit the trend between usability and Boltzmann Entropy as a measure of complexity for image-maps. The complexity of background images has the potential to predict peak usability.

Chapter 6 Automated label placement for point feature based on the complexity of background image and general principles

For the optimization of map symbol load, the last chapter explored the effects of background image complexity on the number of map symbols load. In this chapter, the label placement for image-map is studied, specifically for point features. Both the general principles and the complexity of the background image are taken into consideration in the label placement.

6.1 A complexity-based strategy for automated point label placement

6.1.1 Existing point label placement rules

Point feature label placement (PFLP) is a fundamental task in cartography. Yoeli (1972) proposed a three-step label placement process algorithm for eight potential positions with different weights. The eight potential positions for label placements and the preference of these positions have been reviewed in Section 2.2.3 as shown in Figure 6.1 (a-d), which was taken use of the standard ranking of preference for potential label positions (Christensen et al. 1995, Lan et al. 2020, Cravo et al. 2008). Lower values indicate preferable positions. The initial label placement is the upper right position (ranking 1st in Figure 6.1-a, P_1).

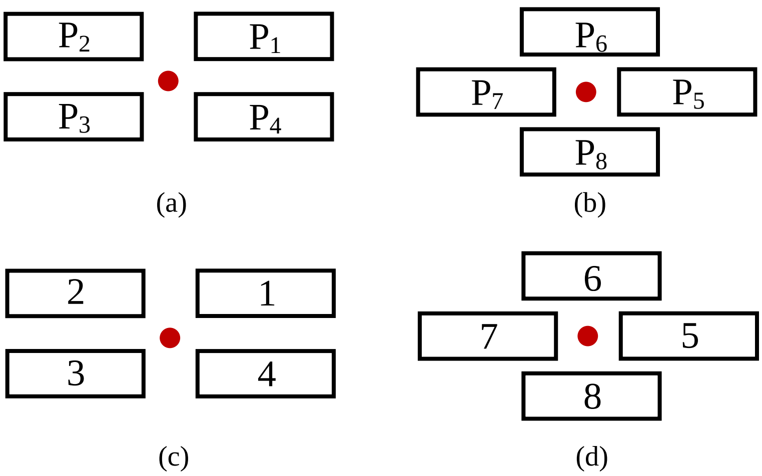

Figure 6.1 A set of potential positions and their preferences: (a & b) potential label positions, $P_1, P_2, \dots, P_8$, (c & d) standard ranking preferences.

6.1.2 Complexity-based rules

For point label placement in image-map generation, the complex background image will influence the visibility of labels. The complexity-based strategy for automated label placement takes the complexity of background images into consideration. The complexity of background images (Absolute Boltzmann Entropy) is computed as Equation 2.7 in chapter 2.3.2. Sorting the complexity of each patch of the background image from smallest to largest, the ranking of each patch is the new preference:

$$\text{Preference Ranking} = \text{argsort}\big((\mathrm{C}_1, \mathrm{C}_2, \ldots, \mathrm{C}_8), '\text{ascending}'\big) \qquad (6.1)$$

where $\mathrm{C}_1, \mathrm{C}_2, \ldots, \mathrm{C}_8$ are the complexity (Absolute Boltzmann Entropy) of the eight patches from background images $(\mathrm{I}_1, \mathrm{I}_2, \ldots, \mathrm{I}_8)$ shown in Figure 6.2. Function argsort is to get the indices that would sort the array in ascending order.

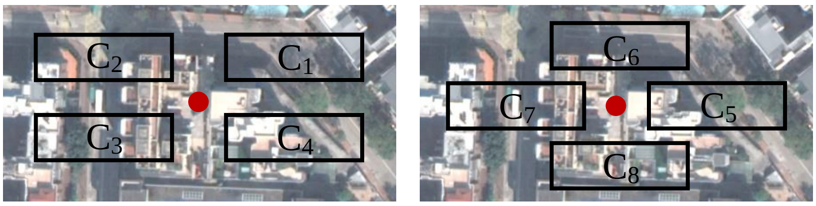

(a) (b)

Figure 6.2 A set of potential positions and their ranking preferences considering the complexity of background images.

Automated labeling can be treated as a combinatorial optimization problem (Papadimitriou and Steiglitz 1998). Rules and optimization techniques/algorithms are required to solve such problems. The rules include the possible positions for labels and the preference ranking. And the optimization algorithms, such as greedy and heuristic optimization algorithms, can be used in this study. Two kinds of PFLP strategies are employed:

- Optimize the point feature labels based on the general principles and standard ranking of preference (Figure 6.1 (c & d)). $\text{Preferences} = \{P_1, P_2, \ldots, P_8\} = \{1,2, \ldots ,8\}$.
- Optimize the point feature labels based on the general principles and ranking of preference based on the complexity of background images (Figure 6.2 (e &

f)). $\text{Preferences} = \{P_1, P_2, \ldots, P_8\} = \text{argsort}\big((\mathrm{C}_1, \mathrm{C}_2, \ldots, \mathrm{C}_8), '\text{ascending}'\big)$.

For automated point label placement, the overlaps among labels and points should be taken into consideration. Overlaps will influence the recognition of points of interests and labels and further affect the usability of maps. Therefore, the optimization of automated point label placement should consider the preference position and overlaps as set as following objective function:

$$\text{Minimize:} \qquad \mathrm{w}_1 \times \mathrm{n}_{\text{overlap}}(\text{Labels}) + \mathrm{w}_2 \times \mathrm{n}_{\text{overlap}}(\text{Points}) \qquad (6.2)$$

where w_1 and w_2 are predefined positive weight values for each kind of overlaps (i.e., those among labels, labels, and points); and $n_{\text{overlap}}(\text{Labels})$ and $n_{\text{overlap}}(\text{Points})$ are the corresponding numbers of overlaps, respectively. These weight values adjust the relative importance of the overlaps. In this study, w_1 and w_2 are equally weighted (i.e., $w_1 = 1$ and $w_2 = 1$).

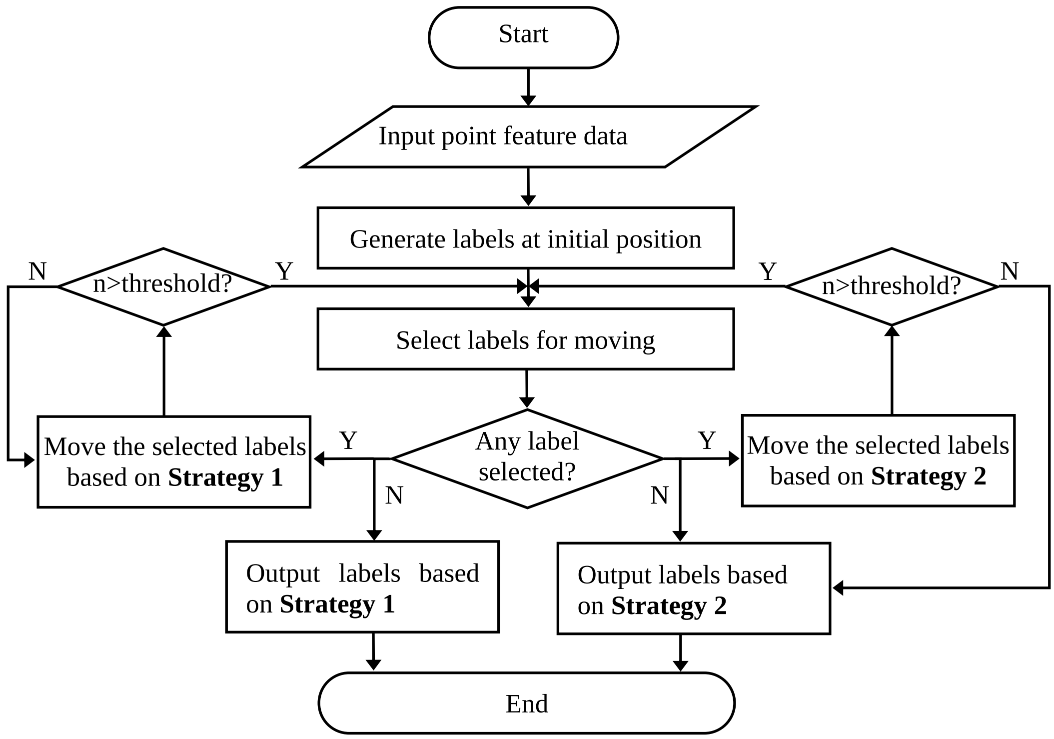

Figure 6.3. The progress of the algorithm for automated labelling with two strategies.

6.2 Generation of image-maps with different strategies for automated label placement

The process of acquiring the optimal solutions of labels by the designed algorithm is shown in Figure 6.3. Firstly, input the point feature data and generate labels for each point at the initial position, i.e., left-right position and the position with the smallest complexity. For each label L, a weight value $\mathrm{W(L)}$ is calculated with reference to the following equation:

$$\mathrm{W(L)} = \begin{cases} 0, & \text{if no overlap exists} \\ \mathrm{w_1} \times \mathrm{n_{overlap}(Labels)} + \mathrm{w_2} \times \mathrm{n_{overlap}(Points)}, & \text{if overlaps exist} \end{cases} \tag{6.3}$$

Where the equation for the situation that overlaps exist is the same as equation (6.2). The labels with $W(L) > 0$ are selected for moving. The selected labels positions were optimized according to the values of $W(L)$ for each label, from large to small. For each label, all potential positions are in order with preference with the two strategies referred above. Only positions with lower preferences with be extracted as optimized positions. When the label moves to a new position, $W(L)$ is updated. If the new $W(L)$ is smaller than previous value, the new position will be updated. Otherwise, the position is rejected, and other potential positions will be chosen one by one.

6.3 Experimental evaluation

6.3.1 Design of image-map series

Experimental validation has been conducted for the proposed automated point label placement for image-map generation. The experimental data includes the images, given by WorldView-4 (Pan-0.3 m, Mul-1.2 m) and Points of Interests (POI) data from vector digital map data (scale: 1:5000), given by the Surveying and Mapping Office, Hong Kong Special Administrative Region (SMO 2019). Three test areas (Figure 6.4) are chosen from the data, each 1.5 km × 1.5 km, with 123, 82, 79 POIs individually. The image-maps of the first test area with point labels, placed at initial positions (Figure 6.5), and generated with strategy 1 and 2 (Figure 6.6 and Figure 6.7) are shown as an example. A ten-grade marking system has been designed for the evaluation, including the “ease level of finding name labels”, “congestion level”, and “satisfaction level”.

(a)

(b)

(c)

Figure 6.4. Three test areas in Hong Kong.

Figure 6.5. Image-map with labels at initial positions.

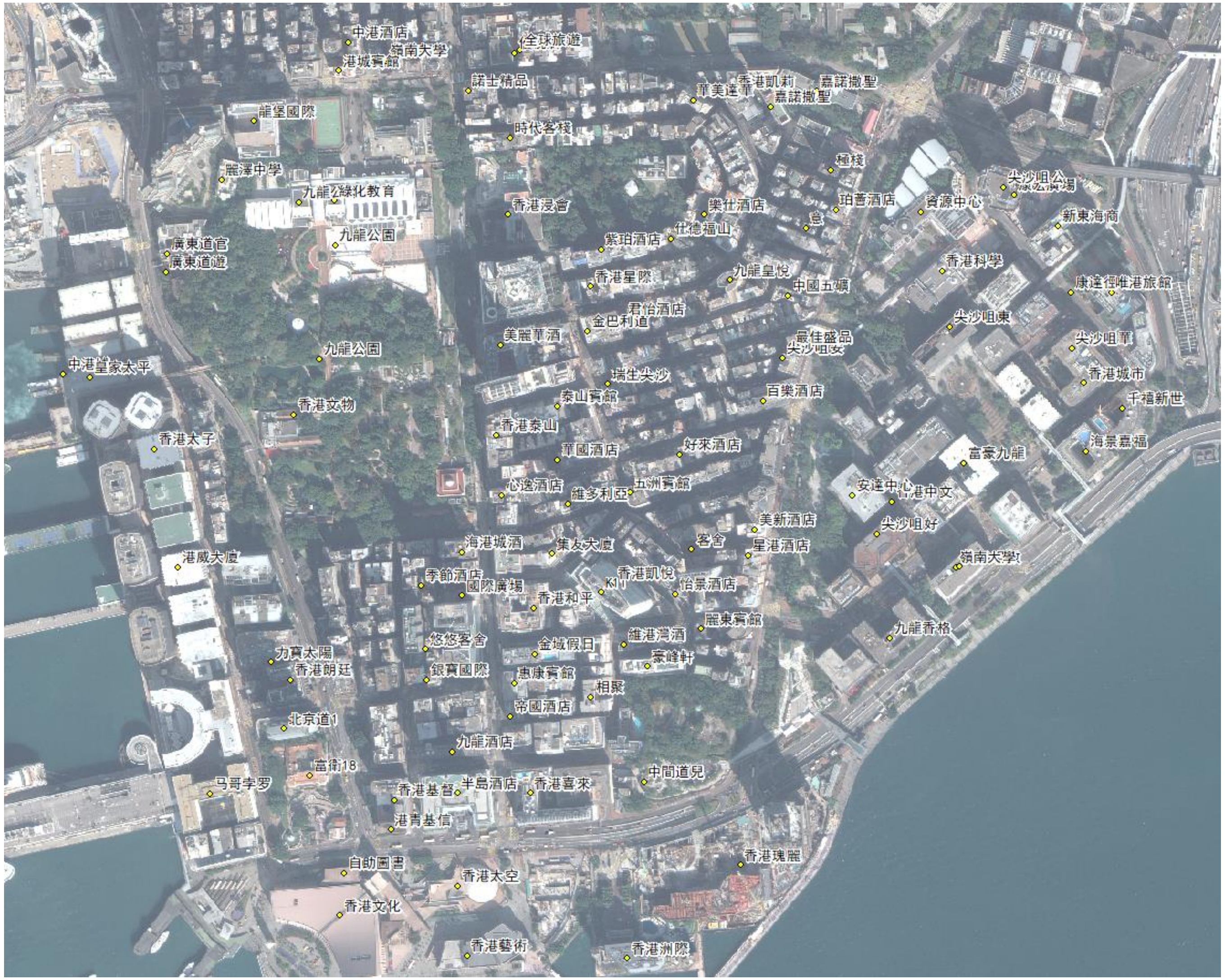

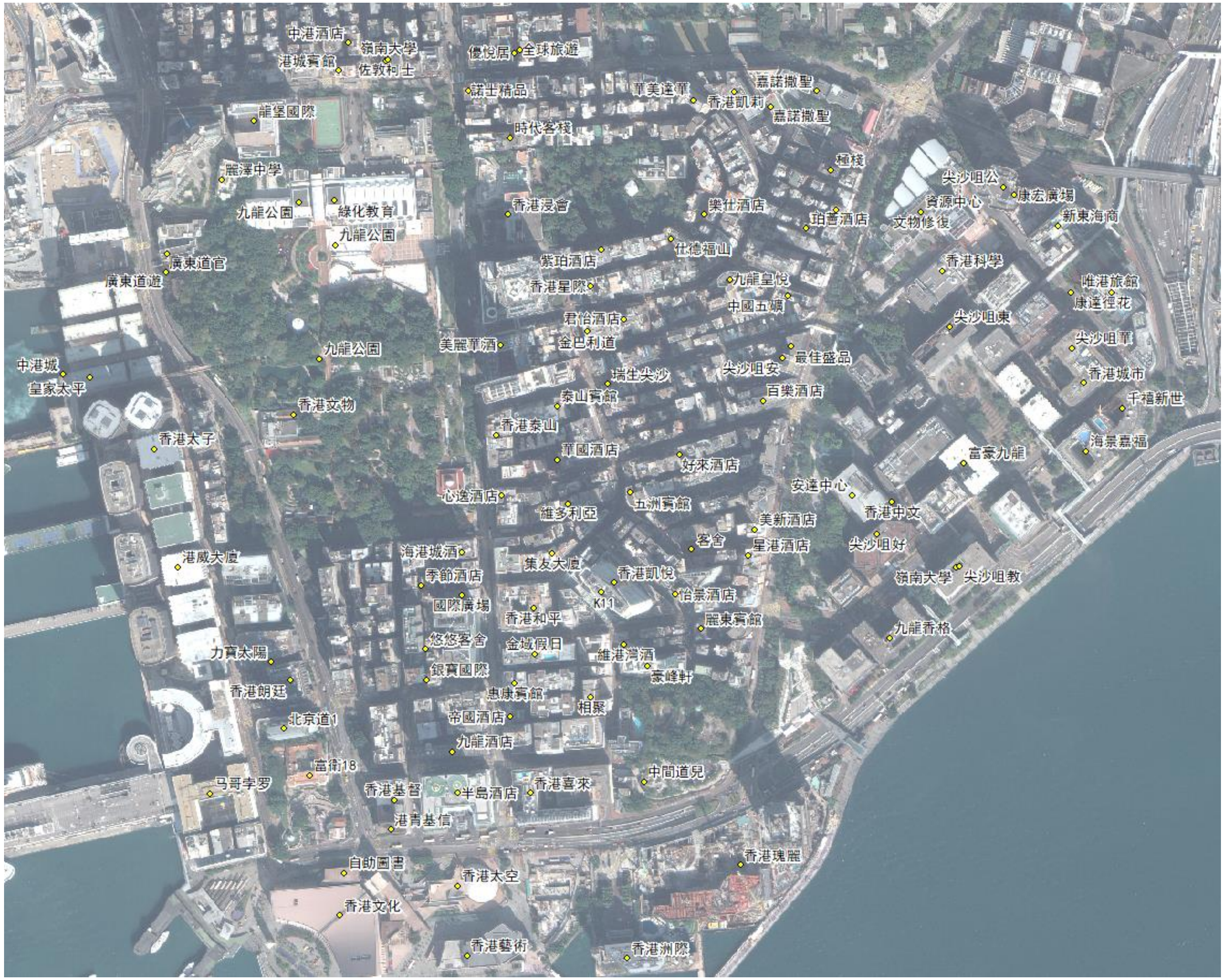

Figure 6.6. Image-map with labels optimized with Strategy 1 (based on general principles and standard ranking of preference).

Figure 6.7. Image-map with labels optimized with Strategy 2 (based on general principles and the complexity of background images).

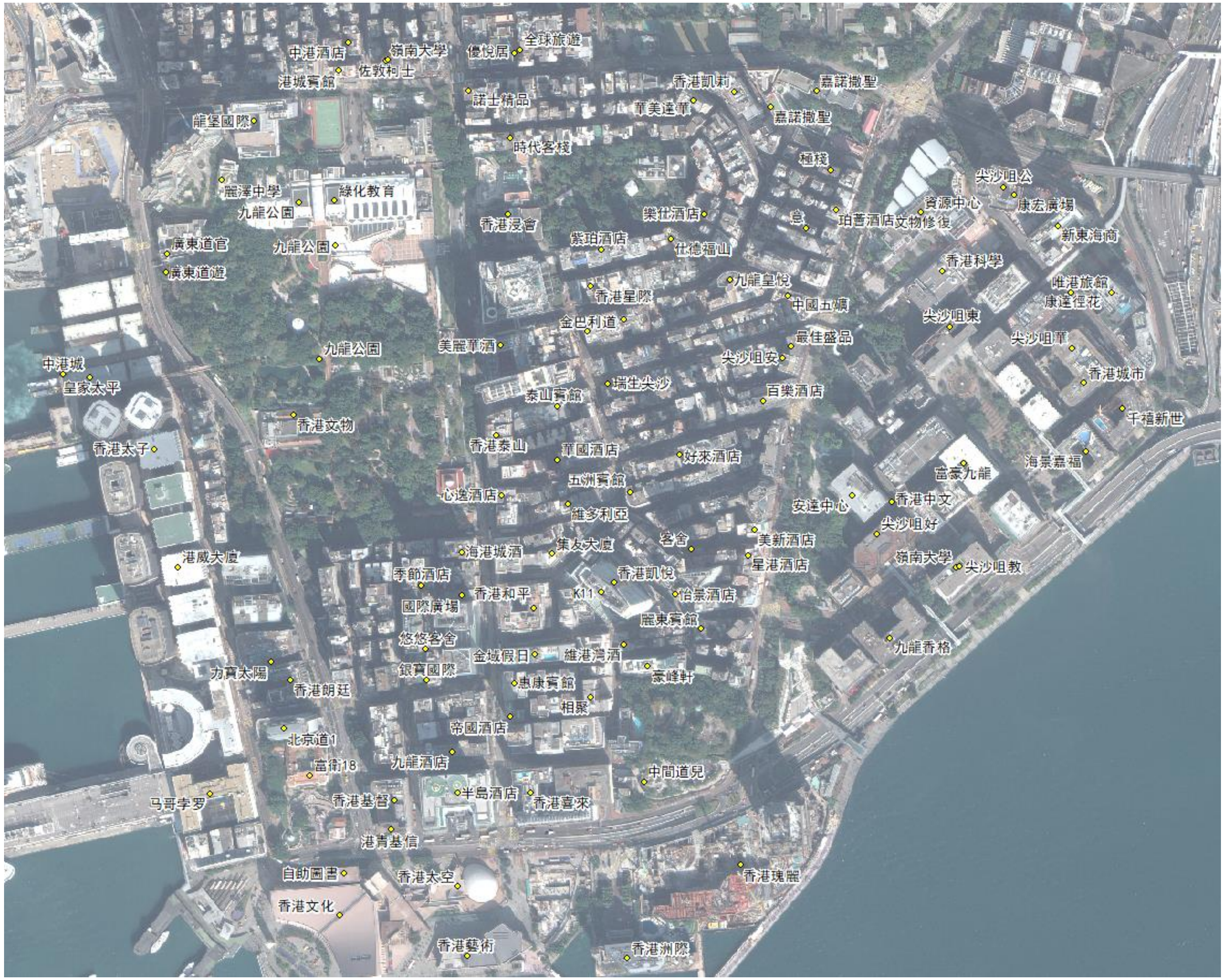

6.3.2 Experimental results and analysis

Participants were recruited via social media networks (https://www.wjx.cn/vj/mBDroXm.aspx). A total of 35 people (15 females and 20 males, aged from 18 to 35) participated in the experiment. The average scores from 30 effective answer sheets are shown in Table 6.1. It can be found the optimized image-maps, with both the two optimization strategies, perform much better than the original ones. But for the results between the two optimized image-maps, the congestion levels are comparable. Both the two optimized methods can get better utilization of space for label placement and reach a higher congestion level. But for the ease level and satisfaction level, the optimized complexity-based strategy can get better results. Considering the complex background images into the optimization of point label placement have better performances in target searching tasks and have better satisfaction.

Table 6.1. Ease level of finding name labels, congestion level, and satisfaction level of the image-maps for three test areas with different label placements.

Test areas		Ease level of finding name labels	Congestion level	Satisfaction level
(a)	Original	3.4	6.4	4.2
	Optimized with strategy 1	4.1	7.4	5.2
	Optimized with strategy 2	**4.5**	**7.8**	**6.4**
(b)	Original	5.4	7.6	5.3
	Optimized with strategy 1	5.8	7.6	5.4
	Optimized with strategy 2	**5.9**	**7.7**	**6.3**
(c)	Original	4.6	7.1	3.2
	Optimized with strategy 1	4.7	7.3	3.3
	Optimized with strategy 2	**5.7**	**7.4**	**3.6**

6.4 Summary

In this chapter, an automated point labeling method is proposed for image-map generation based on the complexity of background image and general principles. The potential positions, general preferences of positions, and the complexity ranking of positions are taken into consideration and integrated into a local optimization algorithm for point label placement. An online user study is conducted with the image-maps generated with the optimization strategies. The experiment evaluated the image-maps from three aspects, including the "ease level of finding name labels", "congestion level", and "satisfaction level". The experiment results showed both the two optimized methods, with general principles and with complexity-based strategy, outperformed the original label placements. What's more, the complexity-based strategy worked better than the strategy with general principles in image-maps.

Chapter 7 Conclusions

7.1 Summary

An image map, as a hybrid design, with the advantage of both maps' high interpretation efficiency and satellite images' realism is desired. However, the quality of such map is criticized by many people. The main factors influenced the quality of image-map generation, include: the generation of background images, overlaying map symbols onto images, and map symbol representation. This study explored the optimization of multi-scale image-map generation and proposed the complexity-based strategies for four aspects. First, the matching between image features and maps' graphic symbols; second, the complexity of background images; third, graphic symbol load; fourth, label placement on complex imagery.

For the first factor, this research developed a complexity-based matching between image resolution and map scale for multi-scale image-map generation. Two levels of complexities for line features were considered for this matching: class level (complexity of line network) and feature level (complexity of individual lines). The horizontal location and visual assessment for the acceptance of image resolutions were evaluated. Experiments showed that the proposed complexity-based method could obtain a good matching between image resolution and map scale in terms of accuracy and users' preference. Complexity-based matching's consideration of LoD differences in multi-scale representations in image-map generation can improve the final matching result between image resolution and map scale.

For the second factor, the usability of image-maps was evaluated in terms of effectiveness and efficiency using image-maps produced with different background image transparency levels. The usability of image-maps is influenced by the transparency of background images. Peak usability occurs at different transparency levels depending on the landscape and scale of image-maps. A quadratic polynomial model can fit the trend between the usability and Boltzmann entropy as a measure of complexity for image-maps. The complexity of background images shows advantages over contrast. This serves as a guideline for the effective use of transparency in image-map design.

For the third factor, the effects of background image complexity on map symbol load were explored through an experiment using eye-tracking and online questionnaire surveying. The usability of image-maps and maps was evaluated with different levels of label density. The effects of background image complexity and map symbol load on image-maps' usability are explored. The complexity of background images influenced the optimum level of map symbol load in image-maps. A quadratic polynomial model can fit the trend between the usability and complexity of image-maps. The complexity of background images has the potential to predict peak usability.

For the fourth factor, an automated point labeling method is proposed for image-map generation based on the complexity of background images and general principles. Both the existing preference and complexity of background images are considered and integrated into the automated labeling optimization algorithm. The image-maps generated using the proposed methods were used to evaluate the "ease level of finding name labels", "congestion level", and "satisfaction level". Image maps generated using the complexity-based strategy outperform those generated using the strategy with general principles and those with original label placements.

7.2 Conclusions

Based on the experimental results, the following conclusions can be drawn:

- Complexity-based matching can improve the matching between image resolution and map scale with consideration of the LoD differences in multi-scale representations.
- The usability of image-maps is influenced by the transparency of background images, mostly with a single peak. The transparency level corresponding to the peak usability decreases as the background complexity increases. The complexity of background images serves as a guideline for the effective use of transparency in image-map design.
- The usability of image-maps is influenced by the complexity of background images, a peak exists for optimum symbol load for an image-map. The optimum levels for symbol load for different image-maps also have a peak when the complexity of background image/image map increases. The

complexity of background images serves as a guideline for optimum map symbol load in image-map design.

- The complexity-based optimization strategy for point label placement, considering not only the general principles and complexity of background images, has better performance in target searching tasks and satisfaction than original placement and strategy with general principles.

7.3 Limitations of this study

The limitations of this study can be considered from four viewpoints.

In the first work, the matching results were influenced by the quality of line networks extracted from images; however, automatic line (road) extraction from Hong Kong images is challenging, given the complex environment, including crowded spaces and high-rise buildings. For this reason, line networks were manually extracted in this experiment. Although vertices can strongly influence individual line features, the length, density, and fractal data for the entire network are not easily influenced by the tightness or sparseness of polyline nodes. The complexity of class-level features also plays a major role in matching. More work could be done to automatically extract line networks from multi-scale-resolution images.

In the second work, the questions in current questionnaires were used to evaluate image-maps' usability based on the main features in the areas studied; however, different types of questions require different information about image-maps and may influence the evaluation of image-maps' usability.

In the third work, only the average time to first view and the average revisits of AOIs were taken and used in the analysis. The other eye movement records, such as the fixation map and heat map, can also be further studied to explore the relationship.

In the fourth work, the current automated complexity-based point labeling method has a limitation, i.e., the complexity is calculated using the patch, where the label is placed. The calculated complexity reflects the local complexity level, but interactions between the label patch and surrounding image values are not considered. For future study, a bigger label patch that considers not only the local patch complexity but also the environment surrounding the label patch could be explored for global optimum label placements.

7.4 Recommendations for future research

Future research is recommended from three viewpoints.

From the aspect of background images, more image generalization methods can be explored for better legibility. The other similar characteristics with transparency referenced in Chapter 4, such as contrast and lightness, can also be explored. In addition, the shadows of high buildings (see examples in Figure 5.4) in background images significantly influenced legibility. Shadows are caused by tilted sunlight, which cannot be avoided in orthophotos. Deep learning methods can be used to further investigate shadow removal (Vasluianu et al. 2021, Fu et al. 2021).

From the aspect of uploaded map symbols, automatic symbol style design based on complex background images is desired for effective use of this kind of map. Many interesting works have been conducted in relative fields, such as the design of continuous hybrid visualizations between ortho-imagery and symbolized vector data (Hoarau and Christophe 2017) and the use of artificial intelligence technologies for map style transfer (Kang et al. 2019).

From the aspect of image and map combination, complex background images violate cartographic design rules in terms of simplicity. This study verified the influence of background images on image maps' usability in Chapter 5. Selective omission of map contents should be explored. The complexity calculated in this study is raster-based. The appearances of different density levels of labels have no significant effect on the overall complexity calculated with raster values. A compromise method that can reflect both the complexity of raster images and the number of vector map symbols could be explored.

References

AGUILAR, M. A., SALDANA, M. M. and AGUILAR, F. J. 2013. Assessing geometric accuracy of the orthorectification process from GeoEye-1 and WorldView-2 panchromatic images. *International Journal of Applied Earth Observation and Geoinformation,* 21, 427-435.

ALBERTZ, J., *et al.*, 1993. Satellite image maps-experiences, problems and chances. ed. *The International Archives of the Photogrammetry, Remote Sensing and Spatial Information Sciences*, 2-14 August 1992 Washington, D.C., USA, 309-314.

ALBERTZ, J. and TAUCH, R. 1994. Mapping from space - cartographic applications of satellite image data. *Geojournal,* 32(1), 29-37.

ALRAJHI, M., *et al.*, 2016. Updating maps using high resolution satellite imagery. ed. *The International Archives of the Photogrammetry, Remote Sensing and Spatial Information Sciences*, 12–19 July 2016 Prague, Czech Republic, 711-719.

ARKESTEIJN, J. G. M., 1968. Dutch experience with photo maps. ed. *Proceedings of the International Symposium on Photo Maps and Orthophoto Maps held in Ottawa, Canada*, September 18-22, 1967 Canadian Institute of Surveying.

ARKIN, E. M., *et al.*, 1991. *An efficiently computable metric for comparing polygonal shapes.* CORNELL UNIV ITHACA NY.

ARUN, K. S., HUANG, T. S. and BLOSTEIN, S. D. 1987. Least-squares fitting of two 3-D point sets. *IEEE Transactions on Pattern Analysis and Machine Intelligence,* 9(5), 698-700.

ASPRS, A. S. F. P. A. R. S. 1990. ASPRS accuracy standards for large-scale maps. *Photogrammetric Engineering and Remote Sensing,* 56(7), 1068-1070.

ASPRS, A. S. F. P. A. R. S., 2014. Positional accuracy standards for digital geospatial data. *Photogrammetric Engineering and Remote Sensing.* A1-A26.

AUTHORITY, T. V., 1998. *Geospatial positioning accuracy standards, part 3: national standard for spatial data accuracy.* Virginia, NV, USA: National Aeronautics and Space Administration.

BARAZZETTI, L., *et al.* 2016. Georeferencing accuracy analysis of a single worldview-3 image collected over milan. *Int. Arch. Photogramm. Remote Sens. Spatial Inf. Sci.,* XLI-B1, 429-434.

BĚLKA, L. 2013. The image map: from broad practical use towards a cartographic concept. *Kartographische Nachrichten,* 4/2013, 196-204.

BĚLKA, L. and VOŽENíLEK, V. 2014. Prototypes of orthoimage maps as tools for geophysical application. *Pure and Applied Geophysics,* 171(6), 1047-1059.

BESL, P. J. and MCKAY, N. D. 1992. A method for registration of 3-D shapes. *IEEE Transactions on Pattern Analysis and Machine Intelligence,* 14(2), 239-256.

BEVAN, N., *et al.*, New ISO standards for usability, usability reports and usability measures. ed. *International Conference on Human-Computer Interaction*, 2016, 268-278.

BJøRKE, J. T. 1996. Framework for entropy-based map evaluation. *Cartography and Geographic Information Systems,* 23(2), 78-95.

BLASBY, D., *et al.*, 2002. *GIS conflation using open source tools.*

BRYCHTOVA, A. and COLTEKIN, A. 2016. An empirical user study for measuring the influence of colour distance and font size in map reading using eye tracking. *The Cartographic Journal,* 53(3), 202-212.

CAMPODONICO, R. M. and MONOPOLI, E. P., 1968. Experience in the production and use of photo maps. ed. *Proceedings of the International Symposium on Photo Maps and Orthophoto Maps held in Ottawa, Canada*, September 18-22, 1967 Canadian Institute of Surveying, Ottawa, Canada.

CARSTENSEN, L. W. 1989. A fractal analysis of cartographic generalization. *The American Cartographer,* 16(3), 181-189.

CASSETTARI, S. 2004. Photo mapping of great britain: a growing opportunity? *The Cartographic Journal,* 41(2), 95-100.

CELIKOYAN, T. M., ALTAN, M. O. and KEMPER, G., 2004. Accuracy investigation for a large scale GIS. ed. *The International Archives of the Photogrammetry, Remote Sensing and Spatial Information Sciences*, 12-23 July 2004 Istanbul, Turkey, 1025-1030.

CHAUDHRY, O. Z., MACKANESS, W. A. and REGNAULD, N. 2009. A functional perspective on map generalisation. *Computers, Environment and Urban Systems,* 33(5), 349-362.

CHEHREGHAN, A. and ALI ABBASPOUR, R. 2017. An assessment of spatial similarity degree between polylines on multi-scale, multi-source maps. *Geocarto International,* 32(5), 471-487.

CHEHREGHAN, A. and ALI ABBASPOUR, R. 2018. An assessment of the efficiency of spatial distances in linear object matching on multi-scale, multi-source maps. *International Journal of Image and Data Fusion,* 9(2), 95-114.

CHEN, J.*, et al.* 2009. Selective omission of road features based on mesh density for automatic map generalization. *International Journal of Geographical Information Science,* 23(8), 1013-1032.

CHRISTENSEN, J., MARKS, J. and SHIEBER, S. 1995. An empirical study of algorithms for point-feature label placement. *ACM Transactions on Graphics (TOG),* 14(3), 203-232.

COLLINS, L. M. 1985. Landsat image maps—the how, why, and how much. *Australian Surveyor,* 32(5), 365-369.

CONGALTON, R. G. and GREEN, K., 2008. *Assessing the accuracy of remotely sensed data: principles and practices.* CRC press.

CONTE, D.*, et al.* 2004. Thirty years of graph matching in pattern recognition. *International journal of Pattern Recognition and Artificial Intelligence,* 18(03), 265-298.

CRAVO, G. L., RIBEIRO, G. M. and LORENA, L. A. N. 2008. A greedy randomized adaptive search procedure for the point-feature cartographic label placement. *Computers & Geosciences,* 34(4), 373-386.

DAHLBERG, R. E. 1993. The design of photo and image maps. *The Cartographic Journal,* 30(2), 112-118.

DAHLBERG, R. E. and LUMAN, D. E., 1987. Towards further development of the satellite image map genre. *Remote Sensing: Towards Operational Cartographic Application.* M. F. Buchroithner and R. Kosta, Eds., Graz, 51-56.

DIGITALGLOBE, 2012. *QuickBird data sheet* [online]. Available from: https://www.spaceimagingme.com/downloads/sensors/datasheets/QuickBird-DS-QB-Web.pdf.

DIGITALGLOBE, 2013. *Digital Globe IKONOS data sheet* [online]. Available from: https://dgv4-cms-production.s3.amazonaws.com/uploads/document/file/133/DG_IKONOS_DS.pdf.

DIGITALGLOBE, 2014. *GeoEye-1 data sheet* [online]. Available from: https://www.digitalglobe.com/resources/data-sheets.

DIGITALGLOBE, 2017a. *WorldView-4 calibration digitalglobe constellation update* [online]. USGS Reston, VA: DigitalGlobe. Available from: https://calval.cr.usgs.gov/wordpress/wp-content/uploads/Chris-Comp.pdf [Accessed 23 October 2018].

DIGITALGLOBE, 2017b. *WorldView-4 data sheet* [online]. Available from: https://dg-cms-uploads-production.s3.amazonaws.com/uploads/document/file/196/DG2017_WorldView-4_DS.pdf.

DO NASCIMENTO, H. A. and EADES, P. 2008. User hints for map labeling. *Journal of Visual Languages & Computing,* 19(1), 39-74.

DODDI, S.*, et al.*, Map labeling and its generalizations. ed. *Proc. 8th Ann. ACM/SIAM Symp. Discrete Algs.(SODA97)*, 1997, 148-157.

DONG, W.*, et al.* 2016. Assessing the Effectiveness and Efficiency of Map Colour for Colour Impairments Using an Eye-tracking Approach. *The Cartographic Journal,* 53(2), 166-176.

DONG, W. H.*, et al.* 2014. Eye tracking to explore the potential of enhanced imagery basemaps in web mapping. *The Cartographic Journal,* 51(4), 313-329.

DUCHOWSKI, A. T., 2017. *Eye tracking methodology: Theory and practice.* Springer.

EBNER, D., KLAU, G. W. and WEISKIRCHER, R., Label Number Maximization in the Slider Model. ed. *Graph Drawing*, 2004, 144-154.

ELSHEHABY, A. R. and TAHA, L. G. E. D. 2011. Assessment of cartographic potential of EgyptSat-1 satellite image (case study in flat areas). *Applied Geomatics,* 3(3), 159-169.

FAIRBAIRN, D. 2006. Measuring map complexity. *The Cartographic Journal,* 43(3), 224-238.

FLEMING, E. A. 1973. Quality of production orthophotos. *Photogrammetric Engineering,* 39(11), 1152-1160.

FRANK, A. U. and TIMPF, S. 1994. Multiple representations for cartographic objects in a multi-scale tree—an intelligent graphical zoom. *Computers & graphics,* 18(6), 823-829.

FRIEDMAN, M. 1937. The use of ranks to avoid the assumption of normality implicit in the analysis of variance. *Journal of the American Statistical Association,* 32(200), 675-701.

FU, L.*, et al.*, Auto-exposure fusion for single-image shadow removal. ed. *Proceedings of the IEEE/CVF Conference on Computer Vision and Pattern Recognition*, 2021, 10571-10580.

GAO, P. C. and LI, Z. L. 2019. Aggregation-based method for computing absolute Boltzmann entropy of landscape gradient with full thermodynamic consistency. *Landscape Ecology,* 34(8), 1837-1847.

GAO, P. C., LI, Z. L. and QIN, Z. 2018. Usability of value-by-alpha maps compared to area cartograms and proportional symbol maps. *Journal of Spatial Science*, 1-17.

GAO, P. C., ZHANG, H. and LI, Z. L. 2017. A hierarchy-based solution to calculate the configurational entropy of landscape gradients. *Landscape Ecology,* 32(6), 1133-1146.

GATRELL, A. C. 1977. Complexity and redundancy in binary maps. *Geographical Analysis,* 9(1), 29-41.

GAZEPOINT, 2021. *GP3 Eye-Tracker* [online]. Available from: https://www.gazept.com [Accessed 11 20 2021].

GONZALEZ, R. C. and WOODS, R. E., 2002. Digital image processing. Prentice hall Upper Saddle River, NJ.

GOODCHILD, M. F. 1980. Fractals and the accuracy of geographical measures. *Mathematical Geology,* 12(2), 85-98.

GUZMáN, P. A. and MEYER, R. L., 1968. Maps and orthophoto maps applied to economic development in El Salvador. ed. *Proceedings of the International Symposium on Photo Maps and Orthophoto Maps held in Ottawa, Canada*, September 18-22, 1967 Canadian Institute of Surveying, Ottawa, Canada.

HACKELOEER, A., *et al.*, 2015. Road network conflation: an iterative hierarchical approach. *Progress in Location-Based Services 2014.* Springer, 137-151.

HACKELöER and ANDREAS, 2016. *Conflation of road networks from digital maps.* (PhD). Technische Universität München.

HARRIE, L. and STIGMAR, H. 2010. An evaluation of measures for quantifying map information. *ISPRS Journal of Photogrammetry and Remote Sensing,* 65(3), 266-274.

HARRIE, L., STIGMAR, H. and DJORDJEVIC, M. 2015. Analytical estimation of map readability. *ISPRS International Journal of Geo-Information,* 4(2), 418-446.

HARRIS, C. G. and STEPHENS, M., A combined corner and edge detector. ed. *Alvey vision conference*, 1988, 10-5244.

HILD, H. and FRITSCH, D. 1998. Integration of vector data and satellite imagery for geocoding. *Iaprs*, 246--251.

HIRSCH, S. A. 1982. An algorithm for automatic name placement around point data. *The American Cartographer,* 9(1), 5-17.

HOARAU, C., Orthoimage or map visualization in use in geoportals, case study on the French geoportal. ed. *Proc. of AutoCarto2012 Conference*, 2012.

HOARAU, C. and CHRISTOPHE, S. 2017. Cartographic continuum rendering based on color and texture interpolation to enhance photo-realism perception. *ISPRS Journal of Photogrammetry and Remote Sensing,* 127, 27-38.

HOARAU, C., CHRISTOPHE, S. and MUSTIèRE, S., Mixing, blending, merging or scrambling topographic maps and orthoimagery in geovisualizations. ed. *International Cartographic Conference*, 2013.

HU, Y. G., *et al.*, 2007. Selection of streets based on mesh density for digital map generalization. *Fourth International Conference on Image and Graphics (ICIG 2007).* 2007, Sichuan, 903-908.

IMHOF, E. 1975. Positioning names on maps. *The American Cartographer,* 2(2), 128-144.

ISO, 2018. Ergonomics of human-system interaction. *Part 11: usability: definitions and concepts.* Switzerland: International Organization for Standardization.

JACOBSEN, K., 1990. Cartographic potential of space images. ed. *The International Archives of the Photogrammetry, Remote Sensing and Spatial Information Sciences*, 8-12 September 1990 Dresden, 127-134.
JACOBSEN, K. 2003. Geometric potential of IKONOS-and QuickBird-images. *Photogrammetric Weeks '03*, 101-110.
JIANG, W., *et al.* 2017. Ortho accuracy validation and analysis of GF-2 PAN imagery based on Beidou satellite navigation system and GPS. *Remote Sensing for Land and Resources,* 29(3), 211-216.
JOHANSSON, O., 1968. Orthophoto maps as a basis for the economic map of Sweden on the scale of 1:10, 000. ed. *Proceedings of the International Symposium on Photo Maps and Orthophoto Maps held in Ottawa, Canada*, September 18-22, 1967 Canadian Institute of Surveying, Ottawa, Canada.
KAMEDA, T. and IMAI, K. 2003. Map label placement for points and curves. *IEICE Transactions on Fundamentals of Electronics, Communications and Computer Sciences,* 86(4), 835-840.
KANG, Y., GAO, S. and ROTH, R. E. 2019. Transferring multiscale map styles using generative adversarial networks. *International Journal of Cartography,* 5(2-3), 115-141.
KENT, R. B. and TOBIAS, T. J. 1990. State atlases: funding sources and thematic content. *The Professional Geographer,* 42(3), 313-323.
KLAU, G. W. and MUTZEL, P. 2003. Optimal labeling of point features in rectangular labeling models. *Mathematical Programming,* 94(2-3), 435-458.
KNOBLOCK, C. A., *et al.*, Automatic alignment of vector data and orthoimagery for the national map. ed. *Proceedings of the 2006 international conference on Digital government research*, 2006, 303-304.
LAM, S. N. and QUATTROCHI, D. A. 1992. On the issues of scale, resolution, and fractal analysis in the mapping sciences. *Professional Geographer,* 44(1), 88-98.
LAN, T., LI, Z. and ZHANG, H. 2019. Urban allometric scaling beneath structural fractality of road networks. *Annals of the American Association of Geographers*, 1-15.
LAN, T., *et al.* 2020. Automated labeling of schematic maps by optimization with knowledge acquired from existing maps. *Transactions in GIS,* 24(6), 1722-1739.
LANDEN, D. 1966. Photomaps for urban planning. *Photogrammetric Engineering,* 32(1), 136-141.
LEUNG, L. F. and LI, Z. L. 2002. Experimental evaluation of the effectiveness of graphic symbols on tourist maps. *Cartography,* 31(1), 11-20.
LI, D. R. and WANG, M. 2012. On-orbit geometric calibration and accuracy assessment of ZY-3. *Spacecraft Recovery and Remote Sensing,* 33(3), 1-6.
LI, L. N. and GOODCHILD, M. F. 2011. An optimisation model for linear feature matching in geographical data conflation. *International Journal of Image and Data Fusion,* 2(4), 309-328.
LI, P. F., *et al.* 2017. An emergency georeferencing framework for GF-4 imagery based on GCP prediction and dynamic RPC refinement. *Remote Sensing,* 9(10), 1053.
LI, Z. L., 2006. *Algorithmic foundation of multi-scale spatial representation.* CRC Press.

LI, Z. L. and HUANG, P. Z. 2002. Quantitative measures for spatial information of maps. *International Journal of Geographical Information Science,* 16(7), 699-709.
LI, Z. L. and TI, P. 2015. Adaptive generation of variable-scale network maps for small displays based on line density distribution. *GeoInformatica,* 19(2), 277-295.
LIAO, H.*, et al.* 2018. Measuring the influence of map label density on perceived complexity: a user study using eye tracking. *Cartography and Geographic Information Science*, 1-18.
LILLESAND, T., KIEFER, R. W. and CHIPMAN, J., 2015. *Remote sensing and image interpretation.* John Wiley & Sons.
LIU, X. L.*, et al.*, Hierarchical image representation based on digital topology for bridging remote sensing and GIS. ed. *Image and Signal Processing, 2008. CISP'08. Congress on*, 2008, 736-740.
LUEBKE, D.*, et al.*, 2003. *Level of detail for 3D graphics.* Morgan Kaufmann.
MA, Z. L.*, et al.* 2017. Geometric positioning for satellite imagery without ground control points by exploiting repeated observation. *Sensors,* 17(2), 240.
MACEACHREN, A. M. 1982. Map complexity: Comparison and measurement. *The American Cartographer,* 9(1), 31-46.
MANDELBROT, B. B., 1983. *The fractal geometry of nature.* New York: W.H. Freeman and Company.
MENG, L. Q.*, et al.* 2017. A review of research works on vgi understanding and image map design. *Kartographische Nachrichten,* 2017(1), 17-22.
MURPHY, C. E., 2014. *Concise image maps-a design approach.* Thesis (PhD). Technische Universität München.
MURPHY, C. E., 2015. Intellectual highlighting of remote sensing imagery for better image map design. ed. *Proceedings of the 27th International Cartographic Conference*, 23–28 August 2015 Rio de Janeiro, Brazil, 1-8.
MURPHY, C. E. 2019. Designing the imagery on image maps – how far can we take it? *International Journal of Cartography,* 5(2-3), 316-331.
NOGUCHI, M.*, et al.* 2004. Accuracy assessment of QuickBird stereo imagery. *The Photogrammetric Record,* 19(106), 128-137.
OLSON, J. M. 1975. Autocorrelation and visual map complexity. *Annals of the Association of American Geographers,* 65(2), 189-204.
PANCHAUD, N. H., ENESCU, I. I. and HURNI, L. 2017. Smart cartographic functionality for improving data visualization in map mashups. *Cartographica: The International Journal for Geographic Information and Geovisualization,* 52(2), 194-211.
PAPADIMITRIOU, C. H. and STEIGLITZ, K., 1998. *Combinatorial optimization: algorithms and complexity.* Courier Corporation.
PETRIE, G. 1977. Orthophotomaps. *Transactions of the Institute of British Geographers*, 49-70.
PHILLIPS, R. J. and NOYES, L. 1982. An investigation of visual clutter in the topographic base of a geological map. *The Cartographic Journal,* 19(2), 122-132.
POHL, C. and VAN GENDEREN, J. L. 1999. Multi‐sensor Image Maps from SPOT, ERS and JERS. *Geocarto International,* 14(2), 34-41.

POLI, D. and TOUTIN, T. 2012. Review of developments in geometric modelling for high resolution satellite pushbroom sensors. *The Photogrammetric Record,* 27(137), 58-73.
POON, S.-H., *et al.* 2004. Labeling points with weights. *Algorithmica,* 38(2), 341-362.
RAIDL, G., A genetic algorithm for labeling point features. ed. *Proceedings of the international conference on imaging science, systems, and technology*, 1998, 189-196.
RAPOSO, P. and BREWER, C. A., Comparison of topographic map designs for overlay on orthoimage backgrounds. ed. *25th International Cartographic Conference, Paris*, 2011.
RAPOSO, P. and BREWER, C. A., Guidelines for consistently readable topographic vectors and labels with toggling backgrounds. ed. *26th International Cartographic Conference, Dresden*, 2013.
RAPOSO, P. and BREWER, C. A. 2014. Landscape preference and map readability in design evaluation of topographic maps with an orthoimage background. *The Cartographic Journal,* 51(1), 25-37.
RIBEIRO, G. M. and LORENA, L. A. N. 2008. Lagrangean relaxation with clusters for point-feature cartographic label placement problems. *Computers & Operations Research,* 35(7), 2129-2140.
ROBINSON, A. H., *et al.*, 1995. *Elements of cartography, 6th edition.* New York: John Wiley & Sons.
ROSENHOLTZ, R., LI, Y. and NAKANO, L. 2007. Measuring visual clutter. *Journal of vision,* 7(2), 17-17.
ROTH, R. E., *et al.* 2017. User studies in cartography: opportunities for empirical research on interactive maps and visualizations. *International Journal of Cartography,* 3(sup1), 61-89.
RUIZ, J., RUBIO, T. and URENA, M. 2011a. Automatic extraction of road intersections from images based on texture characterisation. *Survey review,* 43(321), 212-225.
RUIZ, J. J., *et al.* 2011b. Digital map conflation: a review of the process and a proposal for classification. *International Journal of Geographical Information Science,* 25(9), 1439-1466.
SAALFELD, A. 1988. Conflation automated map compilation. *International Journal of Geographical Information System,* 2(3), 217-228.
SCHNUR, S., BEKTAŞ, K. and ÇöLTEKIN, A. 2018. Measured and perceived visual complexity: a comparative study among three online map providers. *Cartography and Geographic Information Science,* 45(3), 238-254.
SCHNUR, S., *et al.* 2010. A comparison of measured and perceived visual complexity for dynamic web maps. *Proceedings of the GIScience, Zurich, Switzerland,* 14.
SCHWARTGES, N., *et al.*, 2014. Point labeling with sliding labels in interactive maps. *Connecting a Digital Europe Through Location and Place.* Springer, 295-310.
SCHWEINFURTH, G. 1985. Orthophotomaps from digital orthophotos. *Photogrammetria,* 40(2), 77-85.
SISAY, Z. G., BESHA, T. and GESSESSE, B., 2017. Feature orientation and positional accuracy assessment of digital orthophoto and line map for large scale mapping: The case study on bahir dar town, ethiopia. ed. *The International*

Archives of the Photogrammetry, Remote Sensing and Spatial Information Sciences, 6–9 June 2017 Hannover, Germany, 47-53.

Digital map (2019). City: Surveying and mapping office/lands department, the government of the Hong Kong Special Administrative Region.

SONG, W. B.*, et al.* 2009. Automated geospatial conflation of vector road maps to high resolution imagery. *IEEE Transactions on Image Processing,* 18(2), 388-400.

SONG, W. B.*, et al.* 2013. An automated approach for the conflation of vector parcel map with imagery. *Photogrammetric Engineering & Remote Sensing,* 79(6), 535-543.

STIGMAR, H. and HARRIE, L. 2011. Evaluation of analytical measures of map legibility. *The Cartographic Journal,* 48(1), 41-53.

STOREY, J., CHOATE, M. and LEE, K. 2014. Landsat 8 operational land imager on-orbit geometric calibration and performance. *Remote Sensing,* 6(11), 11127-11152.

STRIJK, T. and VAN KREVELD, M. 2002. Practical extensions of point labeling in the slider model. *GeoInformatica,* 6(2), 181-197.

SUKHOV, V. 1970. Application of information theory in generalization of map contents. *International yearbook of cartography,* 10(1), 41-47.

SUNAR ERBEK, F.*, et al.* 2005. The use of satellite image maps for urban planning in Turkey. *International Journal of Remote Sensing,* 26(4), 775-784.

TAUCH, R. and KäHLER, M., 1988. Improving the quality of satellite image maps by various processing techniques. ed. *The International Archives of the Photogrammetry, Remote Sensing and Spatial Information Sciences*, 1-10 July 1988 Kyoto, Japan, 238-247.

THROWER, N. J. W. and JENSEN, J. R. 1976. The orthophoto and orthophotomap: characteristics, development and application. *The American Cartographer,* 3(1), 39-56.

VAJSOVA, B.*, et al.* 2017. New sensors benchmark report on WorldView-4.

VAN KREVELD, M., STRIJK, T. and WOLFF, A. 1999. Point labeling with sliding labels. *Computational Geometry,* 13(1), 21-47.

VASLUIANU, F.-A.*, et al.*, Shadow removal with paired and unpaired learning. ed. *Proceedings of the IEEE/CVF Conference on Computer Vision and Pattern Recognition*, 2021, 826-835.

VELTKAMP, R. C., 2002. Shape matching: similarity measures and algorithms. ed. *Proceedings International Conference on Shape Modeling and Applications*, 7-11 May 2001 Genova, Italy, 188-197.

VOZENILEK, V. and BĚLKA, L., 2016. The cartographic concept of the image map. ed. *The International Archives of the Photogrammetry, Remote Sensing and Spatial Information Sciences*, 12–19 July 2016 Prague, Czech Republic, 605-610.

WALTER, V. and FRITSCH, D. 1999. Matching spatial data sets: a statistical approach. *International Journal of Geographical Information Science,* 13(5), 445-473.

WANG, J. R. and HU, X., 2016. The system overview and geometric image quality of the-TH 1 satellite. ed. *The International Archives of the Photogrammetry, Remote Sensing and Spatial Information Sciences*, 12–19 July 2016 Prague, Czech Republic, 511-516.

WELCH, R. 1972. Photomap image quality. *The Cartographic Journal,* 9(2), 87-92.

WELCH, R. 1985. Cartographic potential of SPOT image data. *Photogrammetric Engineering and Remote Sensing,* 51(8), 1085-1091.
WILLIAMS, T. S., 2000. *Multi-modal registration for image-guided therapy.* Thesis (MSc). Massachusetts Institute of Technology.
WOLFE, R. E., *et al.* 2002. Achieving sub-pixel geolocation accuracy in support of MODIS land science. *Remote Sensing of Environment,* 83(1-2), 31-49.
WOODRUFF, A., LANDAY, J. and STONEBRAKER, M., Constant information density in zoomable interfaces. ed. *Proceedings of the Working Conference on Advanced Visual Interfaces*, 1998, 57-65.
WU, X. Q., *et al.*, Automatic alignment of large-scale aerial rasters to road-maps. ed. *Proceedings of the 15th annual ACM international symposium on Advances in geographic information systems*, 2007, 17.
XIAO, Z., YANG, B. and ZHANG, H. 2014. Positioning accuracy analysis and application for worldview-1 stereo imagery. *Int. Arch. Photogramm. Remote Sens. Spatial Inf. Sci.,* XL-4, 311-314.
XIONG, W. C., *et al.* 2014. Research on HJ-1 A/B satellites data automatic geometric precision correction design. *Engineering Sciences,* 16(3), 37-42.
YAMAMOTO, M., CAMARA, G. and LORENA, L. A. N. 2002. Tabu search heuristic for point-feature cartographic label placement. *GeoInformatica,* 6(1), 77-90.
YANG, B., *et al.* 2017. Large-scale block adjustment without use of ground control points based on the compensation of geometric calibration for ZY-3 images. *ISPRS Journal of Photogrammetry and Remote Sensing,* 134, 1-14.
YOELI, P. 1972. The logic of automated map lettering. *The Cartographic Journal,* 9(2), 99-108.
YUAN, S. X. and TAO, C. 1999. Development of conflation components. *Proceedings of Geoinformatics, Ann Arbor*, 1-13.
ZHANG, H. and LI, Z. L. 2012. Fractality and Self-Similarity in the Structure of Road Networks. *Annals of the Association of American Geographers,* 102(2), 350-365.
ZHANG, J. T., 2013. *A congruent hybrid model for conflation of satellite image and road database.* Thesis (PhD). Technische Universität München.
ZHANG, J. T., ZHU, Y. Q. and MENG, L. Q., Conflation of road network and geo-referenced image using sparse matching. ed. *Proceedings of the 19th ACM SIGSPATIAL International Conference on Advances in Geographic Information Systems*, 2011, 281-288.
ZHANG, M., 2009. *Methods and implementations of road-network matching.* Thesis (PhD). Technischen Universität München.
ZHANG, M., YAO, W. and MENG, L. Q. 2016. Automatic and accurate conflation of different road-network vector data towards multi-modal navigation. *ISPRS International Journal of Geo-Information,* 5(5), 68.
ZHANG, Z. Y. 1994. Iterative point matching for registration of free-form curves and surfaces. *International Journal of Computer Vision,* 13(2), 119-152.
ZUYLEN, V. L. 1969. Production of photomaps. *The Cartographic Journal,* 6(2), 92-102.

Appendix A List of figures

Appendix B List of tables